

AD-765 190

UTILITY OF TSAI'S METHOD FOR SEISMIC  
DISCRIMINATION

Yi-Ben Tsai, et al

Texas Instruments, Incorporated

Prepared for:

Air Force Office of Scientific Research

30 November 1972

DISTRIBUTED BY:

**NTIS**

**National Technical Information Service**  
**U. S. DEPARTMENT OF COMMERCE**  
5285 Port Royal Road, Springfield Va. 22151

**BEST  
AVAILABLE COPY**



AFOSR - TR - 73 - 1014

UTILITY OF TSAI'S METHOD FOR SEISMIC DISCRIMINATION  
FINAL TECHNICAL REPORT

Prepared by

Yi-Ben Tsai and Wen-Wu Shen  
Area Code 703, 836-3882 Ext. 305

T. W. Harley, Program Manager  
Area Code 703, 836-3882 Ext. 300

AD 765190

TEXAS INSTRUMENTS INCORPORATED  
Services Group  
Post Office Box 5621  
Dallas, Texas 75222

Contract No. F44620-71-C-0112  
Amount of Contract: \$47,967  
Beginning 1 July 1971  
Ending 30 September 1972



Prepared for

AIR FORCE OFFICE OF SCIENTIFIC RESEARCH

Sponsored by

ADVANCED RESEARCH PROJECTS AGENCY  
Nuclear Monitoring Research Office  
ARPA Order No. 1827  
ARPA Program Code No. 1F10



30 November 1972

Acknowledgement: This research was supported by the Advanced Research Projects Agency, Nuclear Monitoring Research Office, under Project VELA-UNIFORM, and accomplished under the direction of the Air Force Office of Scientific Research under Contract No. F44620-71-C-0112.

Approved for public release;  
distribution unlimited.

UNCLASSIFIED

Security Classification

DOCUMENT CONTROL DATA - R & D

(Security classification of title, body of abstract and indexing annotation must be entered when the overall report is classified)

|   |   |
|---|---|
| 1. ORIGINATING ACTIVITY (Corporate number)<br>Texas Instruments Incorporated<br>Services Group<br>P. O. Box 5621, Dallas, Texas 75222 | 2a. REPORT SECURITY CLASSIFICATION<br>UNCLASSIFIED<br>2b. GROUP |
|---|---|

3. REPORT TITLE  
 Utility of Tsai's Method for Seismic Discrimination

4. DESCRIPTIVE NOTES (Type of report and inclusive dates)  
 Final

5. AUTHOR(S) (First name, middle initial, last name)  
 Yi-Ben Tsai and Wen-Wu Shen

|                                    |                               |                       |
|------------------------------------|-------------------------------|-----------------------|
| 6. REPORT DATE<br>30 November 1972 | 7a. TOTAL NO. OF PAGES<br>115 | 7b. NO. OF REFS<br>14 |
|------------------------------------|-------------------------------|-----------------------|

|  |  |
|--|--|
| 8a. CONTRACT OR GRANT NO.<br>F44620-71-C-0112<br>b. PROJECT NO.<br>AO 1827<br>c.<br>62701D<br>d. | 9a. ORIGINATOR'S REPORT NUMBER(S)<br><br>9b. OTHER REPORT NO(S) (Any other numbers that may be assigned this report)<br>AFOSR - TR - 73 - 1014 |
|--|--|

10. DISTRIBUTION STATEMENT  
 Approved for public release; distribution unlimited.

|  |  |
|--|--|
| 11. SUPPLEMENTARY NOTES<br>TECH, OTHER | 12. SPONSORING MILITARY ACTIVITY<br>AFOSR/NPG<br>1400 Wilson Blvd<br>Arlington, VA 22209 |
|--|--|

13. ABSTRACT

An automatic spectral-fitting procedure based on a simple least-squares error criterion is devised for determining the source parameters of earthquakes from surface wave data. When this procedure is supplemented by the complex cepstrum technique for removing the spectral modulations due to multipath interference, results are significantly improved. Rayleigh and Love wave spectral data recorded by the VLPE network and the NORSAR long-period array for fifty-one earthquakes in the Eurasian continent are processed by this procedure. The results are discussed on a regional basis. It is found that the surface wave spectral characteristics may vary even among earthquakes located in essentially the same epicentral region. However, the variations are not random but follow certain distinct patterns. With proper data coverage the focal depths of relatively small earthquakes can be estimated within a 20-km range by employing jointly the automatic spectral-fitting procedure and the complex cepstrum technique.

I



---

UTILITY OF TSAI'S METHOD FOR SEISMIC DISCRIMINATION  
FINAL TECHNICAL REPORT

Prepared by

Yi-Ben Tsai and Wen-Wu Shen  
Area Code 703, 836-3882 Ext. 305

T. W. Harley, Program Manager  
Area Code 703, 836-3882 Ext. 300

TEXAS INSTRUMENTS INCORPORATED  
Services Group  
Post Office Box 5621  
Dallas, Texas 75222

Contract No. F44620-71-C-0112  
Amount of Contract: \$47,967  
Beginning 1 July 1971  
Ending 30 September 1972

Prepared for  
AIR FORCE OFFICE OF SCIENTIFIC RESEARCH

Sponsored by  
ADVANCED RESEARCH PROJECTS AGENCY  
Nuclear Monitoring Research Office  
ARPA Order No. 1827  
ARPA Program Code No. 1F10

30 November 1972

Acknowledgement: This research was supported by the Advanced Research Projects Agency, Nuclear Monitoring Research Office, under Project VELA-UNIFORM, and accomplished under the direction of the Air Force Office of Scientific Research under Contract No. F44620-71-C-0112.

## ABSTRACT

An automatic spectral-fitting procedure based on a simple least-squares error criterion is devised for determining the source parameters of earthquakes from surface wave data. When this procedure is supplemented by the complex cepstrum technique for removing the spectral modulations due to multipath interference, results are significantly improved. Rayleigh and Love wave spectral data recorded by the VLPE network and the NORSAR long-period array for fifty-one earthquakes in the Eurasian continent are processed by this procedure. The results are discussed on a regional basis. It is found that the surface wave spectral characteristics may vary even among earthquakes located in essentially the same epicentral region. However, the variations are not random but follow certain distinct patterns. With proper data coverage the focal depths of relatively small earthquakes can be estimated within a 20-km range by employing jointly the automatic spectral-fitting procedure and the complex cepstrum technique.

## TABLE OF CONTENTS

| SECTION | TITLE  | PAGE   |
|---------|--|--------|
|         | ABSTRACT   | iii    |
| I.      | INTRODUCTION   | I-1    |
| II.     | AN AUTOMATIC SPECTRAL-FITTING<br>PROCEDURE FOR DETERMINING EARTH-<br>QUAKE SOURCE PARAMETERS AND FOCAL<br>DEPTH FROM SURFACE WAVES | II-1   |
| III.    | DATA PRESENTATION BY REGION  | III-1  |
|         | A. OUTLINE OF PRESENTATION   | III-1  |
|         | B. EARTHQUAKES IN ITALY  | III-3  |
|         | C. EARTHQUAKES IN GREECE   | III-7  |
|         | D. EARTHQUAKES IN TURKEY   | III-15 |
|         | E. EARTHQUAKES IN THE CAUCASUS   | III-20 |
|         | F. EARTHQUAKES IN IRAN   | III-20 |
|         | G. EARTHQUAKES IN TADZHIK  | III-26 |
|         | H. EARTHQUAKES IN SINKIANG, CHINA  | III-32 |
|         | I. EARTHQUAKES IN TIBET, CHINA   | III-44 |
|         | J. EARTHQUAKES IN NORTHEASTERN<br>ASIA.  | III-49 |
| IV.     | EVALUATION OF THE AUTOMATIC INTER-<br>PRETATION PROCEDURE FOR SURFACE<br>WAVE SPECTRA  | IV-1   |
|         | A. DATA AVAILABILITY FOR THE<br>PRESENT PROCEDURE  | IV-1   |
|         | B. EFFECTS OF THE COMPLEX CEP-<br>STRUM TECHNIQUE ON THE ESTIMATES<br>OF EARTHQUAKE SOURCE PARAMETERS                              | IV-3   |

TABLE OF CONTENTS  
(continued)

| SECTION | TITLE                                    | PAGE  |
|---------|--|-------|
|         | C. EFFECTS OF ATTENUATION<br>CORRECTIONS | IV-3  |
|         | D. MULTIPLE-SITE SPECTRAL<br>FITTING     | IV-10 |
|         | E. ESTIMATION OF SEISMIC<br>MOMENT       | IV-18 |
| V.      | CONCLUSIONS AND DISCUSSIONS              | V-1   |
| VI.     | REFERENCES                               | VI-1  |

## LIST OF FIGURES

| FIGURE | TITLE   | PAGE  |
|--------|---|-------|
| II-1   | LR AND LQ SPECTRA FOR EVENTS<br>17 AND 18 (NORSAR)  | II-8  |
| II-2   | ERROR COUNT VERSUS ESTIMATED<br>FOCAL DEPTH FOR EVENT 17  | II-10 |
| II-3   | ERROR COUNT VERSUS ESTIMATED<br>FOCAL DEPTH FOR EVENT 18  | II-11 |
| II-4   | LR AND LQ SPECTRA FOR EVENTS<br>19 AND 20 (KON)   | II-14 |
| II-5   | ERROR COUNT VERSUS ESTIMATED<br>FOCAL DEPTH FOR EVENT 19  | II-16 |
| II-6   | ERROR COUNT VERSUS ESTIMATED<br>FOCAL DEPTH FOR EVENT 20  | II-17 |
| II-7   | LR AND LQ SPECTRA FOR EVENTS<br>21 (KON) AND 22 (NORSAR)  | II-18 |
| II-8   | ERROR COUNT VERSUS ESTIMATED<br>FOCAL DEPTH FOR EVENT 21  | II-19 |
| II-9   | ERROR COUNT VERSUS ESTIMATED<br>FOCAL DEPTH FOR EVENT 22  | II-20 |
| III-1  | FIFTY-ONE EARTHQUAKES IN NINE<br>REGIONS STUDIED IN THIS REPORT   | III-2 |
| III-2  | LR AND LQ SPECTRA FOR EVENTS<br>1 AND 2 (KON) AND THE CORRESPOND-<br>ING DISTRIBUTIONS OF ESTIMATED<br>FOCAL DEPTH    | III-6 |
| III-3  | LR AND LQ SPECTRA FOR EVENT 3<br>(KON, OGD, TLO) AND THE CORRES-<br>PONDING DISTRIBUTION OF ESTIMATED<br>FOCAL DEPTHS | III-8 |
| III-4  | LR AND LQ SPECTRA FOR EVENTS 4<br>AND 6 (KON) AND THE CORRESPONDING<br>DISTRIBUTION OF ESTIMATED FOCAL<br>DEPTHS      | III-9 |

LIST OF FIGURES  
(continued)

| FIGURE | TITLE   | PAGE   |
|--------|---|--------|
| III-5  | LR AND LQ SPECTRA FOR EVENT 5 (KON) AND THE CORRESPONDING DISTRIBUTION OF ESTIMATED FOCAL DEPTHS                        | III-10 |
| III-6  | LR AND LQ SPECTRA FOR EVENTS 7 AND 8 (NORSAR) AND THE CORRESPONDING DISTRIBUTION OF ESTIMATED FOCAL DEPTHS              | III-13 |
| III-7  | LR AND LQ SPECTRA FOR EVENTS 9 AND 10 (NORSAR) AND THE CORRESPONDING DISTRIBUTION OF ESTIMATED FOCAL DEPTHS             | III-14 |
| III-8  | LR AND LQ SPECTRA FOR EVENTS 11 AND 12 (NORSAR) AND THE CORRESPONDING DISTRIBUTION OF ESTIMATED FOCAL DEPTHS            | III-18 |
| III-9  | LR AND LQ SPECTRA FOR EVENT 13 (KON) AND THE CORRESPONDING DISTRIBUTION OF ESTIMATED FOCAL DEPTHS                       | III-19 |
| III-10 | LR AND LQ SPECTRA FOR EVENT 14 (KON, TLO) AND THE CORRESPONDING DISTRIBUTION OF ESTIMATED FOCAL DEPTHS                  | III-21 |
| III-11 | LR AND LQ SPECTRA FOR EVENTS 15 AND 16 (NORSAR) AND THE CORRESPONDING DISTRIBUTION OF ESTIMATED FOCAL DEPTHS            | III-22 |
| III-12 | LR AND LQ SPECTRA FOR EVENT 23 (NORSAR) AND EVENT 24 (KON) AND THE CORRESPONDING DISTRIBUTION OF ESTIMATED FOCAL DEPTHS | III-25 |
| III-13 | LR AND LQ SPECTRA FOR EVENT 25 (KON, CHG) AND THE CORRESPONDING DISTRIBUTION OF ESTIMATED FOCAL DEPTHS                  | III-27 |

LIST OF FIGURES  
(continued)

| FIGURE | TITLE  | PAGE   |
|--------|--|--------|
| III-14 | LR AND LQ SPECTRA FOR EVENTS 26 AND 27 (KON) AND THE CORRESPONDING DISTRIBUTION OF ESTIMATED FOCAL DEPTHS    | III-28 |
| III-15 | LR AND LQ SPECTRA FOR EVENT 28 (KON) AND THE CORRESPONDING DISTRIBUTION OF ESTIMATED FOCAL DEPTHS            | III-29 |
| III-16 | LR AND LQ SPECTRA FOR EVENTS 29 AND 30 (NORSAR) AND THE CORRESPONDING DISTRIBUTION OF ESTIMATED FOCAL DEPTHS | III-33 |
| III-17 | LR AND LQ SPECTRA FOR EVENT 31 (NORSAR) AND THE CORRESPONDING DISTRIBUTION OF ESTIMATED FOCAL DEPTHS         | III-34 |
| III-18 | LR AND LQ SPECTRA FOR EVENTS 32 AND 33 (NORSAR) AND THE CORRESPONDING DISTRIBUTION OF ESTIMATED FOCAL DEPTHS | III-35 |
| III-19 | LR AND LQ SPECTRA FOR EVENTS 34 AND 35 (NORSAR) AND THE CORRESPONDING DISTRIBUTION OF ESTIMATED FOCAL DEPTHS | III-39 |
| III-20 | LR AND LQ SPECTRA FOR EVENTS 36 AND 37 (NORSAR) AND THE CORRESPONDING DISTRIBUTION OF ESTIMATED FOCAL DEPTHS | III-40 |
| III-21 | LR AND LQ SPECTRA FOR EVENTS 38 AND 39 (NORSAR) AND THE CORRESPONDING DISTRIBUTION OF ESTIMATED FOCAL DEPTHS | III-41 |
| III-22 | LR AND LQ SPECTRA FOR EVENTS 40 AND 41 (NORSAR) AND THE CORRESPONDING DISTRIBUTION OF ESTIMATED FOCAL DEPTHS | III-42 |

LIST OF FIGURES  
(continued)

| FIGURE | TITLE  | PAGE   |
|--------|--|--------|
| III-23 | LR AND LQ SPECTRA FOR EVENTS 42 AND 43 (NORSAR) AND THE CORRESPONDING DISTRIBUTION OF ESTIMATED FOCAL DEPTHS | III-43 |
| III-24 | LR AND LQ SPECTRA FOR EVENTS 44 AND 45 (NORSAR) AND THE CORRESPONDING DISTRIBUTION OF ESTIMATED FOCAL DEPTHS | III-47 |
| III-25 | LR AND LQ SPECTRA FOR EVENTS 46 AND 47 (NORSAR) AND THE CORRESPONDING DISTRIBUTION OF ESTIMATED FOCAL DEPTHS | III-48 |
| III-26 | LR AND LQ SPECTRA FOR EVENT 48 (NORSAR) AND THE CORRESPONDING DISTRIBUTION OF ESTIMATED FOCAL DEPTHS         | III-50 |
| III-27 | LR AND LQ SPECTRA FOR EVENT 49 (NORSAR) AND THE CORRESPONDING DISTRIBUTION OF ESTIMATED FOCAL DEPTHS         | III-53 |
| III-28 | LR AND LQ SPECTRA FOR EVENTS 50 AND 51 (NORSAR) AND THE CORRESPONDING DISTRIBUTION OF ESTIMATED FOCAL DEPTHS | III-54 |
| IV-1   | LR ATTENUATION COEFFICIENT CURVES MEASURED BY THE PRESENT STUDY AND BY TRYGGVASSON (1965)                    | IV-8   |
| IV-2   | COMPARISON OF SPECTRAL FITTINGS FOR EVENT 3 AMONG VARIOUS SITE COMBINATIONS                                  | IV-11  |
| IV-3   | COMPARISON OF SPECTRAL FITTINGS FOR EVENT 21 AMONG VARIOUS SITE COMBINATIONS                                 | IV-15  |

LIST OF FIGURES  
(continued)

| FIGURE | TITLE   | PAGE  |
|--------|---|-------|
| IV-4   | COMPARISON OF SPECTRAL FITTINGS<br>FOR EVENT 21 AMONG VARIOUS SITE<br>COMBINATIONS            | IV-16 |
| IV-5   | THE OBSERVED AND THEORETICAL<br>RELATIONSHIPS OF SEISMIC MOMENT<br>VERSUS THE $m_b$ MAGNITUDE | IV-19 |

## LIST OF TABLES

| TABLE  | TITLE  | PAGE   |
|--------|--|--------|
| II-1   | PDE INFORMATION FOR EARTHQUAKE -<br>EVENTS IN CAUCASUS                                   | II-7   |
| II-2   | THEORETICAL SOLUTION OF SOURCE<br>MECHANISM FOR EARTHQUAKE -<br>EVENTS IN CAUCASUS       | II-13  |
| III-1  | PDE INFORMATION FOR EVENTS IN<br>ITALY   | III-4  |
| III-2  | THEORETICAL SOLUTION OF SOURCE<br>MECHANISM FOR EVENTS IN ITALY                          | III-5  |
| III-3  | PDE INFORMATION FOR EVENTS IN<br>GREECE  | III-11 |
| III-4  | THEORETICAL SOLUTION OF SOURCE<br>MECHANISM FOR EVENTS IN GREECE                         | III-12 |
| III-5  | PDE INFORMATION FOR EVENTS IN<br>TURKEY  | III-16 |
| III-6  | THEORETICAL SOLUTION OF SOURCE<br>MECHANISM FOR EVENTS IN TURKEY                         | III-17 |
| III-7  | PDE INFORMATION FOR EARTHQUAKE -<br>EVENTS IN IRAN                                       | III-23 |
| III-8  | THEORETICAL SOLUTION OF SOURCE<br>MECHANISM FOR EARTHQUAKE -EVENTS<br>IN IRAN            | III-24 |
| III-9  | PDE INFORMATION FOR EVENTS IN<br>TADZHIK   | III-30 |
| III-10 | THEORETICAL SOLUTION OF SOURCE<br>MECHANISM FOR EARTHQUAKE -EVENTS<br>IN TADZHIK         | III-31 |
| III-11 | PDE INFORMATION FOR EARTHQUAKE -<br>EVENTS IN SINKIANG, CHINA                            | III-36 |
| III-12 | THEORETICAL SOLUTION OF SOURCE<br>MECHANISM FOR EARTHQUAKE -EVENTS<br>IN SINKIANG, CHINA | III-37 |
| III-13 | PDE INFORMATION FOR EARTHQUAKE -<br>EVENTS IN TIBET, CHINA                               | III-45 |

LIST OF TABLES  
(continued)

| TABLE  | TITLE   | PAGE   |
|--------|---|--------|
| III-14 | THEORETICAL SOLUTION OF SOURCE MECHANISM FOR EARTHQUAKE-EVENTS IN TIBET, CHINA                                | III-46 |
| III-15 | PDE INFORMATION FOR EARTHQUAKE-EVENTS IN NORTHEASTERN ASIA  | III-51 |
| III-16 | THEORETICAL SOLUTION OF SOURCE MECHANISM FOR EARTHQUAKES IN NORTHEASTERN ASIA                                 | III-52 |
| IV-1   | BODY-WAVE MAGNITUDE VS. DISTANCES FROM THE VLPE DATA  | IV-2   |
| IV-2   | COMPARISON OF RESOLUTION ERROR BETWEEN THE VLPE DATA (CEPSTRUM APPLIED) AND NORSAR DATA (NO CEPSTRUM APPLIED) | IV-4   |
| IV-3   | EVENTS USED FOR ATTENUATION MEASUREMENTS (FROM PDE BULLETIN)  | IV-6   |
| IV-4   | TEST OF SOLUTIONS FOR SOURCE MECHANISM DUE TO VARIOUS ATTENUATION COEFFICIENTS                                | IV-9   |
| IV-5   | COMPARISON OF MULTI-SITES AND SINGLE-SITE SOLUTION FOR EVENT LX/CITLY/134                                     | IV-13  |
| IV-6   | COMPARISON OF MULTI-SITES AND SINGLE-SITE SOLUTIONS FOR EVENT LX/CAUCA/724                                    | IV-17  |

## SECTION I

### INTRODUCTION

It has been shown that the amplitude spectra of surface waves observed at a few sites can be used to give reasonable focal depth estimates for earthquakes whose source mechanisms are known (Tsai and Aki, 1970a, b; Mendiguren, 1971; Canitez and Toksoz, 1972). Some people have voiced serious doubts about the validity of this approach (e. g., McGarr, 1972). Thus, a thorough evaluation of the method using a large ensemble of earthquake data has been undertaken in the past fifteen months. The results are presented in this report.

Because of our primary concern for adapting the method for small magnitude earthquakes, we have to start with the assumption that (1) no prior knowledge about an earthquake source mechanism will be available, and (2) for a given earthquake reliable surface wave spectral data will be available only at a small number of sites. The first condition requires that, besides focal depth, other source parameters such as dip angle, slip angle, strike direction and the seismic moment all have to be treated as unknown variables. The second condition rules out the more familiar approach of using radiation patterns of individual frequencies for which a good azimuthal coverage is essential. As an alternative, simultaneous usage of Rayleigh and Love wave amplitude spectra over the frequency band from 0.02 to 0.05 Hz will be made. A method which takes into account the conditions mentioned above is devised by using a least-squares error criterion. A detailed description of the method is given in Section II.

Preliminary tests of the method on a small number of earthquakes were carried out and the results, as previously presented in the first

semi-annual report (Tsai, 1972a), were promising enough to suggest further evaluations of the method. Since then, we have embarked on an effort to apply the method for determining the source parameters and focal depths of a large number of earthquakes, fifty-one in total, located in the Eurasian continent. In order to study the spectral characteristics of surface-waves on a regional basis, we have classified these events into nine groups according to their epicentral locations. The results are presented in Section III.

Remembering that our method employs the theoretical spectra of Love and Rayleigh waves calculated from a layered half space of non-dissipating elastic medium to compare with their observed counterparts, it becomes necessary to make corrections for attenuation due to anelasticity and to remove the spectral modulations due to interference of multipath arrivals from the observed spectra before comparisons can be made. For the attenuation corrections we shall use smooth curves for attenuation coefficients. Unfortunately, these curves are not well determined for the frequency band concerned, namely from 0.02 to 0.05 Hz, especially for the Eurasian continent. We have obtained an attenuation coefficient curve by using Rayleigh waves recorded at Chiang Mai, Thailand (CHG) and Toldeo, Spain (TLO) from six earthquakes in the Moluccas-New Guinea area. The curve is subsequently applied to all our data. Since the propagation path between CHG and TLO is far from typical of most continental paths with which we are concerned, we have made a comparative study of the estimates of source parameters and focal depths using different curves of attenuation coefficients. The results are discussed in Section IV. As for the removal of the spectral modulations due to interference of multipath arrivals, it has been demonstrated in our earlier report (Tsai, 1972a) that the complex cepstrum technique is highly suitable for this purpose. We have applied this technique to some of our data. A comparison is made between the outcomes obtained with and without use of the complex cepstrum technique and is presented in Section IV.

The method is designed to handle surface wave spectral data at one or more sites. Limited by the availability of data at the time when this study was conducted, all except two of the fifty-one earthquakes have single-site coverage. The remaining two have data available at three sites. Thus, it is possible to make a very preliminary investigation on outcomes of multiple-site coverage as compared with single-site coverage. The results are discussed in the last part of Section IV.

Finally, Section V gives a summary of the results gained to date. We shall also venture to draw some conclusions from what is accomplished with regard to the performance of the method employed for the surface wave spectral analysis.

SECTION II

AN AUTOMATIC SPECTRAL-FITTING PROCEDURE FOR  
DETERMINING EARTHQUAKE SOURCE PARAMETERS  
AND FOCAL DEPTH FROM SURFACE WAVES

We shall attempt to determine the earthquake source parameters and focal depth from the amplitude spectra of surface waves obtained at a limited number of recording sites. This approach is particularly suitable for earthquakes of relatively small magnitudes whose source parameters and focal depths are otherwise difficult to determine. In terms of data utility the method about to be described is designed to take advantages of the increasing availability of digital seismograms furnished by the long-period array stations, such as NORSAR and ALPA, and by the newly installed VLPE Network. Since the method makes use of the theoretical surface wave spectra as its core element, we shall start with a brief discussion on these theoretical spectra.

The earthquake source is represented by a double couple which varies as a step function in time. The strength of the double couple is called seismic moment and designated as  $M$ . The Fourier spectra of Love and Rayleigh waves due to a point source of this kind buried in a layered half-space can be expressed in terms of normal mode solutions for respective wave types (Haskell, 1964; Harkrider, 1964; Ben-Menahem and Harkrider, 1964; and Saito, 1967). We shall follow Saito's formulation in the present study. The lengthy expressions for computing the theoretical surface wave spectra due to this particular case of source representation can be found elsewhere (Tsai and Aki, 1970), and so will not be given here. It is sufficient to say that the spectral values of Love and Rayleigh waves of a given frequency depend on a total of six parameters. Two of the six parameters, namely the dip angle  $\delta$

and the slip angle  $\lambda$ , specify the orientation of the double couple. The third source parameter is the seismic moment  $M$  which represents the strength of the double couple. The fourth parameter  $h$  indicates the depth at which the equivalent point source of the earthquake dislocation is located in the layered half-space. The remaining two parameters  $r$  and  $\theta$ , specify the cylindrical coordinates of the observation point with respect to the epicenter.  $\theta$  is azimuth angle measured counterclockwise from the strike direction  $\phi$  of the dislocation plane. Because the distance parameter  $r$  appears only in the geometrical spreading factor as  $r^{-1/2}$  and in the attenuation factor as  $e^{-nr}$  which are independent of the source characteristics, it can be conveniently handled by specifying a constant value, say 2000 km, for it in computing all the theoretical spectra. In the meantime observations made at distances other than the specified one would have to be equalized by making proper corrections for the geometrical spreading and attenuation. Thus, there remain five parameters to be determined: the seismic moment  $M$ , the dip angle  $\delta$ , the slip angle  $\lambda$ , the strike direction  $\phi$ , and finally the focal depth  $h$ . One common approach to this problem is to study the radiation patterns of Love and Rayleigh waves formed by spectral amplitudes of a single frequency observed at a multitude of azimuths. In this case a good azimuthal coverage of recording sites is essential. Unfortunately, for earthquakes of relatively small magnitudes which are our main concern, it will be extremely difficult, if not impossible, to have enough azimuthal coverage to yield meaningful radiation patterns. Hence, this approach is not suitable for our purpose. As an alternative, we shall adopt a spectral approach which makes use of the spectral shapes of both Love and Rayleigh waves formed by individual spectral moduli of a number of successive frequencies within a given frequency band, say from 0.02 to 0.05 Hz. In this case we can take maximum advantage of those good-quality spectral data available at only a small number of recording sites.

If the fault plane solution is available for an earthquake from observations of the first motions of body waves, it is possible to determine

three of the remaining five parameters, namely,  $\delta$ ,  $\lambda$  and  $\phi$ . Like using surface wave radiation patterns, this approach is practical only if there is enough coverage of recording sites. Our primary concern with relatively small earthquakes again imposes a severe limit on this possibility. Consequently, we shall proceed on the assumption that no prior knowledge on  $\delta$ ,  $\lambda$  and  $\phi$  will be available. In other words, all the five parameters, i. e.,  $\delta$ ,  $\lambda$ ,  $\phi$ ,  $h$  and  $M$  will be treated as unknowns in our approach toward interpreting the surface wave spectra. A detailed description of our method follows.

The amplitude spectra of Rayleigh and Love waves from an earthquake are obtained by using the fast Fourier transform technique. If necessary, the complex cepstrum technique is applied to remove the spectral modulations caused by multipath interference. For a detailed discussion of this technique the readers are referred to one of our previous reports (Tsai, 1972a). A sample rate of one sample per six seconds is adopted by decimating the original time traces which use a sample rate of one sample per two seconds. Prior to transforming, a time trace of any length is filled with additional zeros at its end to make up 2048 time points. This results in 1025 spectral points at frequencies ranging from zero Hz to the folding frequency at  $(1/12)$  Hz. with a fixed frequency increment of  $(1/6 \times 2048)$  Hz. For the present study we shall focus our attention on the spectral behavior in the frequency band between 0.02 and 0.05 Hz which is dictated largely by the instrumental response of the long-period seismographs in operation. This is done by selecting twelve evenly-spaced frequencies ranging from  $(40/2048)$  Hz to  $(106/2048)$  Hz. The spectral values at these frequencies are first corrected for the instrumental response, the geometrical spreading and attenuation, and then compared with their theoretical counterparts to yield estimates on the five earthquake source parameters. A simple least-squares error criterion is adopted for judging the goodness of fit between the observed spectral curves of Love and Rayleigh waves defined at the twelve discrete frequencies and their theoretical counter-

parts computed for a given set of source parameters. The curve-fitting procedure is described below.

Let  $X_{ij}^R$  and  $X_{ij}^L$  denote the observed Rayleigh and Love wave spectral amplitudes, respectively, for  $i^{\text{th}}$  frequency and at  $j^{\text{th}}$  site.  $Y_{ij}^R$  and  $Y_{ij}^L$  denote the corresponding theoretical spectra for a seismic moment of one dyne-cm. The sum of the squares of residuals  $\epsilon$  is defined as:

$$\epsilon = \sum_j \sum_i \left[ (X_{ij}^R - MY_{ij}^R)^2 + (X_{ij}^L - MY_{ij}^L)^2 \right] \quad (1)$$

where  $M$  represents the seismic moment of the earthquake source. For a given set of  $Y_{ij}^R$  and  $Y_{ij}^L$  which are functions of the four source parameters ( $\delta, \lambda, \phi$  and  $h$ ), the error count is minimized by finding the seismic moment  $M$  according to the following equation.

$$M = \frac{\sum_j \sum_i \left[ X_{ij}^R Y_{ij}^R + X_{ij}^L Y_{ij}^L \right]}{\sum_j \sum_i \left[ Y_{ij}^R Y_{ij}^R + Y_{ij}^L Y_{ij}^L \right]} \quad (2)$$

In other words, for a given combination of  $\delta, \lambda, \phi$  and  $h$ , we first find the optimum seismic moment  $M$  from equation (2). This is followed by inserting the resultant  $M$  value in equation (1) to compute the minimum error count for this particular set of source parameters. We then proceed to vary the four source parameters,  $\delta, \lambda, \phi$  and  $h$ , in a systematic manner so as to cover a wide range of source mechanisms and focal depth. In the mean time the error count  $\epsilon$  is used as a convenient criterion for judging the goodness of fit between the observed and the theoretical surface wave spectra among various sets of source parameters. In the end we shall take as our final solution the one set of source parameters whose theoretical surface wave spectra fit most closely with their observed counterparts. To the extent that the prescribed layered earth model provides an adequate approximation of the real world, this method can be expected to provide reasonable estimates of the earthquake

source parameters on a routine basis from the long-period digital seismograms. Preliminary tests on the method were conducted during the early part of this project and the results, as described in our previous report (Tsai, 1972a), are quite encouraging. Since then, we have undertaken a more thorough evaluation of the method by applying it to the surface wave spectral data of a large ensemble of fifty-one earthquakes taking place during 1971-1972 in the Eurasian continent. The results are presented in Section III. Before looking into the outcome of individual cases, it should help at this point to provide an outline of the procedure through which the final solution is found. To begin with the range and the increment are specified for each of the four source parameters to be varied as follows:

| <u>Parameters</u>           | <u>Range</u>              | <u>Increment</u> |
|-----------------------------|---------------------------|------------------|
| Dip Angle ( $\delta$ )      | $60^\circ \sim 90^\circ$  | $10^\circ$       |
| Slip Angle ( $\lambda$ )    | $-90^\circ \sim 90^\circ$ | $30^\circ$       |
| Focal depth (h)             | 0 ~ 125 km                | 5 km             |
| Strike direction ( $\phi$ ) | 0 ~ $180^\circ$           | $10^\circ$       |

The strike direction  $\phi$  is measured clockwise from the North direction. In order to cover every one of the specified cases, the four parameters are varied in sequence. For a given source mechanism defined by the first two parameters,  $\delta$  and  $\lambda$ , the focal depth  $h$  is increased from 0 km to 125 km by a fixed increment of 5 km. For each focal depth, the strike direction  $\phi$  is varied from  $0^\circ$  to  $180^\circ$  in even increments of  $10^\circ$ . At each combination of  $\delta$ ,  $\lambda$ ,  $h$  and  $\phi$ , the theoretical Love and Rayleigh wave spectral amplitudes are computed at the twelve frequencies mentioned earlier for those azimuths in which the corresponding spectral data are available. Both the theoretical and the observed spectral amplitudes are then inserted into equations 1 and 2 to yield an estimate of  $\epsilon$  and  $M$ , respectively. At each increment of  $\phi$ , if the new error count is smaller than the existing error count, then it will replace the existing one for next comparison. All the source parameters and the

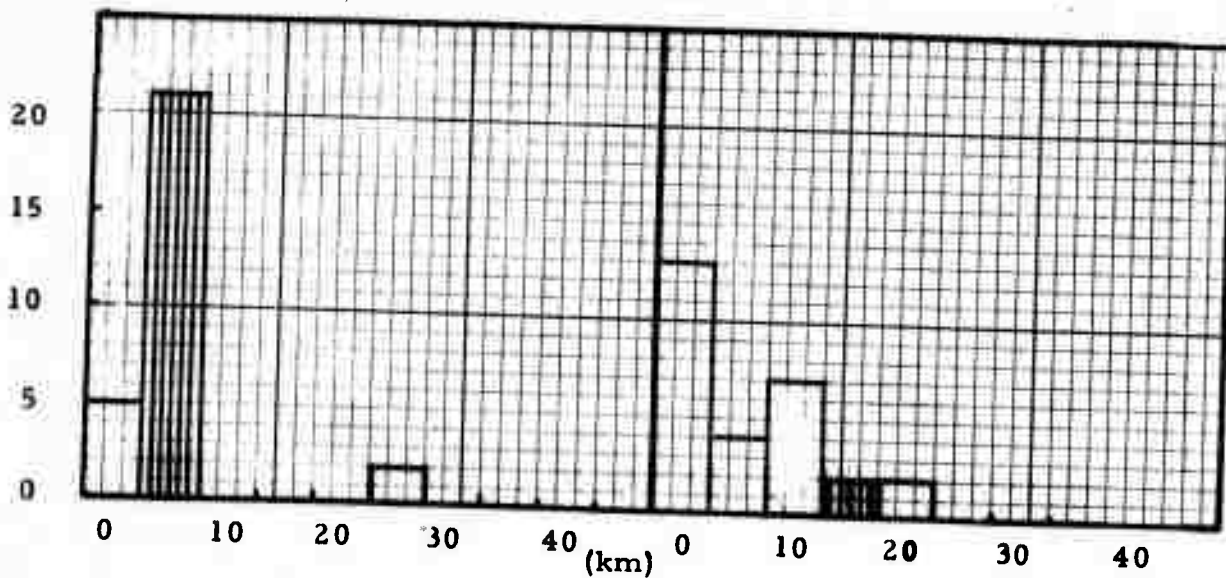
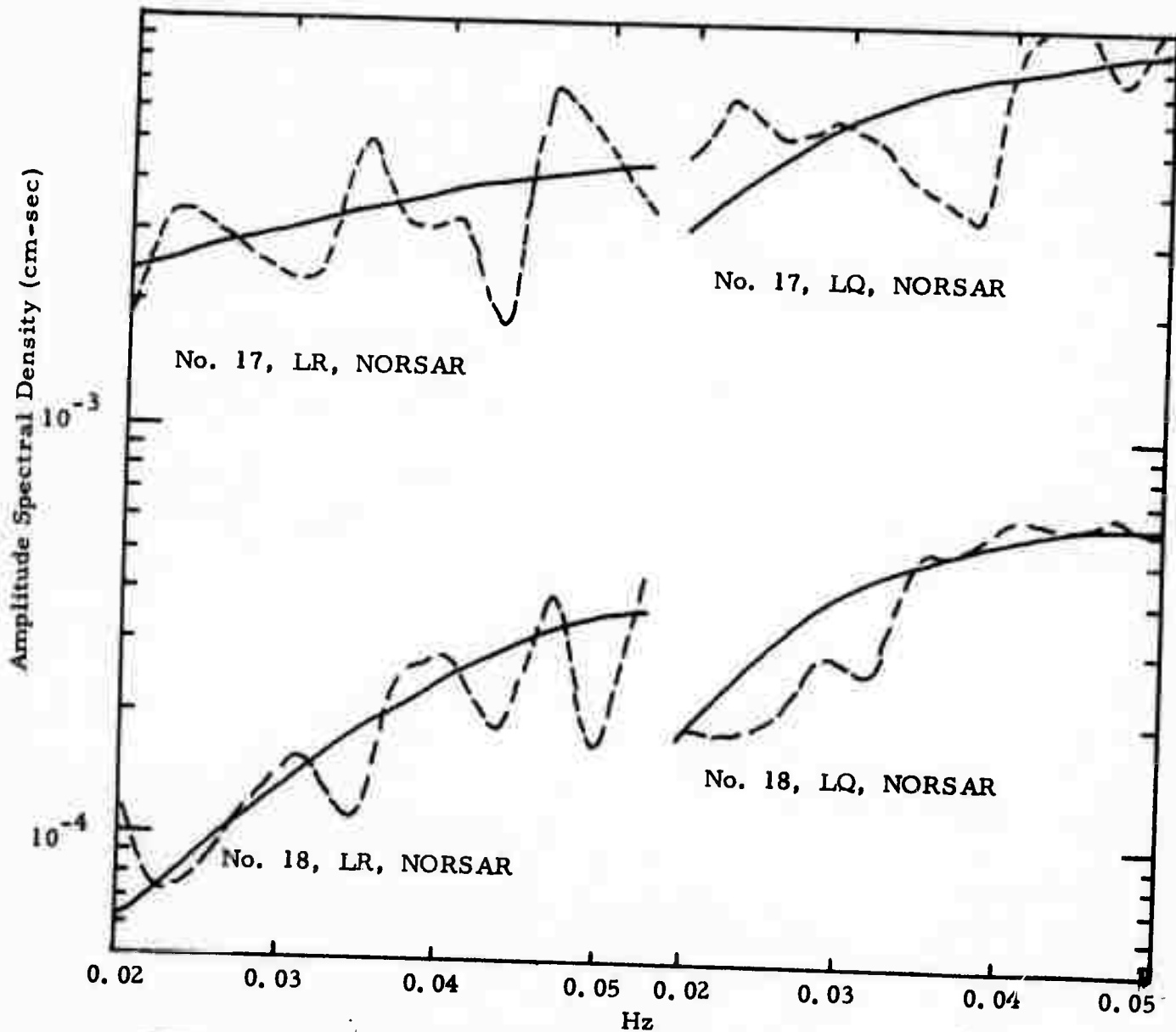
theoretical spectra associated with this new error count are also carried over until the next replacement by an even smaller error count takes place. In this way, we arrive at the optimum strike direction  $\phi$  for this particular source mechanism at a particular focal depth. This same procedure is applied throughout all of the specified focal depths. At the end we find a focal depth with the "best-fit" theoretical surface wave spectra. For every combination of  $\delta$  and  $\lambda$  we keep this optimum focal depth together with the error count  $\epsilon$ , the strike direction  $\phi$ , the seismic moment  $M$  and the theoretical surface wave spectra. There are a total of twenty-eight cases of source mechanism tested for each earthquake. We shall look into the distribution of the corresponding twenty-eight best estimates of focal depth. By so doing we hope to establish a probable range of focal depth for an earthquake regardless of its source mechanism because knowledge of focal depth of an earthquake can be very useful for seismic discrimination purposes.

Following the general description of the method given in the preceding paragraphs, it is appropriate at this point to look into the outcome of actual application of this method to a few earthquakes. For this purpose we choose six earthquakes that occurred in the Caucasus region during 1971-1972 for which surface wave spectral data are available. The PDE information for these events is listed in Table II-1. It is interesting to note that the magnitudes of these events, ranging from  $m_b = 4.0$  to  $m_b = 5.1$ , are relatively small. Data are available for three events with code names starting with 'LX' at KON, a VLPE station at Kongsberg, Norway. Data are also available at the NORSAR long-period array, located in Norway, for the other three events with their code name ending with 'NL'. The complex cepstrum technique has been applied to the first group of data at KON, but not for the second group at NORSAR. Following is an examination of the results of the individual events.

Figure II-1 shows the results for Events No. 17 and 18 which are code named as TRS/251/22NL and CAU/283/09NL, respectively. Event

TABLE II-1  
PDE INFORMATION FOR EARTHQUAKE-EVENTS IN CAUCASUS

| I. D. No. | Event Name   | Date     | Time     | Location |           | Focal Depth | $m_b$ | Data Site |
|-----------|--------------|----------|----------|----------|-----------|-------------|-------|-----------|
|           |              |          |          | Latitude | Longitude |             |       |           |
| 17        | TRS/251/22NL | 09/08/71 | 22.35.16 | 41.1N    | 43.8E     | N           | 4.8   | NORSAR    |
| 18        | CAU/283/09NL | 10/10/71 | 09.06.06 | 43.1N    | 43.8E     | 15          | 4.0   | NORSAR    |
| 19        | LX/CAUCA/688 | 02/09/72 | 11.22.52 | 43.2N    | 46.0E     | 36          | 4.5   | KON       |
| 20        | LX/CAUCA/606 | 12/20/71 | 07.53.11 | 41.2N    | 48.3E     | N           | 4.8   | KON       |
| 21        | LX/CAUCA/724 | 02/03/72 | 02.29.22 | 40.7N    | 48.4E     | 39          | 5.1   | KON       |
| 22        | CAU/288/17NL | 10/15/71 | 17.08.06 | 41.4N    | 48.6E     | N           | 4.9   | NORSAR    |



No. 17 TRS/251/22NL

No. 18 CAU/283/09NL

FIGURE II-1

LR AND LQ SPECTRA FOR EVENTS 17 AND 18 (NORSAR)

No. 17 is located near the Caucasus-Turkey border region. The spectra of Rayleigh and Love waves recorded at NORSAR are shown, respectively in the upper left and upper right of Figure II-1. Both of the observed spectra, as shown in dashed curves, are contaminated by modulations due to multipath interference. The solid curves represent the "best-fit" theoretical spectra which result in a minimum error count  $\epsilon$ . The corresponding focal depth is 5 km. The histogram of focal depth determinations of the twenty-eight cases of source mechanism tested for this earthquake is shown in the lower left of Figure II-1. For all but two cases of source mechanism, the focal depth is set at 0 or 5 km. We should hasten to point out that this high concentration of focal depth estimates in a narrow range does not necessarily mean a high quality of focal depth determination. This can be seen more clearly if we take a look at Figure II-2 in which the error count is plotted against the corresponding focal depth estimate for the twenty-eight cases of source mechanism. In this figure all except four cases have nearly identical values of error count which simply means poor resolution for favoring a particular source mechanism based on the error count criterion. Such phenomenon is to be expected for highly modulated spectral data. Thus, it is important to take into account the quality of spectral data in judging the quality of the "best-fit" solution.

The spectral data obtained at NORSAR for Event No. 18 are shown by the dashed curves in the middle part of Figure II-1, with Rayleigh waves on the left side and Love waves on the right. The corresponding "best-fit" theoretical spectra are given by the solid curves. The histogram of focal depth estimates is shown in the lower right part of Figure II-1. All focal depth estimates in this case is confined in the upper 20 km with the "best-fit" focal depth located at 15 km. The error count is plotted against focal depth in Figure II-3. Judging from the distribution of error counts and the goodness of fit between the observed and theoretical spectra, we are inclined to take 15 km as a reasonably good estimate of the focal depth.



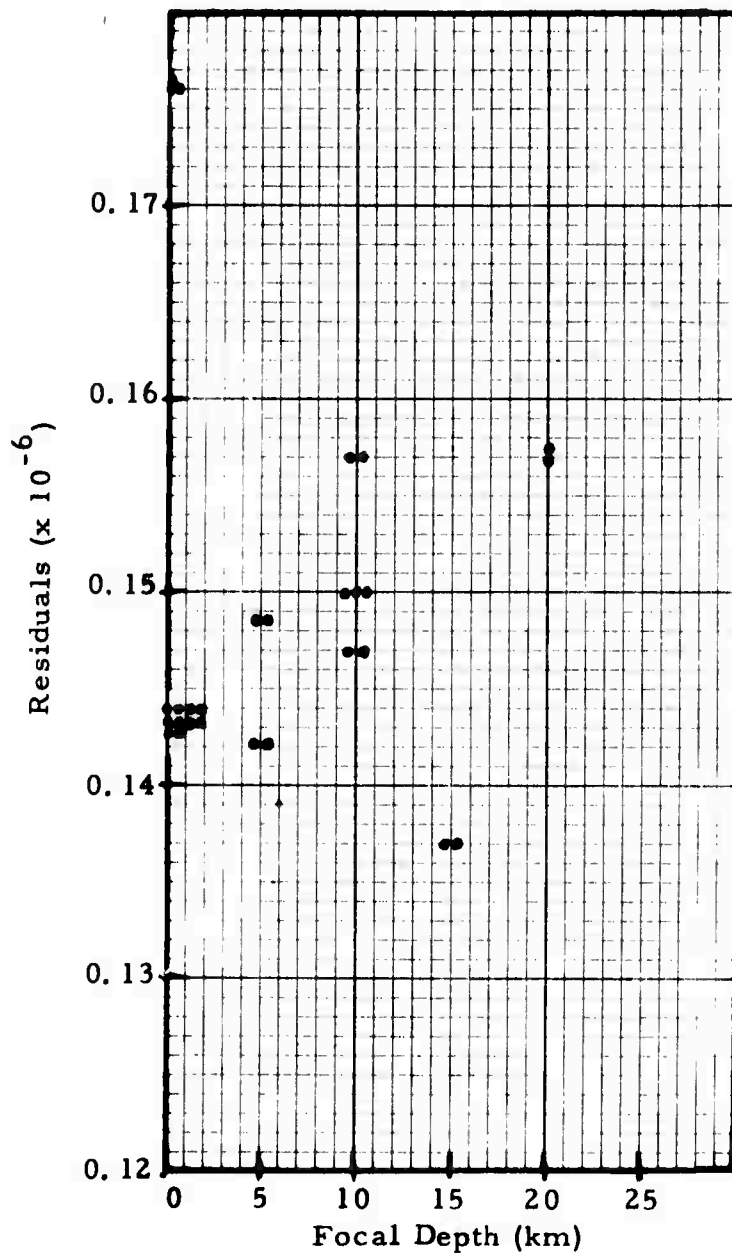


FIGURE II-3

ERROR COUNT VERSUS ESTIMATED FOCAL DEPTH FOR EVENT 18

Other source parameters corresponding to the best-fit spectra for the preceding two earthquakes are listed in Table II-2. According to these parameters Event No. 17 is an oblique-slip dislocation with its strike in N140° E whereas Event No. 18 is a normal dislocation on a vertical plane striking in N30° E. It must be cautioned that these dislocation parameters contain certain ambiguities due to the symmetry conditions of surface wave radiation from a double couple point source. These ambiguities can not be resolved by using surface wave data alone.

The observed spectra of Rayleigh (LR) and Love (LQ) waves at KON from Events No. 19 and 20 are shown by the dashed lines in Figure II-4. As indicated in Table II-1, Event No. 19 is located a few degrees to the Northwest of Event No. 20. These spectra have been processed by the complex cepstrum technique so that they are considerably free of modulations. The spectral behaviors of both LR and LQ waves are somewhat similar. The best-fit theoretical spectra are given by the solid curves in the same figure. The agreement between the observed and theoretical spectra is generally good except for the unsightly presence of theoretical LR spectral notches. It should be emphasized here that the spectral analysis technique for determining the source parameters of an earthquake does not rely solely on the presence of the spectral notches. Instead, the technique really depends more on the general shapes of, and the relative levels between, LR and LQ spectra. The source parameters related to the best-fit theoretical spectra shown in Figure II-4 for both Events No. 19 and 20, as listed in Table II-2, suggest that they are all associated with oblique-slip dislocation; one being 40 km deep, and the other 25 km deep. Realizing that the method being used for the present study can not be expected to yield an exact estimate of focal depth for an earthquake, it is perhaps more instructive to set a probability range for the focal depth than to pinpoint it at a particular value. For this purpose the histograms of twenty-eight focal depth estimates for both Events No. 19 and 20 are shown on Figure II-4. For Event No. 19 the estimated focal depth is confined mostly

TABLE II-2  
THEORETICAL SOLUTION OF SOURCE MECHANISM FOR  
EARTHQUAKE-EVENTS IN CAUCASUS

| I. D. No. | Event Name   | Strike  | Dip Angle | Slip Angle | Focal Depth (km) | Moment $M(x10^{25}$ dyne-cm) |
|-----------|--------------|---------|-----------|------------|------------------|------------------------------|
| 17        | TRS/251/22NL | N 140°E | 60        | -60        | 5                | 0.39x10 <sup>-1</sup>        |
| 18        | CAU/283/09NL | N 30°E  | 90        | 90         | 15               | 0.06x10 <sup>-1</sup>        |
| 19        | LX/CAUCA/688 | N 10°E  | 70        | 30         | 40               | 0.10x10 <sup>-1</sup>        |
| 20        | LX/CAUCA/606 | N 100°E | 60        | -30        | 25               | 0.74x10 <sup>-1</sup>        |
| 21        | LX/CAUCA/724 | N 160°E | 60        | 30         | 45               | 0.28x10 <sup>-1</sup>        |
| 22        | CAU/288/17NL | N 0°E   | 70        | 30         | 55               | 0.19x10 <sup>-1</sup>        |

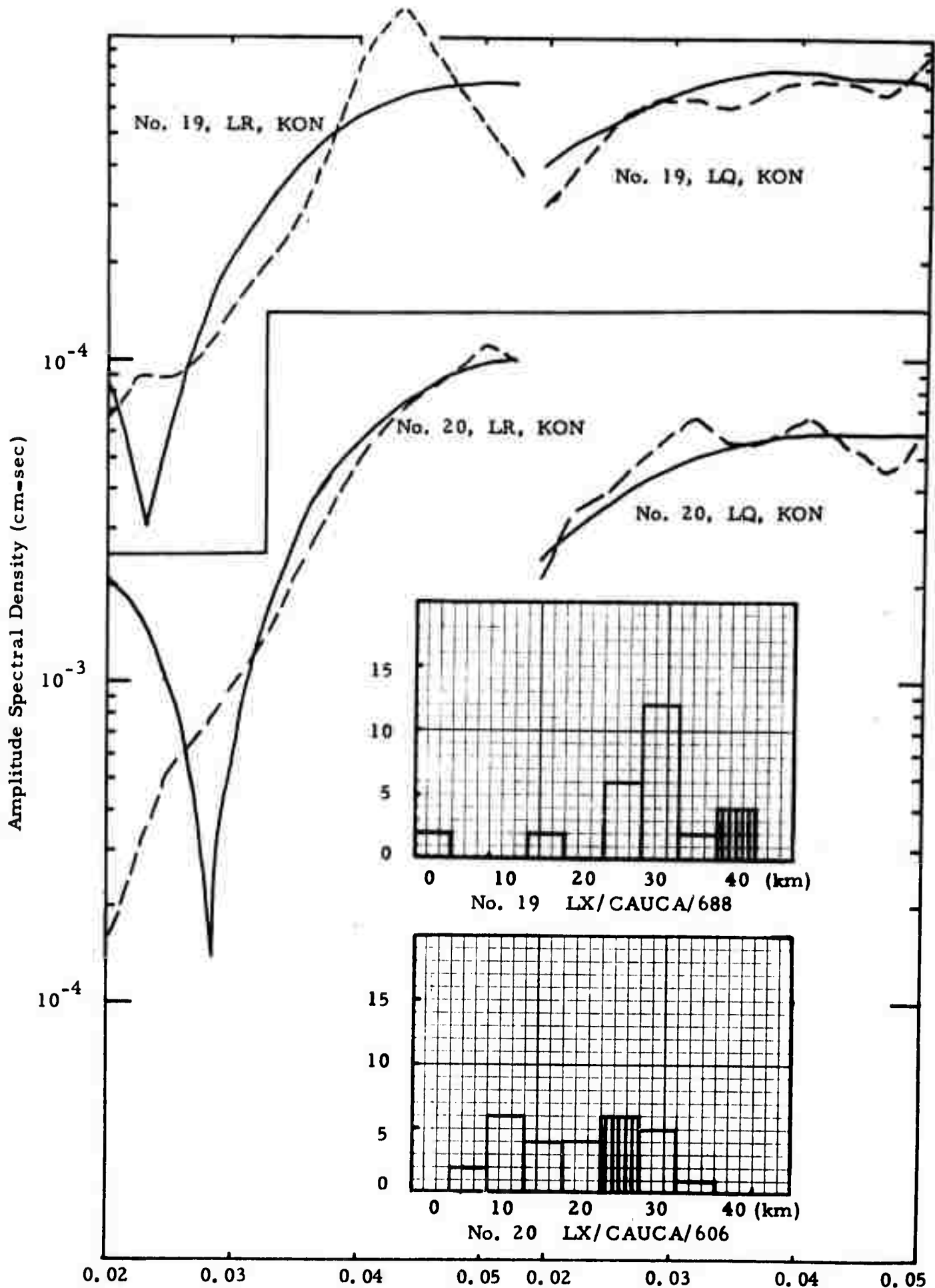


FIGURE II-4  
LR AND LQ SPECTRA FOR EVENTS 19 AND 20 (KON)

between 25 and 40 km. A study of the profile of the corresponding twenty-eight error counts, as shown in Figure II-5, further narrows this range to between 30 and 40 km in which many relatively small error counts take place. As for Event No. 20, the focal depth estimates spread over a rather wide range from 5 to 35 km. Again a glance of the profile of error counts, as shown in Figure II-6, reveals that the most probable focal depth range for this earthquake should be between 15 and 35 km.

The LR and LQ spectra of the last two earthquakes in the Caucasus area listed in Table II-1 as Events No. 21 and 22 are shown in the upper part of Figure II-7. The data for Event No. 21 are obtained by the VLPE instruments located at KON and are processed by the complex cepstrum technique. The data for Event No. 22 are obtained at NORSAR and are not processed with the complex cepstrum technique. A comparison of the spectra between these two events clearly shows the spectral improvement brought about by the complex cepstrum technique. Once again, the solid curves represent the "best-fit" theoretical spectra for which the source parameters are listed in Table II-2. Both events are shown to be related with oblique-slip dislocation ( $\delta = 70^\circ$ ,  $\lambda = 30^\circ$ ). The corresponding focal depth is determined to be 45 km and 55 km, respectively, for Events No. 21 and 22. The distributions of focal depth estimates for the twenty-eight cases of source mechanism for the two events are shown in the lower part of Figure II-7. For Event No. 21 the estimated focal depth ranges from 25 to 50 km. Further examination of the associated error counts shown in Figure II-8 suggests that the most likely value of focal depth for this earthquake lies between 45 and 50 km. With regard to Event No. 22, we find a small range, from 45 to 55 km, of focal depth distribution which is related to poor quality spectral data. The error counts in this case tend to have similar values, as shown in Figure II-9, which in turn makes it difficult to reach a clearcut solution for the source parameters.

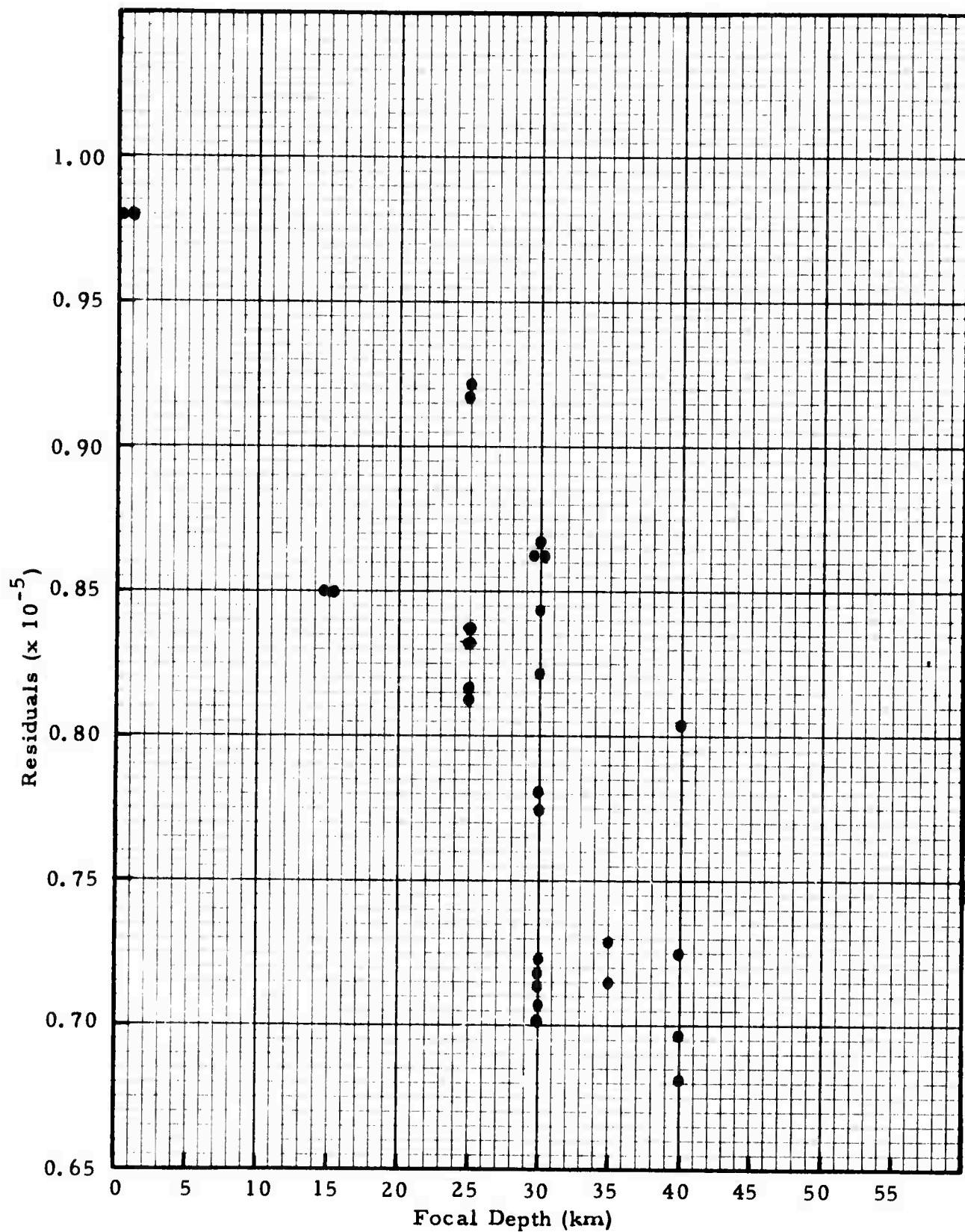


FIGURE II-5

ERROR COUNT VERSUS ESTIMATED FOCAL DEPTH FOR EVENT 19

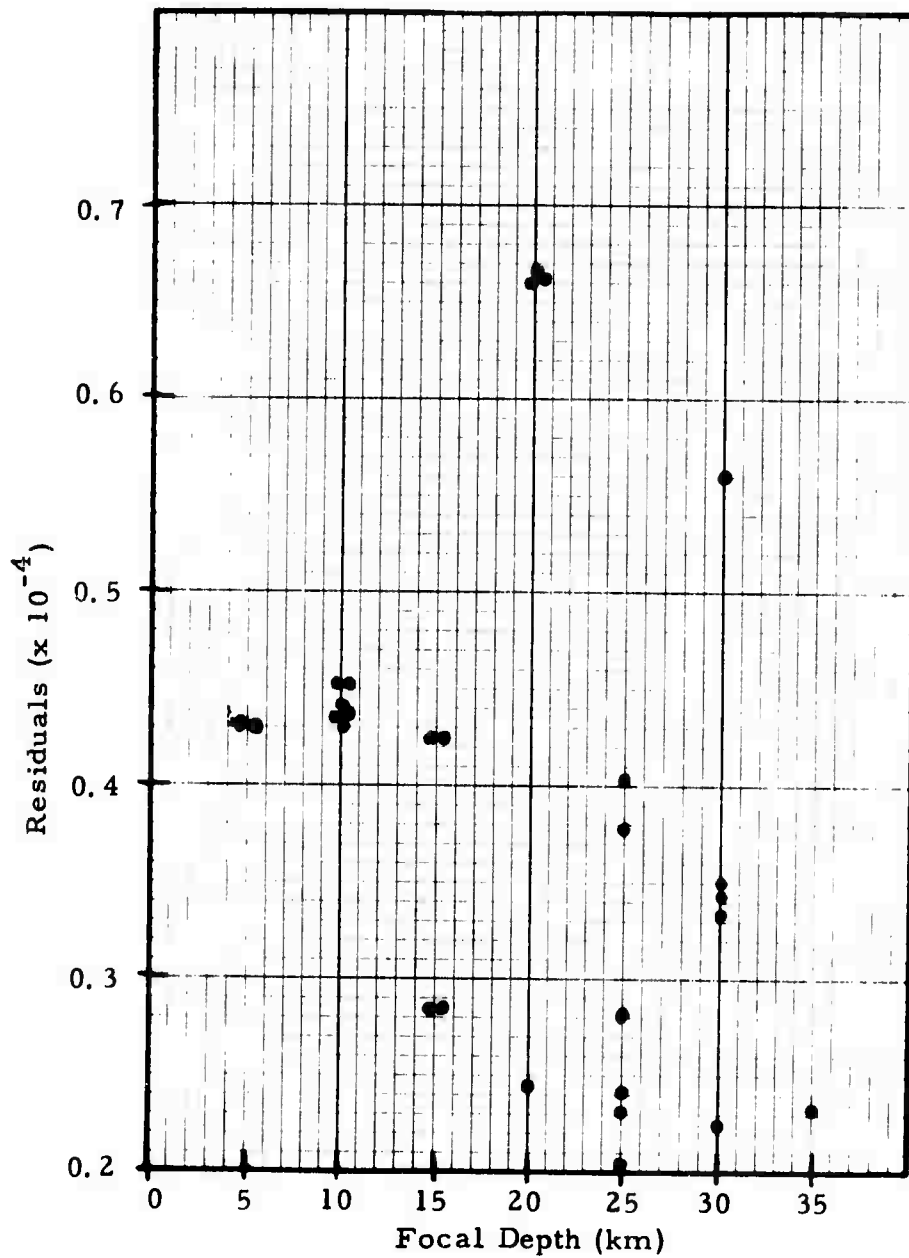


FIGURE II-6

ERROR COUNT VERSUS ESTIMATED FOCAL DEPTH FOR EVENT 20

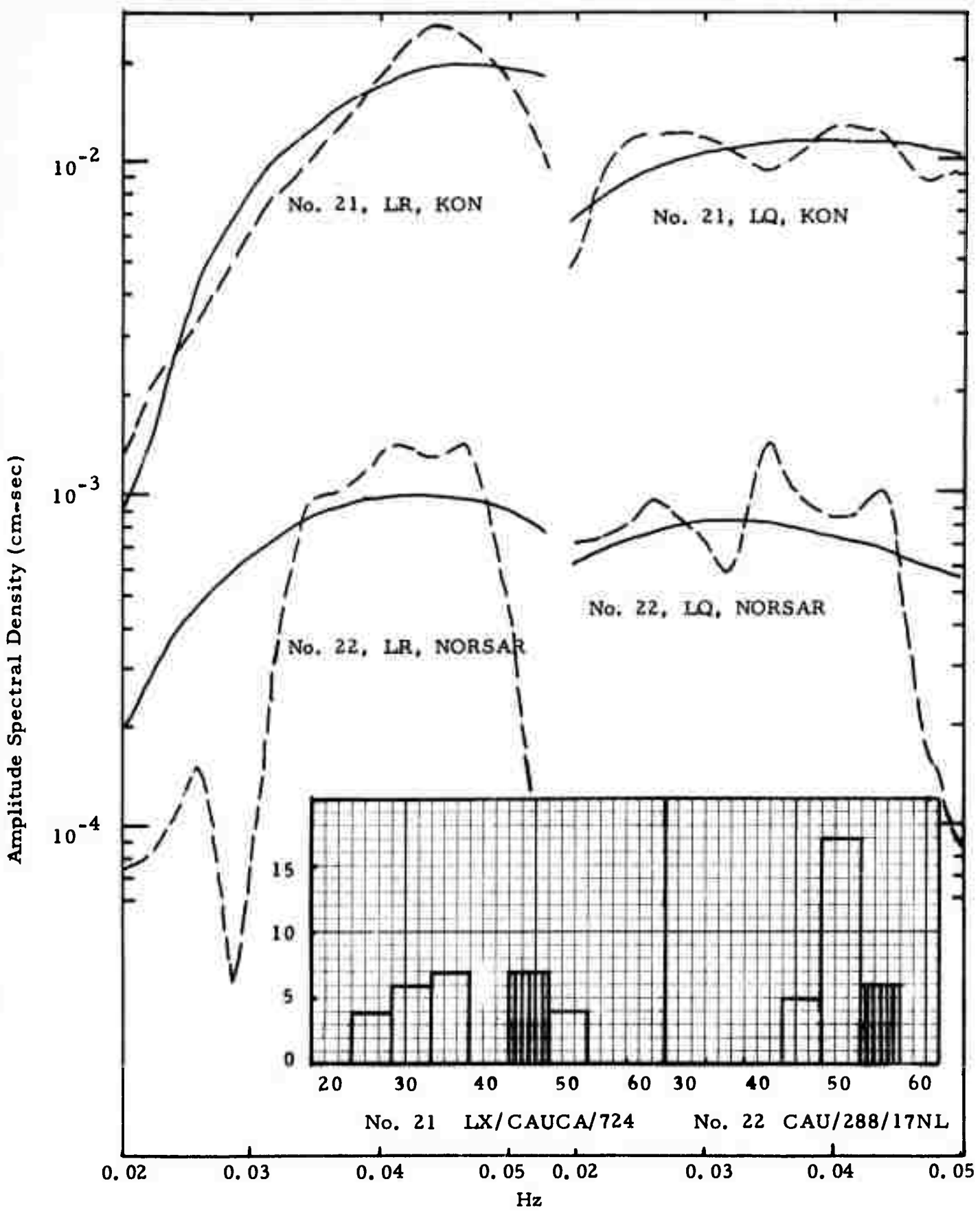


FIGURE II-7  
 LR AND LQ SPECTRA FOR EVENTS 21 (KON) AND 22 (NORSAR)

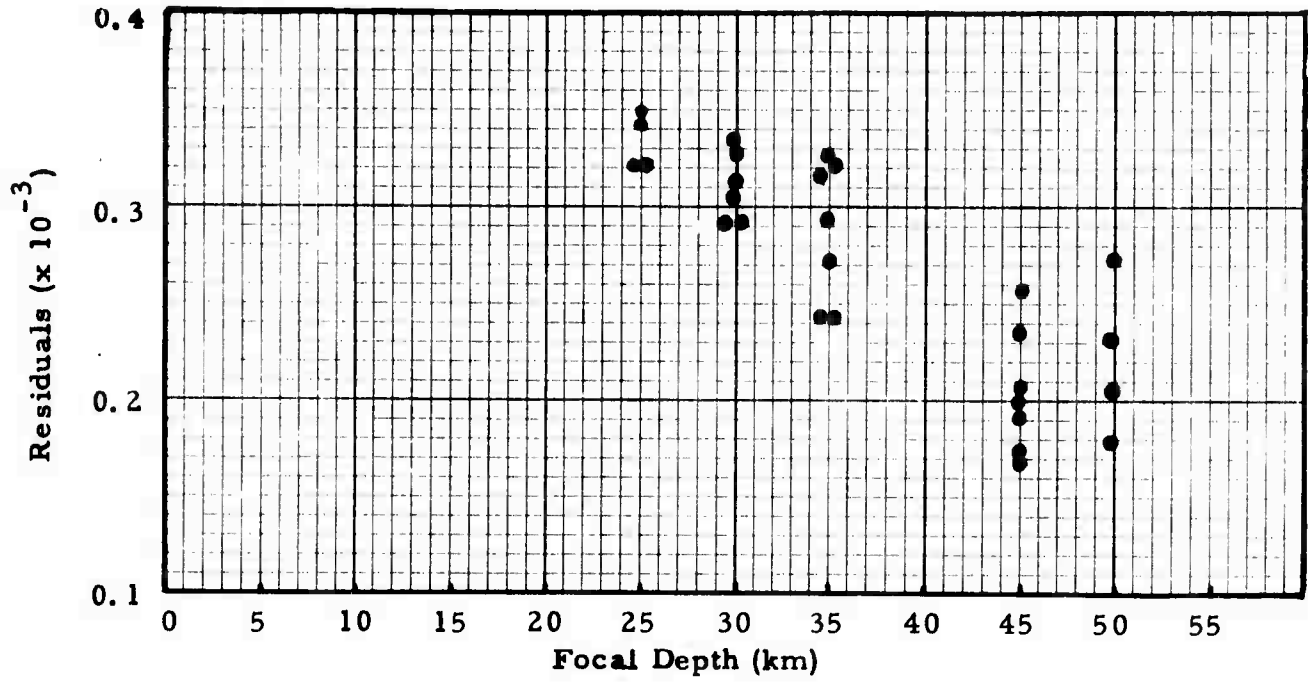


FIGURE II-8

ERROR COUNT VERSUS ESTIMATED FOCAL DEPTH FOR EVENT 21

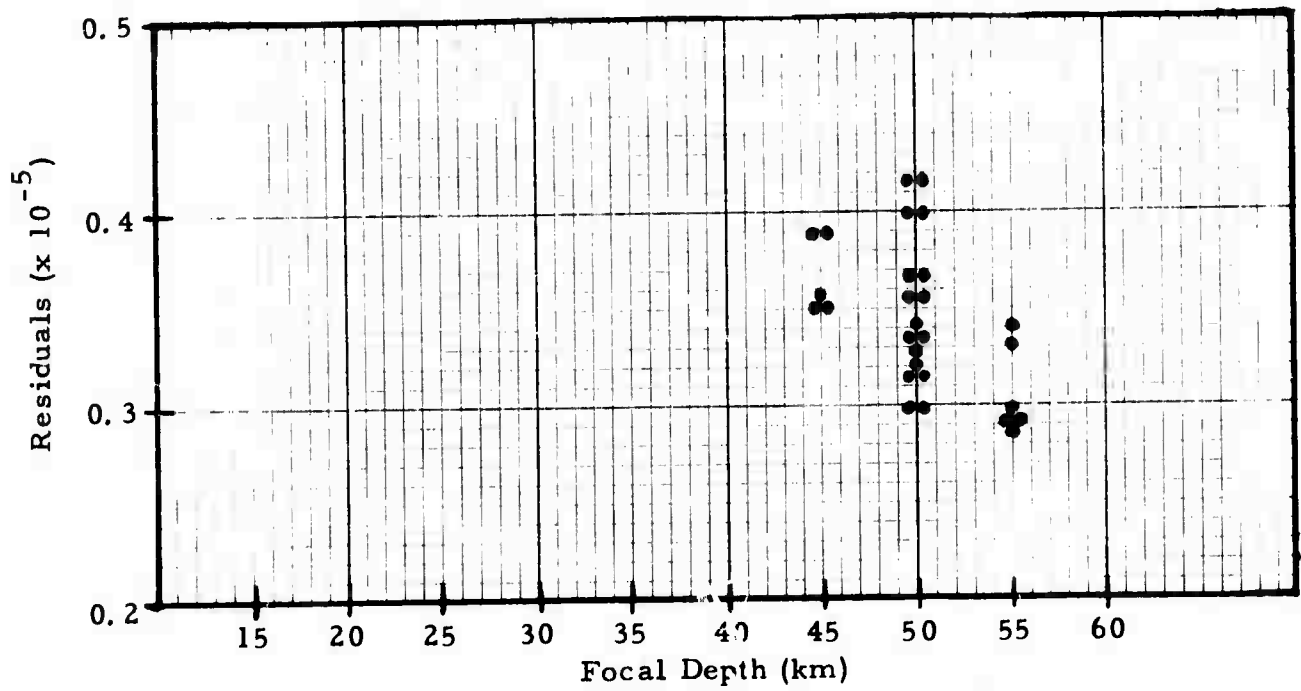


FIGURE II-9

ERROR COUNT VERSUS ESTIMATED FOCAL DEPTH FOR EVENT 22

In summary, the preceding examples of six earthquakes in the Caucasus area clearly indicate that the complex cepstrum technique can bring about highly desirable improvement on the quality of spectral data and in turn make the present method more effective. Judging from the results obtained by applying our method to the single-site surface wave spectral data for Events No. 19, 20, and 21 to which the complex cepstrum technique was applied, it is not unreasonable to say that the focal depth of an earthquake, regardless of its source mechanism, can be determined within a range of about 20 km. It should be emphasized that for the present method to be effective, especially for relatively small earthquakes whose surface waves are expected to be recorded with sufficient quality only at a very small number of sites, simultaneous use of both LR and LQ spectral data is essential.

We have applied the method described in the preceding paragraphs to fifty-one earthquakes in the Eurasian continent, including the six earthquakes in the Caucasus area just discussed above. The spectral data of these earthquakes are obtained from LP seismograms recorded by either the Very Long Period Experiment (VLPE) network or the Norwegian Seismic Array (NORSAR). The VLPE instruments were installed and operated by Lamont-Doherty Geological Observatory of Columbia University. A copy of the data tapes was made available to the Seismic Data Analysis Center (SDAC) where routine processing and analysis was performed by Texas Instruments Incorporated. A detailed description of the computer programs written for this task is given in the Documentation of Very Long Period Experiment Software Package (Texas Instruments Incorporated, 1971a). For the present study, only those earthquakes whose surface waves have sufficient signal-to-noise ratio are selected for analysis. The VLPE data are processed by the complex cepstrum technique in addition to a bandpass filtering operation for the pass band between 0.017 and 0.070 Hz to remove the spectral modulations due to multipath interference. Sixteen out of the fifty-one earthquakes presented in this report depend on the VLPE data and are identified by event codes beginning with 'LX'.

In addition each event code contains five letters in the middle block indicating the geographical location of the earthquake and in the last block three numerical digits for bookkeeping purposes in the VLPE routine processing. For example, Event No. 20 discussed previously is given an event code LX/CAUCA/606 to indicate that the VLPE data are used for the analysis of the earthquake located in Caucasus and is to be identified as Event No. 606 in the VLPE data series.

Because the VLPE network was still in experimental stages during the period when this study was undertaken, the amount of VLPE data suitable for this study was relatively small. As an alternative, a substantial quantity of the NORSAR data was taken for our analysis. This was conveniently accomplished because Texas Instruments Incorporated was also responsible for performing routine processing and analysis of the NORSAR data. Detailed information on this aspect can be found in the Documentation of the Array Evaluation Software Package (Texas Instruments Incorporated, 1971b). The NORSAR data selected for use in this study were the beamsteered output of surface wave trains with sufficiently large signal-to-noise ratio. The complex cepstrum technique was not applied to this set of data for thirty-five earthquakes. Each event code for the NORSAR data is set to begin with the first three letters indicating its geographical location and end with two letters 'NL' identifying itself as long-period NORSAR data. In between there are five numerical digits showing the Julian date and the hour in which the event takes place.

The results of our analysis of these fifty-one earthquakes will be discussed on a regional basis. In total, they are divided into nine groups according to the geographical location of each earthquake epicenter. For illustrative purposes the results of six earthquakes in Caucasus already have been presented as a group in the preceding paragraphs. Results obtained in this study for the remaining forty-five earthquakes which are divided into eight geographical groups are described in the following section.

SECTION III  
DATA PRESENTATION BY REGION

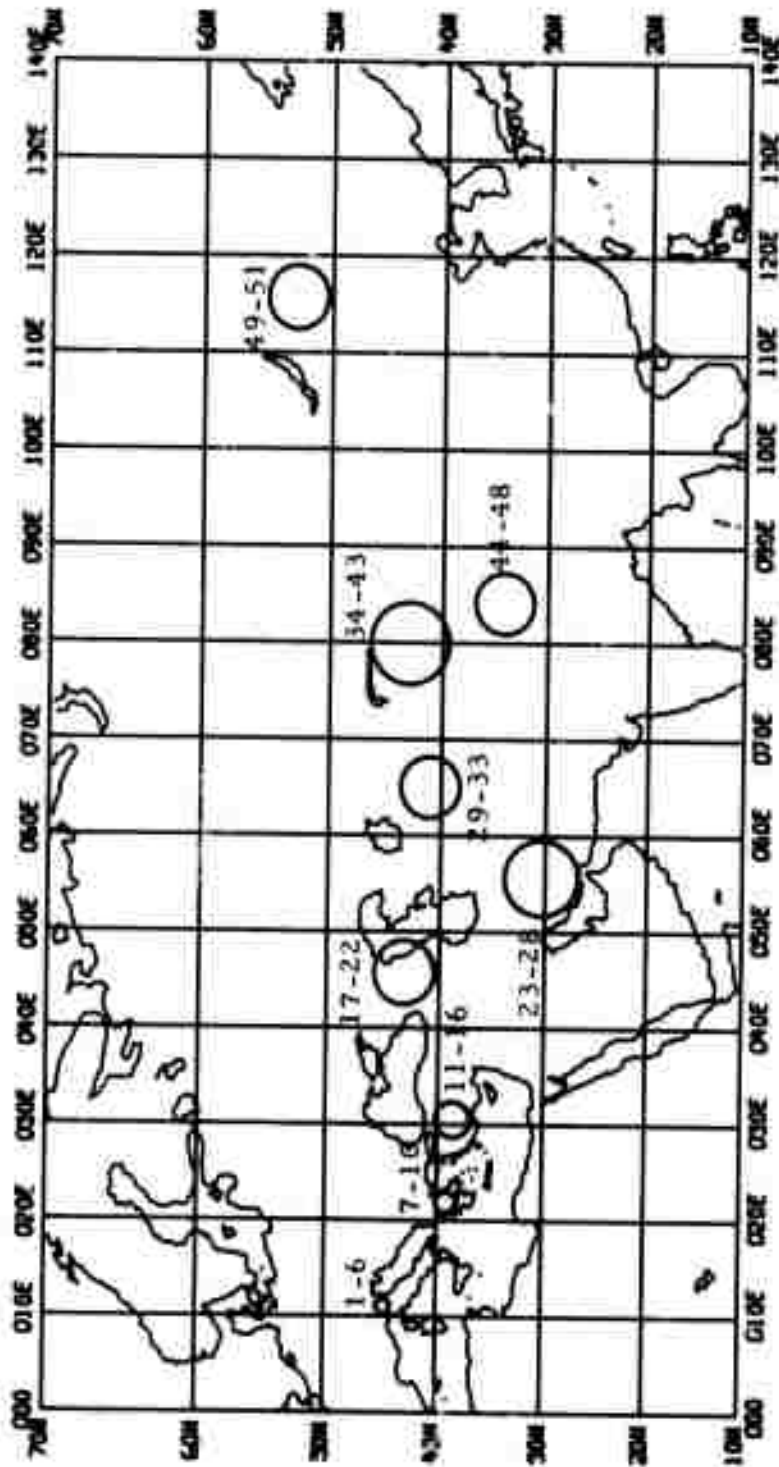
A. OUTLINE OF PRESENTATION

There is reason to believe that the source mechanism for earthquakes may be related to regional tectonic structures. Hence, it is of particular interest to examine the surface wave spectra and their solutions of earthquake parameters on a regional basis. For this purpose, fifty-one events are grouped into nine regions:

|    | <u>Region</u>     | <u>Event Numbers</u> |
|----|-------------------|----------------------|
| 1. | Italy             | 1-6                  |
| 2. | Greece            | 7-10                 |
| 3. | Turkey            | 11-16                |
| 4. | Caucasus          | 17-22                |
| 5. | Iran              | 23-28                |
| 6. | Tadzhik           | 29-33                |
| 7. | Sinkiang          | 34-43                |
| 8. | Tibet             | 44-48                |
| 9. | Northeastern Asia | 49-51                |

The nine regions with their associated events are identified in Figure III-1.

In the following discussion, the nine regions (except region 4 - Caucasus, which was presented in Section II) are examined in detail, with the observed as well as the 'best-fit' spectra presented. Qualitative judgements on the matching of the 'best-fit' spectra with the observed spectra will be left to the reader. In making any judgments, one should bear in mind the procedure used in determining the 'best-fit' spectra. First, the least squares procedure involves determining the minimum residual from the total energy in



MILLER MODIFIED MERCATOR PROJECTION  
 MAP SCALE: 0.500 IN. / 10 DEG. LONGITUDE

FIGURE III-1  
 FIFTY-ONE EARTHQUAKES IN NINE REGIONS STUDIED IN THIS REPORT

both the Rayleigh and Love waves, and the resulting solution is not determined by fitting the Rayleigh or Love wave spectra individually. Secondly, since the earthquake focal depth is the most important source parameter for discrimination purposes, our discussions of the outcomes from the least-squares procedure will be made with special emphasis on the focal depth. In the lower part of each spectral illustration, the distribution of focal depths obtained from the 28 sets of dip and slip angles is grouped and plotted as the number of appearances versus the focal depth. The shaded group in this plot contains the minimum residual depth, and this depth along with the other source parameters is used to calculate the 'best-fit' spectra shown on the associated spectral plots.

#### B. EARTHQUAKES IN ITALY

For the region in Northern Italy, six events have been examined. The PDE information for these events are given in Table III-1, with the theoretically determined source parameters given in Table III-2.

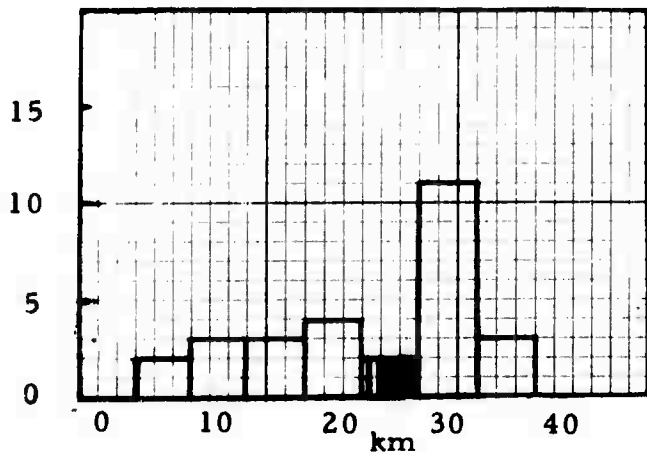
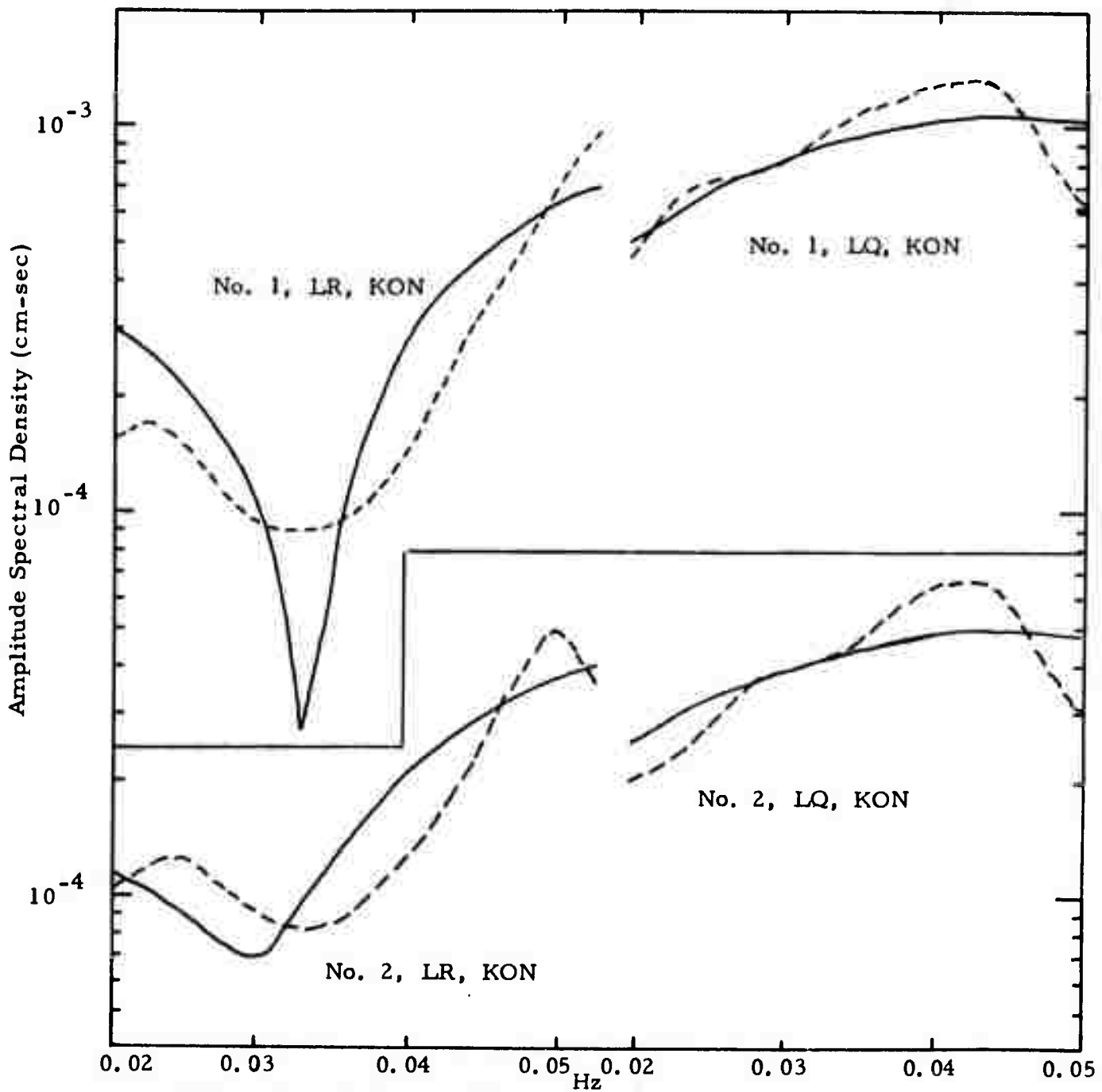
From the shape of the Fourier amplitude spectra of the Rayleigh and Love waves, the Italian events can be placed in two subgroups (Events 1, 2 and Events 3-6). The first subgroup (Events 1 and 2), as shown in Figure III-2, is characterized by a prominent trough in the LR spectra between 0.03 and 0.04 Hz. Although these events have similar spectral shapes for both the Rayleigh and Love waves, the 'best-fit' theoretical spectra are somewhat different. For Event 1, the node at 0.035 Hz is over-characterized by the computed Rayleigh-wave spectrum. A vertical strike-slip fault is suggested for this earthquake, with the focal depth in the range from 5 to 35 km having a minimum residual at 25 km (Table III-2). For Event 2, the suggested mechanism is also a vertical strike-slip fault with the focal depth in the range from 5 to 40 km and having a minimum residual at 30 km. It is interesting to note that the solution for both events yields a strike-direction of  $N130^{\circ}E$ .

TABLE III-1  
PDE INFORMATION FOR EVENTS IN ITALY

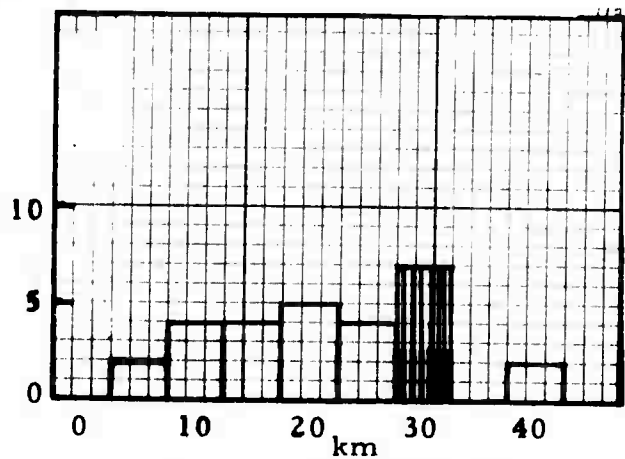
| I. D. No. | Event Name   | Date     | Time       | Location |           | Focal Depth | $m_b$ | Data Site        |
|-----------|--------------|----------|------------|----------|-----------|-------------|-------|------------------|
|           |              |          |            | Latitude | Longitude |             |       |                  |
| 1         | LX/ITALY/665 | 02/04/72 | 09. 18. 32 | 43. 9N   | 13. 2E    | 23          | 4. 4  | KON              |
| 2         | LX/ITALY/672 | 02/04/72 | 07. 08. 13 | 43. 9N   | 13. 3E    | 33          | 4. 7  | KON              |
| 3         | LX/CITLY/134 | 02/04/72 | 17. 19. 52 | 43. 8N   | 13. 3E    | 23          | 4. 4  | T LO, KON<br>OGD |
| 4         | LX/ITALY/667 | 02/04/72 | 18. 17. 30 | 43. 8N   | 13. 4E    | 33          | 4. 8  | KON              |
| 5         | LX/ITALY/671 | 02/05/72 | 05. 05. 51 | 43. 7N   | 13. 4E    | 33          | 4. 6  | KON              |
| 6         | LX/ITALY/674 | 02/05/72 | 15. 14. 48 | 43. 7N   | 13. 4E    | 35          | 4. 7  | KON              |

TABLE III-2  
 THEORETICAL SOLUTION OF SOURCE MECHANISM FOR  
 EVENTS IN ITALY

| I. D. No. | Event Name   | Strike  | Dip Angle | Slip Angle | Focal Depth (km) | Moment $M(x10^{25} \text{ dyne-cm})$ |
|-----------|--------------|---------|-----------|------------|------------------|--------------------------------------|
| 1         | LX/ITALY/665 | N 130°E | 90        | 0.0        | 25               | $0.92 \times 10^{-2}$                |
| 2         | LX/ITALY/672 | N 130°E | 80        | 0.0        | 30               | $0.47 \times 10^{-2}$                |
| 3         | LX/CITLY/134 | N 170°E | 90        | -60.0      | 30               | $0.72 \times 10^{-2}$                |
| 4         | LX/ITALY/667 | N 110°E | 60        | -30.0      | 35               | $0.19 \times 10^{-2}$                |
| 5         | LX/ITALY/671 | N 40°E  | 80        | -30.0      | 45               | $0.40 \times 10^{-2}$                |
| 6         | LX/ITALY/674 | N 10°E  | 70        | -60.0      | 40               | $0.89 \times 10^{-2}$                |



No. 1 LX/ITALY/665



No. 2 LX/ITALY/672

FIGURE III-2

LR AND LQ SPECTRA FOR EVENTS 1 AND 2 (KON) AND THE CORRESPONDING DISTRIBUTIONS OF ESTIMATED FOCAL DEPTH III-6

Event 3 represents a multiple station fit (Figure III-3). The 'best-fit' source parameters are given in Table III-2. According to these source parameters, the earthquake is related to oblique-slip dislocation. The focal depth falls mostly in the range from 25 to 40 km with six exceptions at 0 km. More discussion on this event will be made in the next section.

The amplitude spectra for Events 4 and 6 are shown in Figure III-4. For Events 4 and 6, the 'best-fit' dip and slip angles given in Table III-2 suggest oblique-slip dislocation source mechanisms. The focal depth estimates for Event 4 predominantly fall in the range of 30 to 45 km. Both Events 4 and 6 have nearly the same residual-profile, with the latter having a focal depth in the range of 35 to 45 km. The strike directions for these two events are  $110^{\circ}\text{E}$  and  $\text{N}10^{\circ}\text{E}$ , respectively, which probably represent conjugate planes. On the basis of surface wave data alone, it is not possible to make a choice.

Spectra for Event 5 are shown in Figure III-5. The residuals have the same profile as those for Events 3, 4, and 6, with the focal depth in the 40-45 km range.

In general, we can group Events 1 and 2 and Events 3, 4, 5, and 6, by similar spectral shapes and similar residual profiles. The first group has a strike-slip source mechanism whereas the second group has oblique slip source mechanisms. Also, the first group seems to be located at slightly shallower depths.

### C. EARTHQUAKES IN GREECE

Four events have been studied for the region in Greece (Table III-3). The data for these events were obtained from NORSAR. The best-fit solutions are given in Table III-4.

From the observed spectral shapes of the Rayleigh and Love waves, the four events can be classified into two subgroups; Events 7 and 8 in Western Greece (Figure III-6) and Events 9 and 10 in Eastern Greece (Figure III-7).

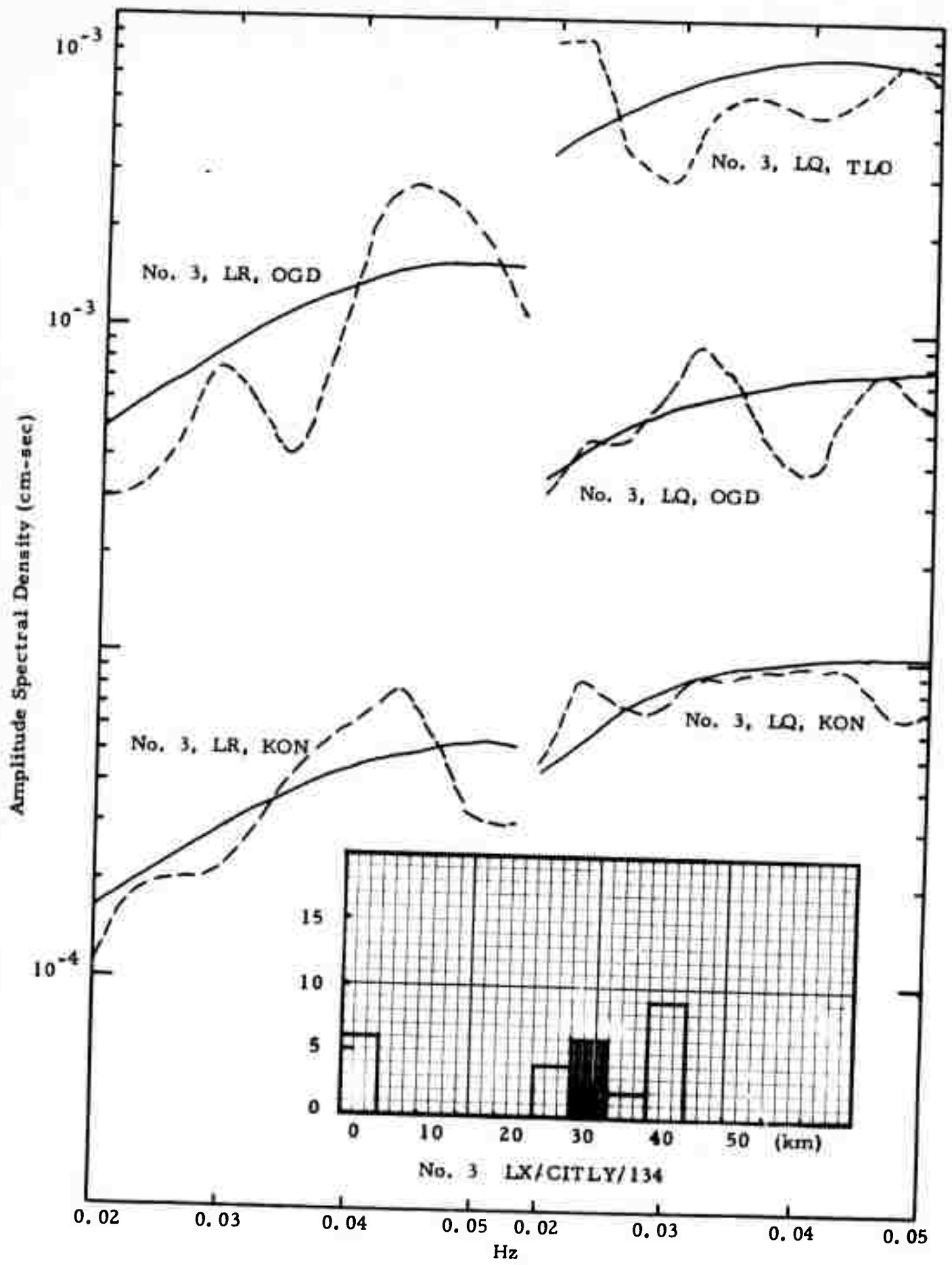


FIGURE III-3

LR AND LQ SPECTRA FOR EVENT 3 (KON, OGD, TLO) AND THE CORRESPONDING DISTRIBUTION OF ESTIMATED FOCAL DEPTHS

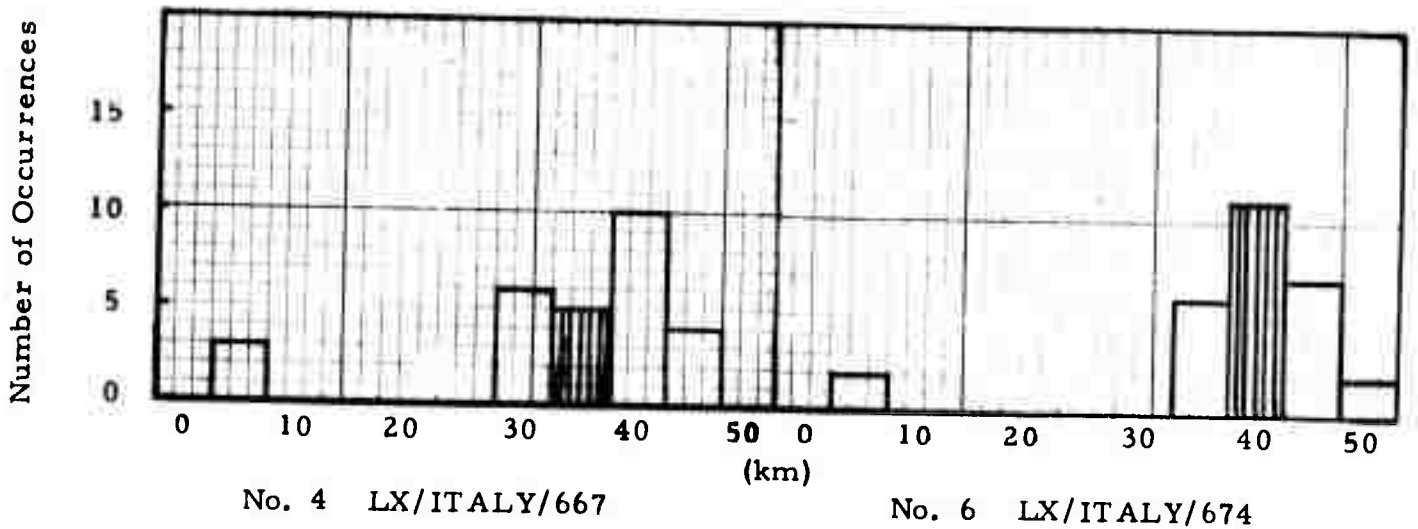
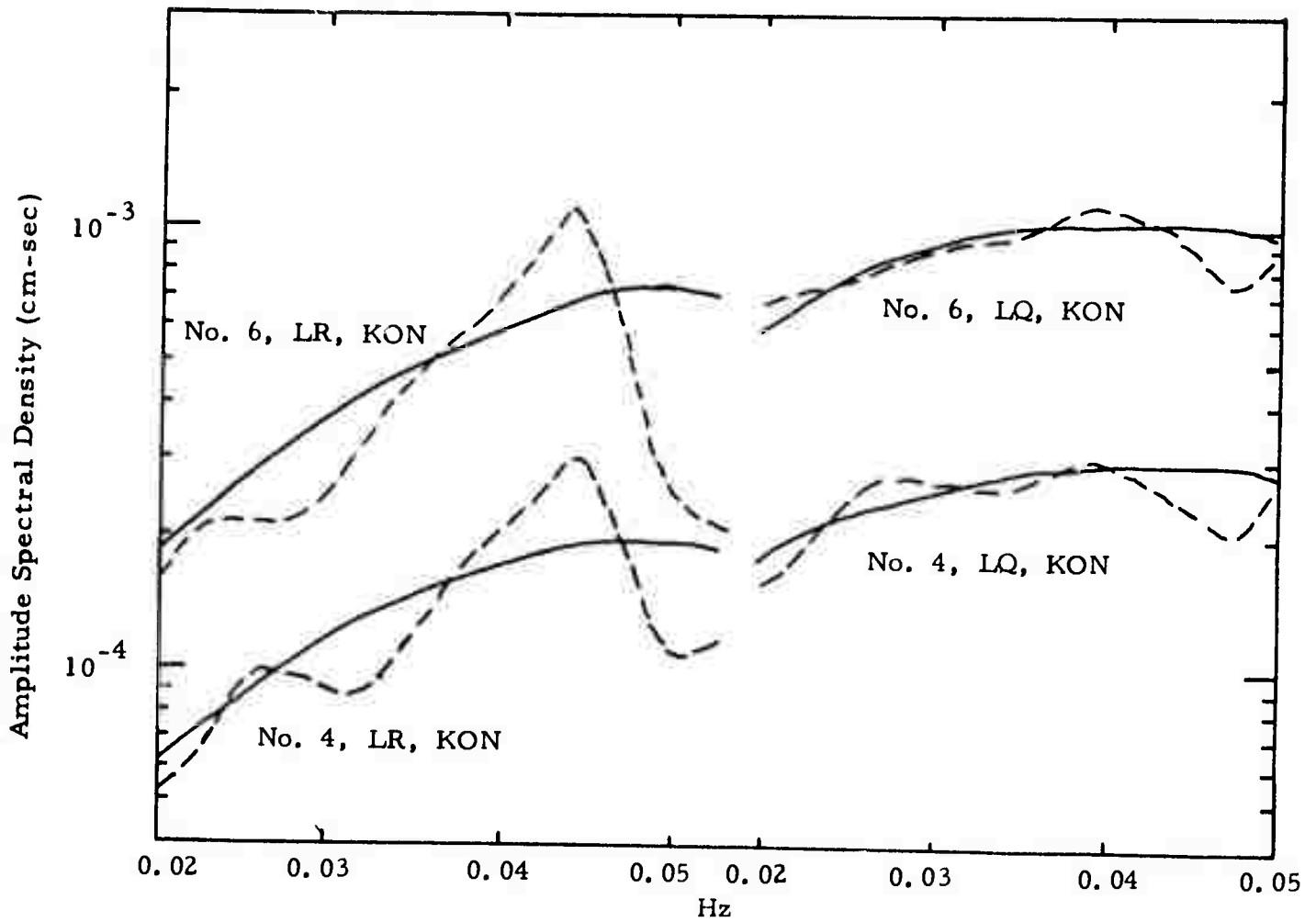


FIGURE III-4

LR AND LQ SPECTRA FOR EVENTS 4 AND 6 (KON) AND THE CORRESPONDING DISTRIBUTION OF ESTIMATED FOCAL DEPTHS

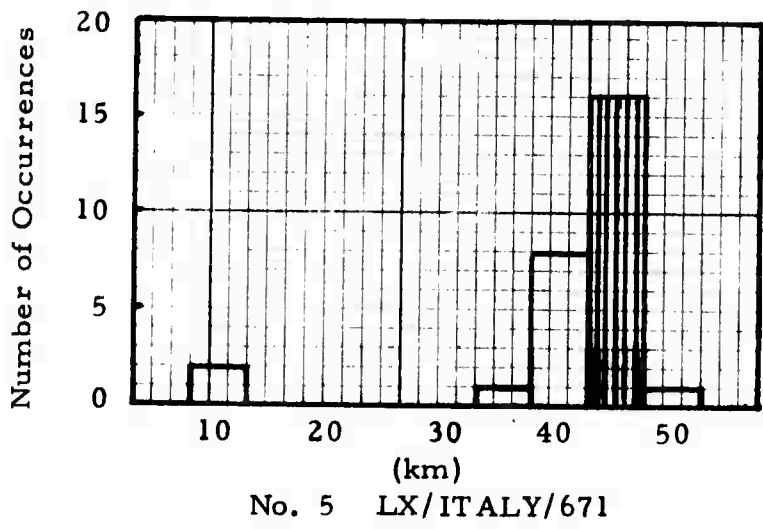
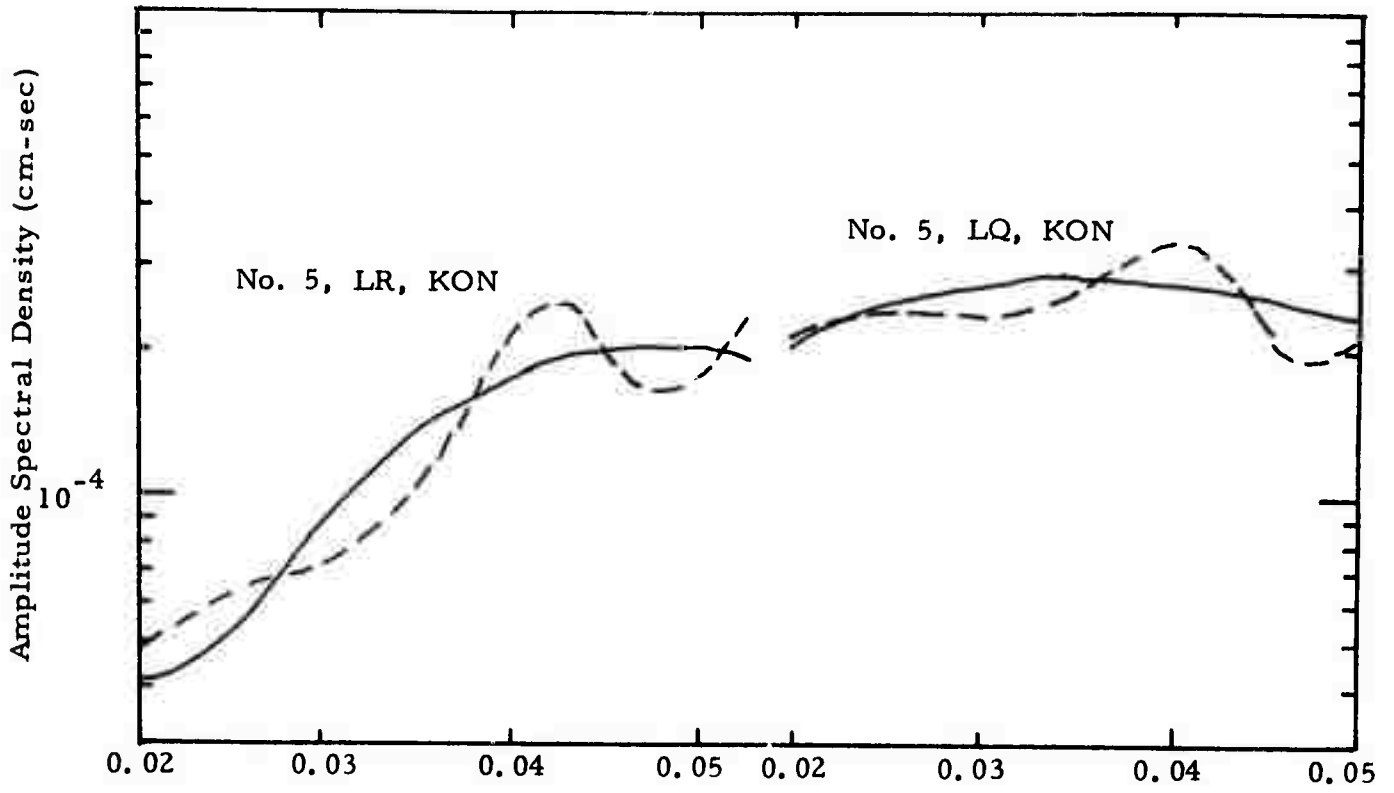


FIGURE III-5  
 LR AND LQ SPECTRA FOR EVENT 5 (KON) AND THE CORRESPONDING  
 DISTRIBUTION OF ESTIMATED FOCAL DEPTHS

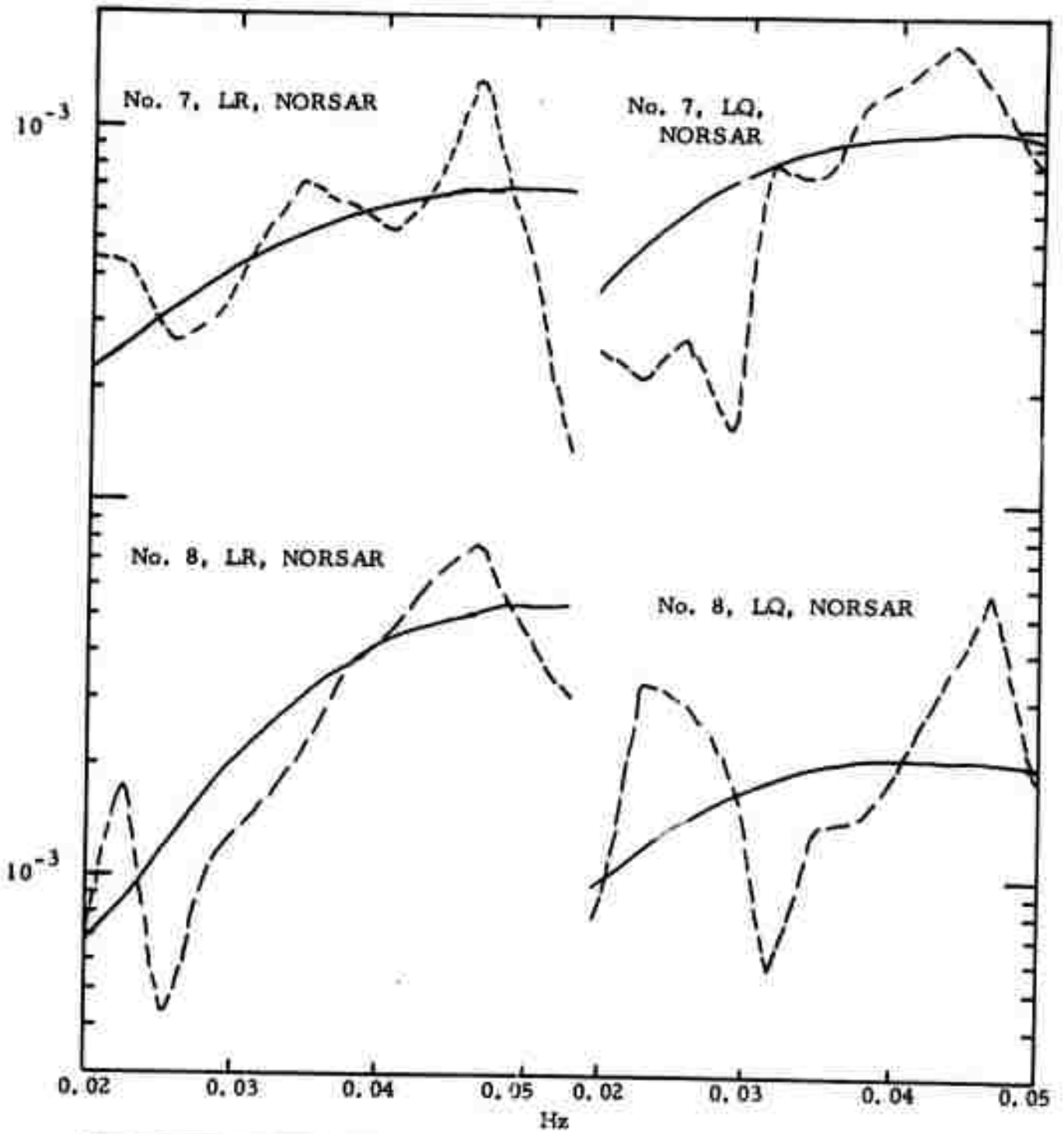
TABLE III-3  
PDE INFORMATION FOR EVENTS IN GREECE

| I. D. No. | Event Name   | Date     | Time     | Location |           | Focal Depth | $m_b$ | Data Site |
|-----------|--------------|----------|----------|----------|-----------|-------------|-------|-----------|
|           |              |          |          | Latitude | Longitude |             |       |           |
| 7         | GRE*033*21NL | 02/02/72 | 21.19.49 | 38.9N    | 21.2E     | 44          | 4.6   | NORSAR    |
| 8         | GRE*012*13NL | 01/12/72 | 13.51.20 | 35.0N    | 23.5E     | 48          | 4.9   | NORSAR    |
| 9         | GRE*044*13NL | 02/13/72 | 13.07.11 | 37.1N    | 24.0E     | 27          | 4.5   | NORSAR    |
| 10        | GRE*047*00NL | 02/16/72 | 00.42.24 | 36.3N    | 24.2E     | N           | 4.5   | NORSAR    |

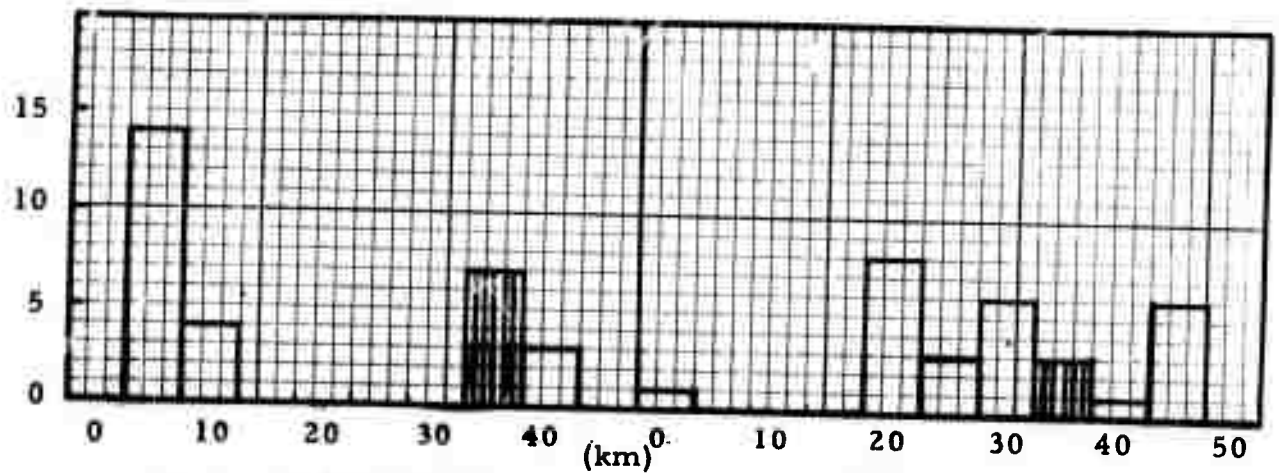
TABLE III-4  
THEORETICAL SOLUTION OF SOURCE MECHANISM FOR  
EVENTS IN GREECE

| I. D. No. | Event Name   | Strike  | Dip Angle | Slip Angle | Focal Depth (km) | Moment $M(x10^{25} \text{ dyne-cm})$ |
|-----------|--------------|---------|-----------|------------|------------------|--------------------------------------|
| 7         | GRE*033*21NL | N 0°E   | 80        | -90        | 35               | $0.87 \times 10^{-2}$                |
| 8         | GRE*012*13NL | N 140°E | 60        | 60         | 35               | $0.32 \times 10^{-2}$                |
| 9         | GRE*044*13NL | N 110°E | 60        | 30         | 5                | $0.41 \times 10^{-2}$                |
| 10        | GRE*047*00NL | N 160°E | 60        | 30         | 10               | $0.35 \times 10^{-2}$                |

Amplitude Spectral Density (cm-sec)

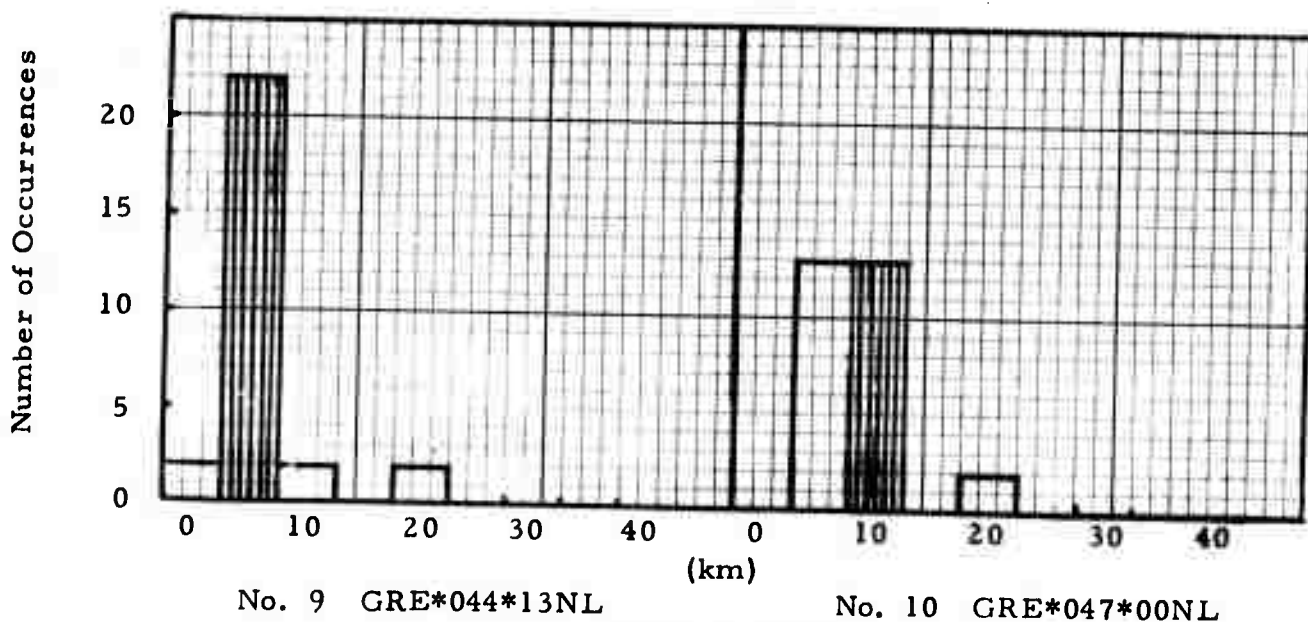
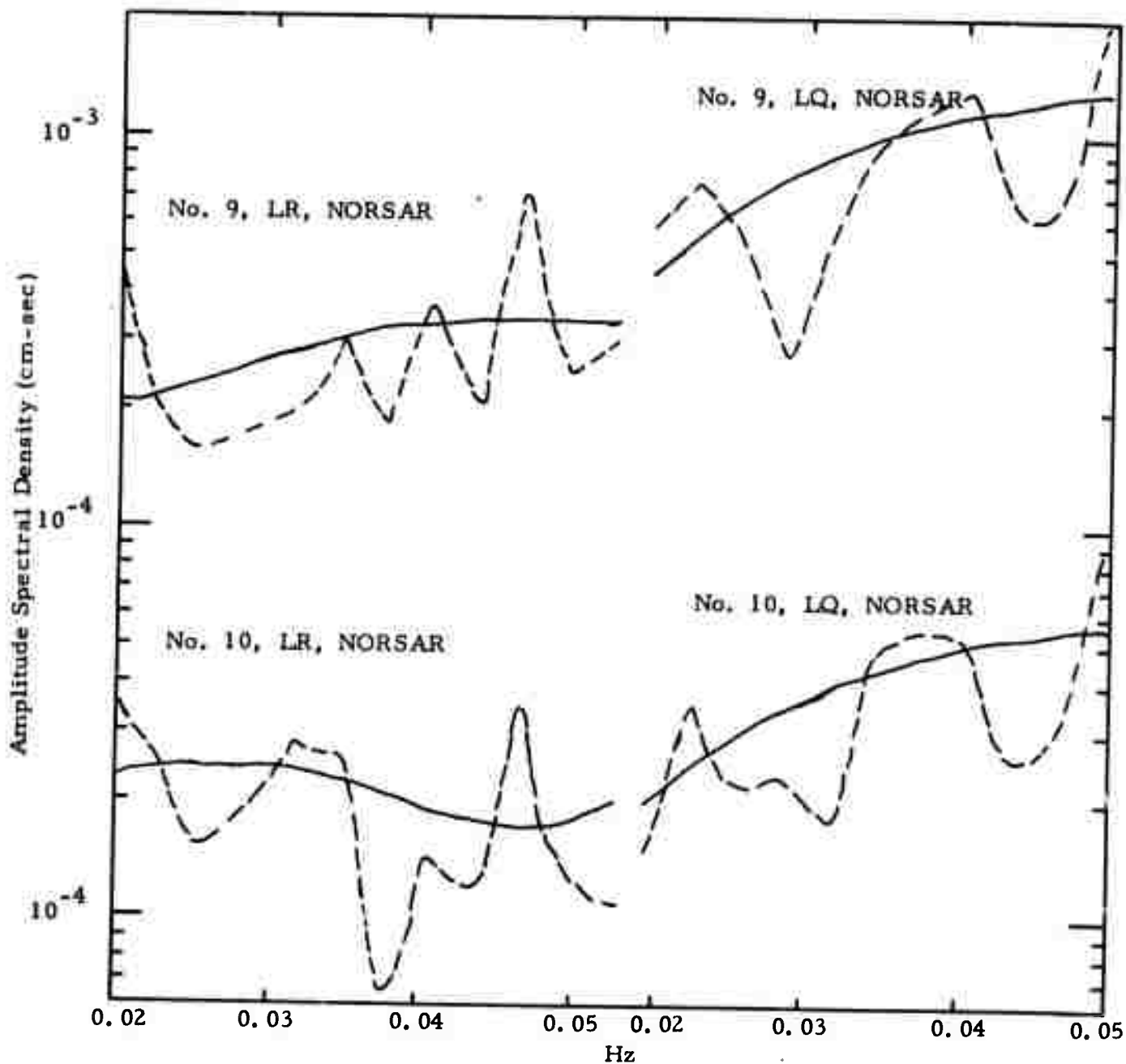


Number of Occurrences



No. 7 GRE\*033\*21NL **FIGURE III-6** No. 8 GRE\*012\*13NL

LR AND LQ SPECTRA FOR EVENTS 7 AND 8(NORSAR) AND THE CORRESPONDING DISTRIBUTION OF ESTIMATED FOCAL DEPTHS



No. 9 GRE\*044\*13NL                      No. 10 GRE\*047\*00NL  
**FIGURE III-7**  
**LR AND LQ SPECTRA FOR EVENTS 9 AND 10 (NORSAR) AND THE**  
**CORRESPONDING DISTRIBUTION OF ESTIMATED FOCAL DEPTHS**

For Event 7, the differences of the residuals are small and one cannot make a clear estimate of the dip and slip angles. The focal depth could be in either the range from 5 to 10 km or from 35 to 40 km. For Event 8, it would seem impossible that the computed Love-wave spectra would yield a node at 0.035 Hz for the theoretical model. The best-fit solution yields an oblique faulting, with a focal depth in the 20 to 45 km range.

For Events 9 and 10, the residuals are distributed for 5 to 10 km focal depths and are not sufficiently varied to make a clear selection of the earthquake parameters.

None of the Greek events were processed with the complex cepstrum technique, so the solutions should be taken with caution.

#### D. EARTHQUAKES IN TURKEY

Six events have been studied for the region in Turkey, and these data sites are indicated in Table III-5. The 'best-fit' earthquake parameters are given in Table III-6.

For Event 11, the 'best-fit' solution suggests an oblique-slip source mechanism. The focal depth is found in the range of 5 to 10 km (Figure III-8). The observed Rayleigh-wave spectrum for Event 12 has a node at 0.047 Hz which is not reproduced by its 'best-fit' theoretical counterpart. The minimum residuals are about equally distributed in two ranges of focal depth, 5 to 15 km and 35 to 45 km. Although a clearcut choice is difficult, the shallower depth range is slightly preferred because of the spectral similarity between this event and Event 11.

Event 13 (Figure III-9) has its minimum residuals narrowly distributed in the range of 45 to 55 km focal depths, with the best estimate of the focal depth being 50 km. The difference in both Rayleigh and Love wave spectral shapes between this event and Events 11, 12 is remarkable.

TABLE III-5  
PDE INFORMATION FOR EVENTS IN TURKEY

| I. D. No. | Event Name    | Date     | Time     | Location |           | Focal Depth | m <sub>b</sub> | Data Site |
|-----------|---------------|----------|----------|----------|-----------|-------------|----------------|-----------|
|           |               |          |          | Latitude | Longitude |             |                |           |
| 11        | TUR/126/04BE  | 05/06/71 | 04.24.34 | 39.0N    | 29.7E     | N           | 4.6            | NORSAR    |
| 12        | TUR/219/17NL  | 08/07/71 | 17.07.24 | 38.9N    | 29.9E     | 20          | 4.5            | NORSAR    |
| 13        | LX/TURKY/265  | 10/06/71 | 01.46.38 | 38.3N    | 30.2E     | 19          | 4.6            | KON       |
| 14        | LX/TURKE/047* | 01/12/72 | 06.38.28 | 37.7N    | 30.0E     | N           | 4.4            | TLO, KON  |
| 15        | TUR/221/04NL  | 08/09/71 | 04.40.47 | 37.6N    | 29.8E     | 11          | 4.8            | NORSAR    |
| 16        | TUR/143/01NL  | 05/23/71 | 01.02.55 | 37.6N    | 30.1E     | N           | 4.4            | NORSAR    |

\* = LASA Bulletin

TABLE III-6  
 THEORETICAL SOLUTION OF SOURCE MECHANISM FOR  
 EVENTS IN TURKEY

| I. D. No. | Event Name   | Strike  | Dip Angle | Slip Angle | Focal Depth (km) | Moment $M(\times 10^{25} \text{ dyne-cm})$ |
|-----------|--------------|---------|-----------|------------|------------------|--|
| 11        | TUR/126/04BE | N 60°E  | 60        | -60        | 5                | 0.23x10 <sup>-1</sup>                      |
| 12        | TUR/219/17NL | N 40°E  | 90        | 90         | 45               | 0.23x10 <sup>-1</sup>                      |
| 13        | LX/TURKY/265 | N 60°E  | 90        | 0.0        | 50               | 0.40x10 <sup>-1</sup>                      |
| 14        | LX/TURKE/047 | N 160°E | 80        | 60         | 35               | 0.13x10 <sup>-1</sup>                      |
| 15        | TUR/221/04NL | N 50°E  | 80        | 60         | 60               | 0.16x10 <sup>-1</sup>                      |
| 16        | TUR/143/01NL | N 150°E | 60        | 60         | 5                | 0.39x10 <sup>-1</sup>                      |

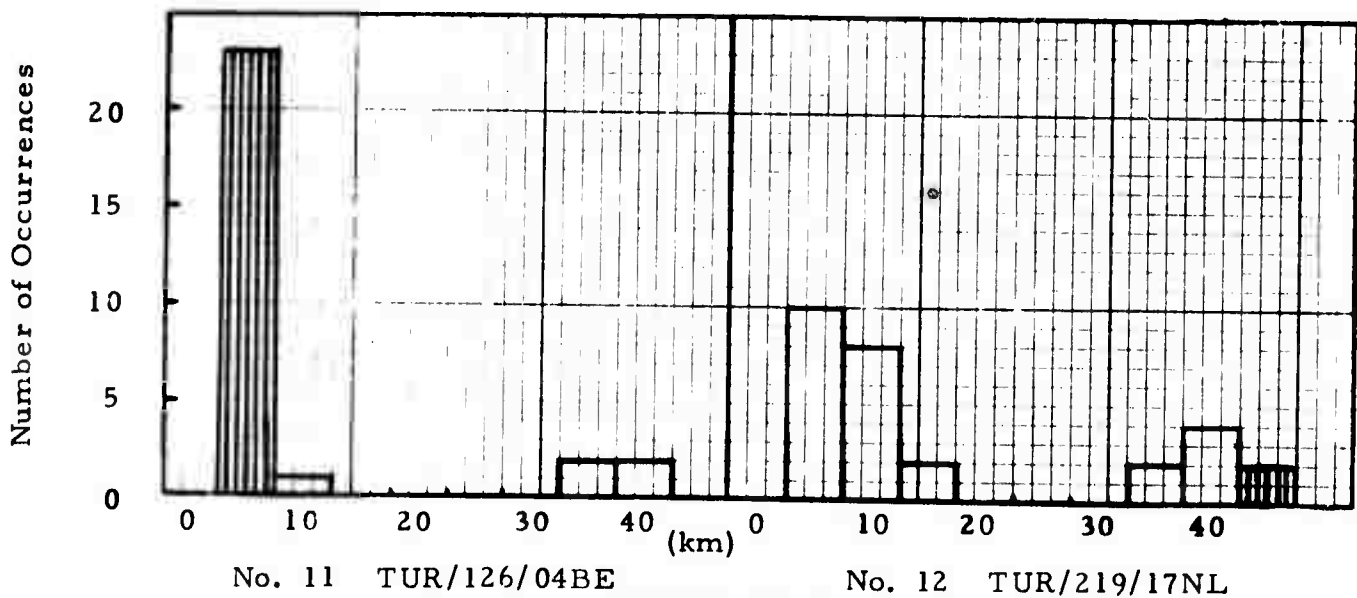
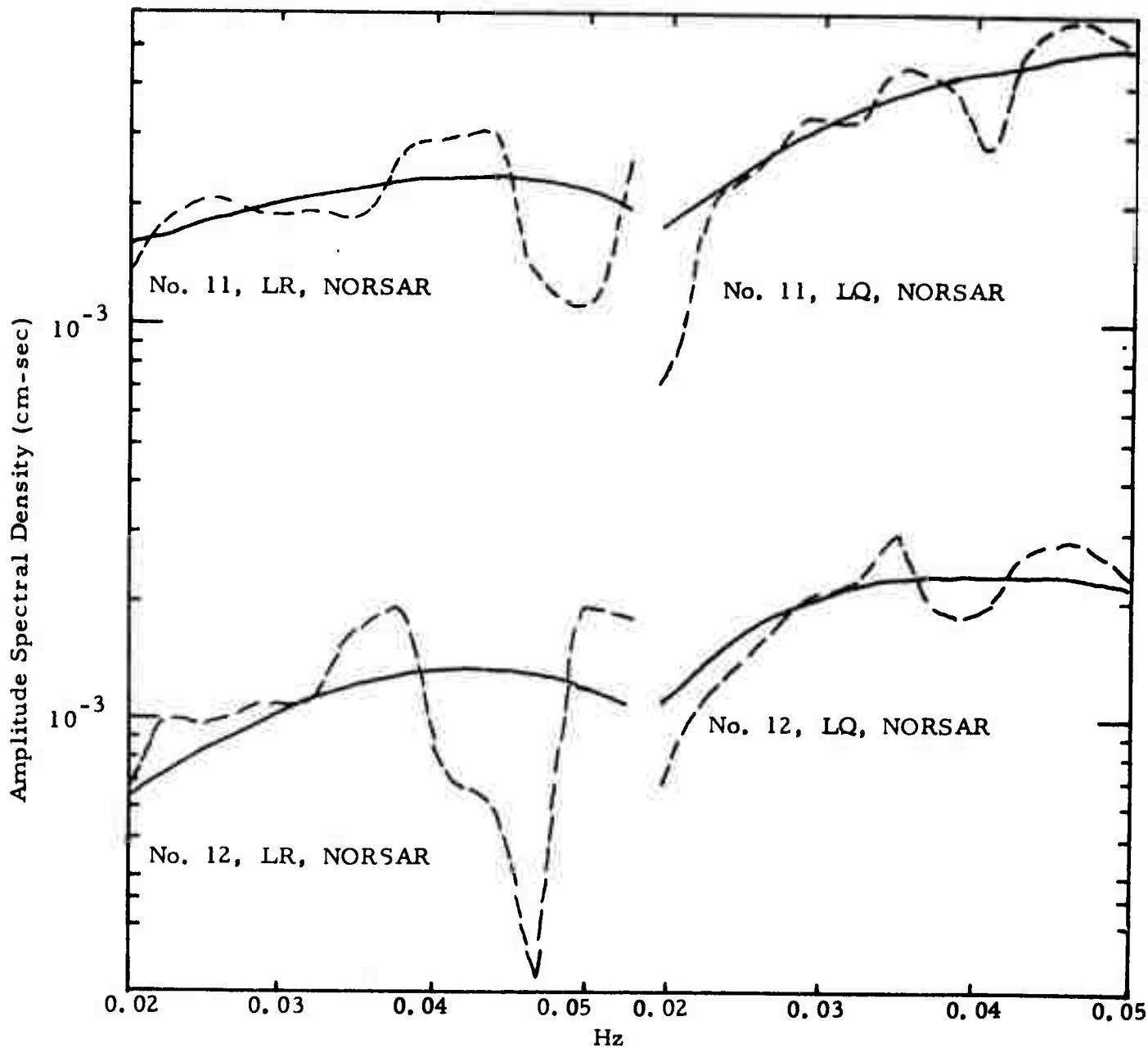
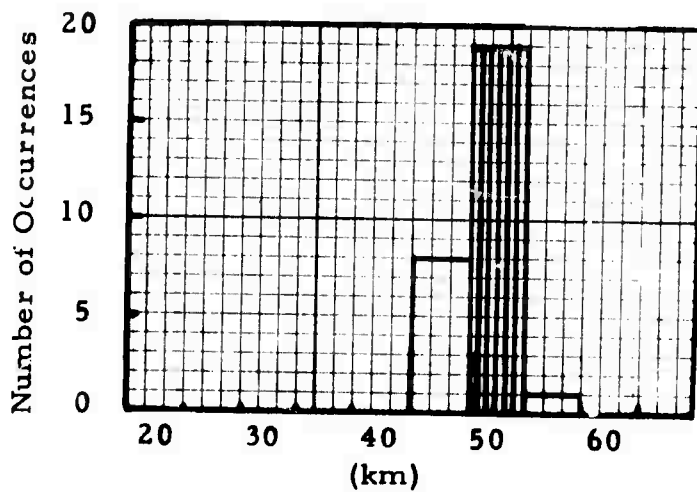
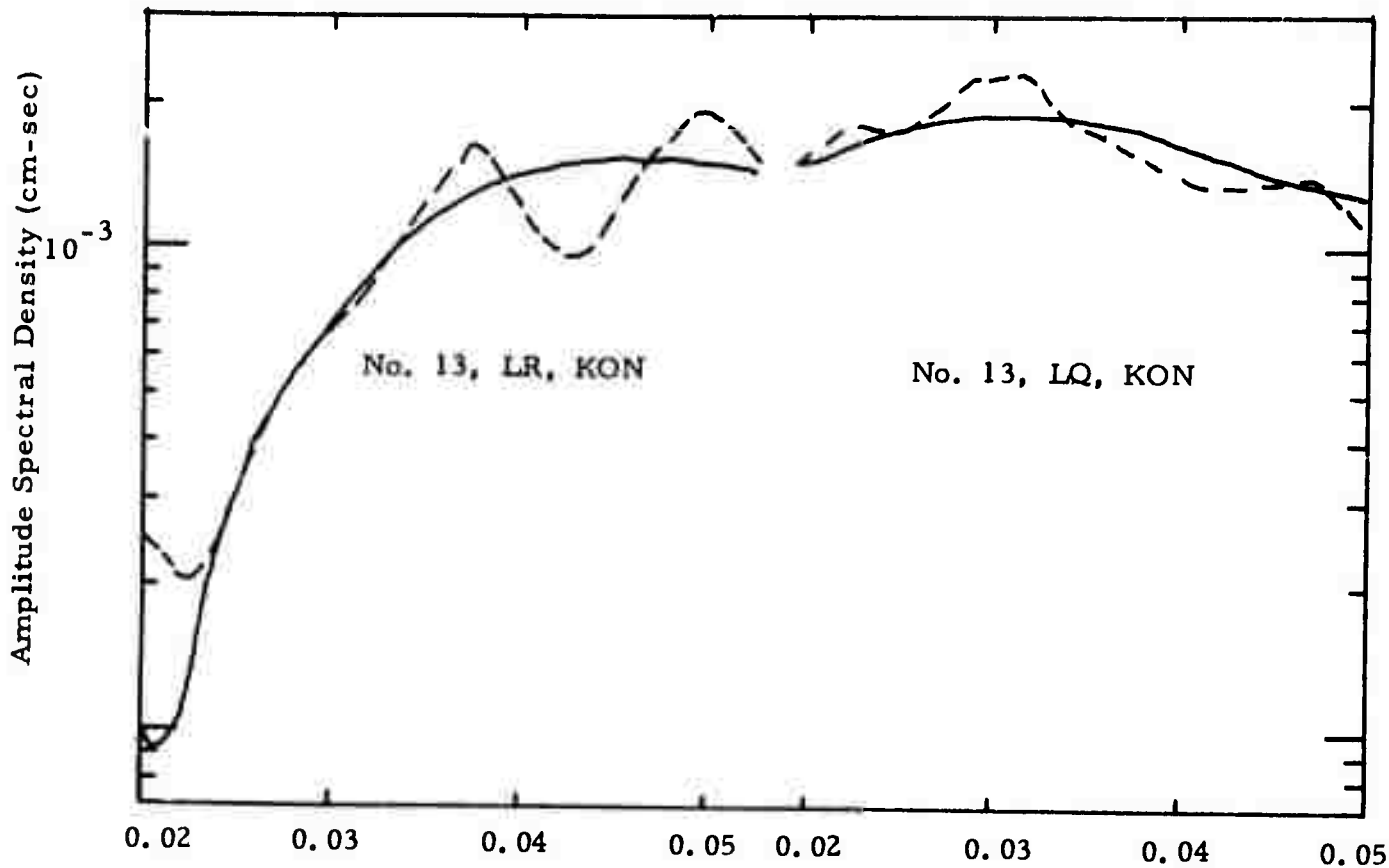


FIGURE III-8

LR AND LQ SPECTRA FOR EVENTS 11 AND 12 (NORSAR) AND THE  
CORRESPONDING DISTRIBUTION OF ESTIMATED FOCAL DEPTHS



No. 13 LX/TURKEY/265

FIGURE III-9

LR AND LQ SPECTRA FOR EVENT 13 (KON) AND THE CORRESPONDING DISTRIBUTION OF ESTIMATED FOCAL DEPTHS

Event 14 is a multiple station fit (Figure III-10), with the event information obtained from LASA bulletins. The minimum residual gives a focal depth in the range of 35 to 40 km. The best-fit solution suggests an oblique slip source mechanism with the strike direction either  $N160^{\circ}E$  or its orthogonal direction.

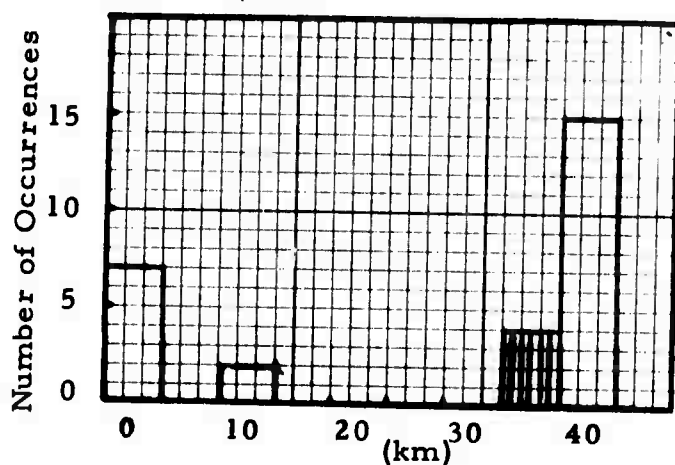
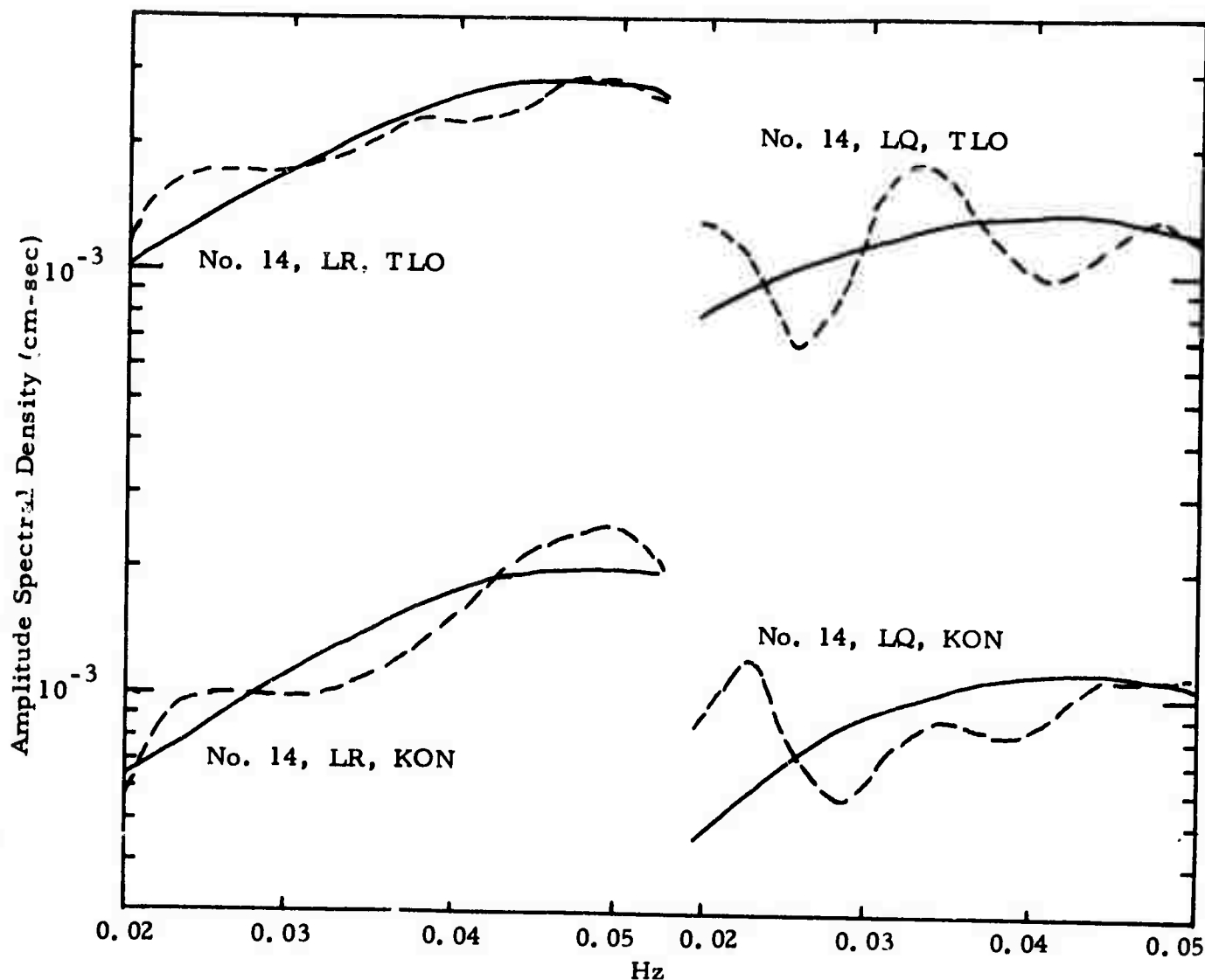
The spectral data for Events 15 and 16 as shown in Figure III-11, are contaminated by modulations, especially for Love waves. For Event 15, the residual errors are narrowly distributed in the range of 55 to 70 km, but a clear selection of the earthquake parameters is difficult. The Love waves for Event 16 have a sharp node at 0.038 Hz which probably is due to propagation effects. The residual errors are distributed equally in two narrow ranges, 5 to 10 km and 45 to 55 km, making a clear choice of focal depth difficult. According to the best-fit solutions, both Events 15 and 16 have oblique-slip source mechanisms. In view of the poor data quality these solutions should be taken with caution.

E. EARTHQUAKES IN THE CAUCASUS (See Section II)

F. EARTHQUAKES IN IRAN

Six events were studied for the region in Iran (Table III-7), and the source parameters obtained for these events are given in Table III-8. In general, the Love wave amplitude spectra have much higher levels than the Rayleigh wave amplitude spectra for the events in this region.

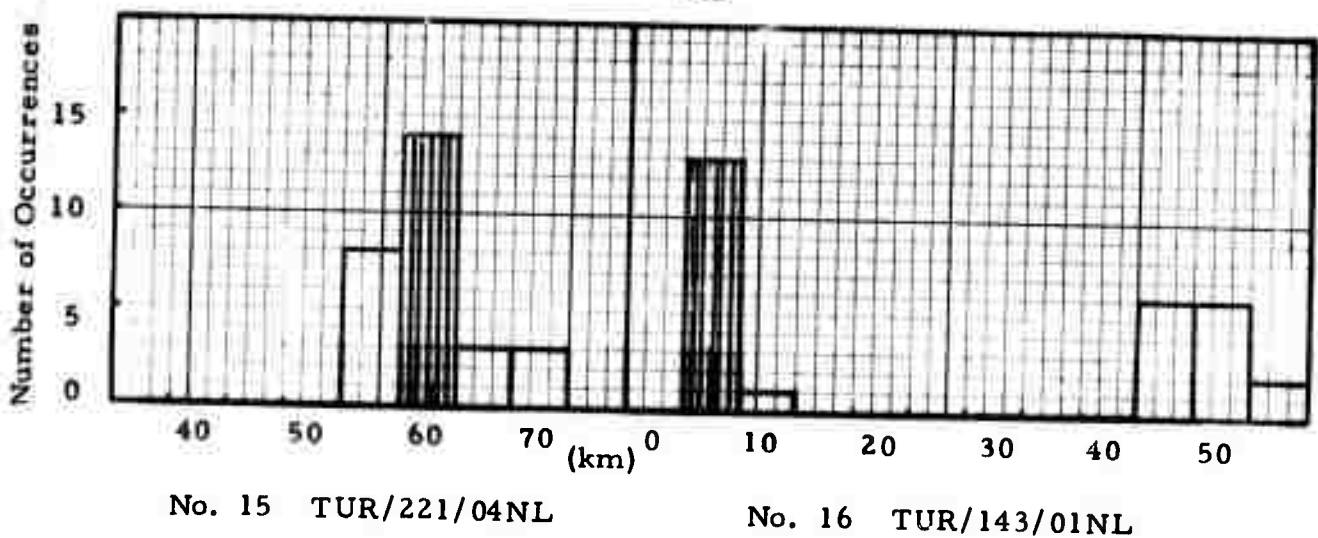
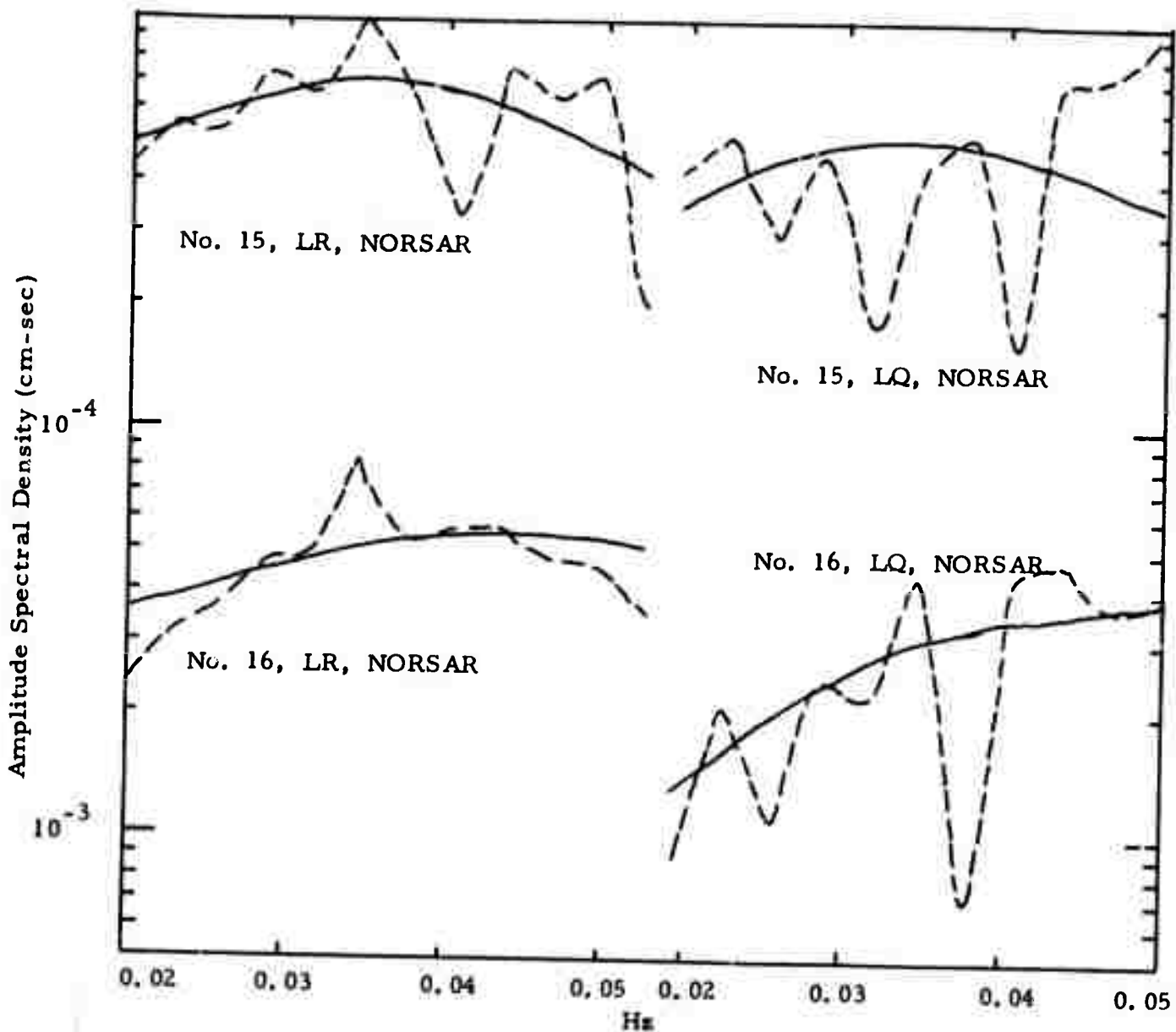
For Event 23 (Figure III-12), the nodes are not consistent between the 'best-fit' theoretical and the observed Rayleigh-wave spectra. The residuals from the twenty-eight subsets are distributed in the narrow range of focal depth from 45 to 50 km, with the 'best-fit' solution indicating a vertical strike-slip source mechanism. The residuals for Event 24 indicate a depth range of 70 to 90 km.



No. 14 LX/TURKE/047

FIGURE III-10

LR AND LQ SPECTRA FOR EVENT 14 (KON, TLO) AND THE CORRESPONDING DISTRIBUTION OF ESTIMATED FOCAL DEPTHS



No. 15 TUR/221/04NL

No. 16 TUR/143/01NL

FIGURE III-11

LR AND LQ SPECTRA FOR EVENTS 15 AND 16 (NORSAR) AND THE CORRESPONDING DISTRIBUTION OF ESTIMATED FOCAL DEPTHS

TABLE III-7  
PDE INFORMATION FOR EARTHQUAKE-EVENTS IN IRAN

| I. D. No. | Event Name   | Date     | Time     | Location |           | Focal Depth | $m_b$ | Data Site |
|-----------|--------------|----------|----------|----------|-----------|-------------|-------|-----------|
|           |              |          |          | Latitude | Longitude |             |       |           |
| 23        | IRA*006*09NL | 01/06/72 | 09.41.33 | 30.3N    | 50.0E     | 41          | 5.2   | NORSAR    |
| 24        | LX/IRANN/264 | 10/05/71 | 22.45.04 | 31.6N    | 50.7E     | 66          | 4.1   | KON       |
| 25        | LX/SIRAN/273 | 10/23/71 | 11.49.21 | 29.6N    | 51.3E     | 33          | 4.5   | KON, CHG  |
| 26        | LX/SIRAN/289 | 11/08/71 | 03.06.36 | 27.1N    | 54.5E     | 36          | 5.6   | KON       |
| 27        | LX/SIRAN/290 | 11/09/71 | 00.16.58 | 27.0N    | 54.5E     | 33          | 4.8   | KON       |
| 28        | LX/SIRAN/276 | 10/05/71 | 18.31.18 | 27.2N    | 55.8E     | 39          | 5.1   | KON       |

TABLE III-8  
THEORETICAL SOLUTION OF SOURCE MECHANISM FOR  
EARTHQUAKE-EVENTS IN IRAN

| I. D. No. | Event Name   | Strike  | Dip Angle | Slip Angle | Focal Depth (km) | Moment $M(\times 10^{25} \text{ dyne-cm})$ |
|-----------|--------------|---------|-----------|------------|------------------|--|
| 23        | IRA*006*09NL | N 70°E  | 90        | 0          | 45               | $0.27 \times 10^{-1}$                      |
| 24        | LX/IRANN/264 | N 100°E | 90        | 0          | 80               | $0.16 \times 10^{-1}$                      |
| 25        | LX/SIRAN/273 | N 20°E  | 70        | 30         | 80               | $0.85 \times 10^{-1}$                      |
| 26        | LX/SIRAN/289 | N 140°E | 90        | 0          | 80               | 4.3  |
| 27        | LX/SIRAN/290 | N 140°E | 60        | 30         | 65               | $0.41 \times 10^{-1}$                      |
| 28        | LX/SIRAN/276 | N 110°E | 80        | -30        | 60               | $0.37 \times 10^{-1}$                      |

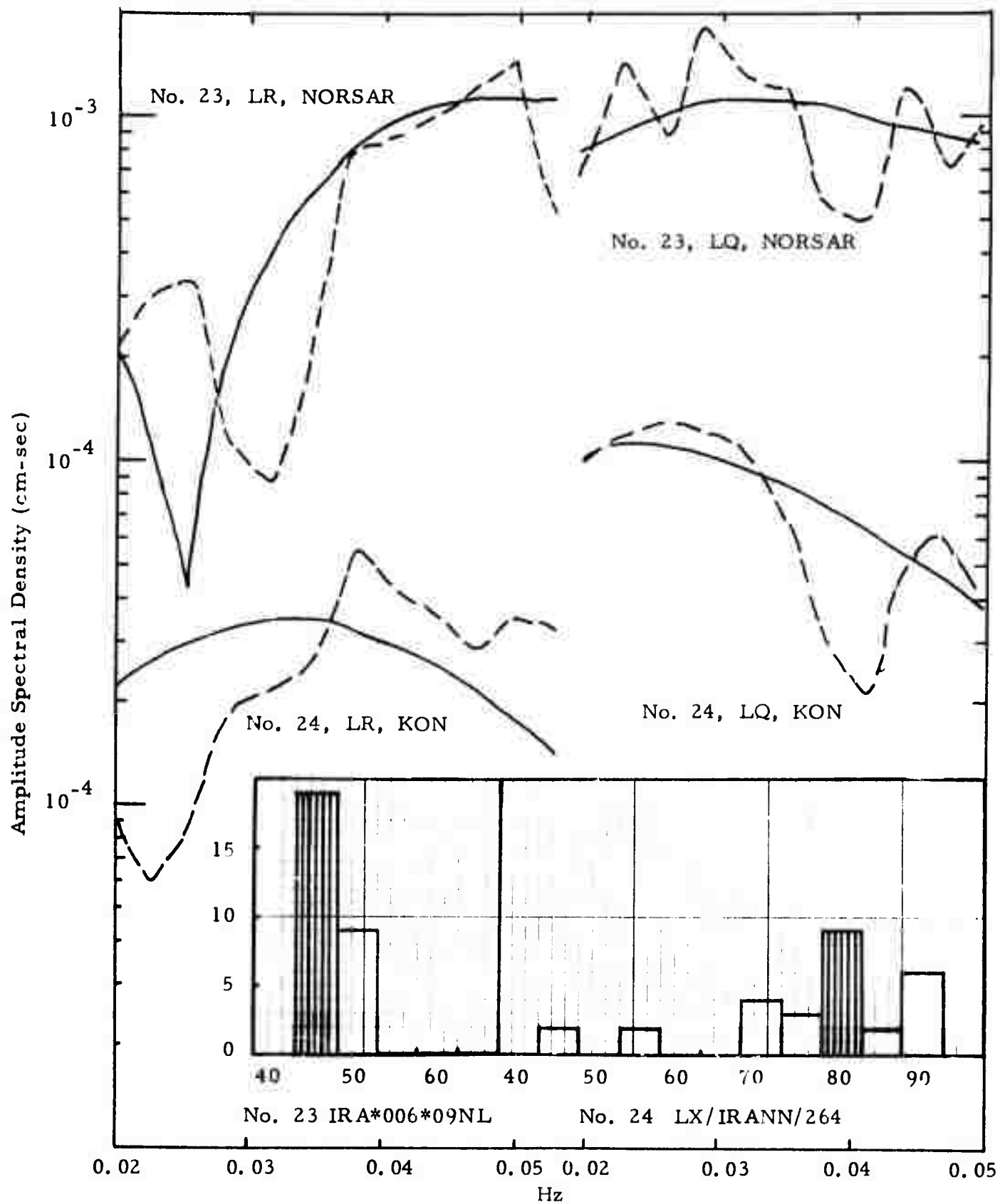


FIGURE III-12

LR AND LQ SPECTRA FOR EVENT 23 (NORSAR) AND EVENT 24 (KON)  
AND THE CORRESPONDING DISTRIBUTION OF ESTIMATED FOCAL DEPTHS

Event 25 (Figure III-13) has a profile of residual-errors which indicates that the focal depth may be in the range from 60 to 90 km for this earthquake. The best-fit solution for the strike-direction, dip angle, and slip angle suggests an oblique-slip source mechanism.

For Event 26 (Figure III-14), both the Rayleigh and Love waves have a high spectral amplitude level. The residual errors are scattered in a wide range from 45 to 105 km with the minimum value taking place at 80 km. A strike-slip source mechanism is suggested by the best-fit solution. The residual errors for Event 27 are distributed in the narrow range of 60 to 70 km (Figure III-14). According to the best-fit solution, the event has an oblique-slip source mechanism. Since Events 26 and 27 are located at the same place and their spectra are not too different, the difference in the inferred source mechanisms is probably not real but merely reflects poor resolution.

The focal depth for Event 28 (Figure III-15) is put in the range of 55 to 70 km. The other earthquake parameters suggest an oblique-slip source mechanism for the event.

Examining all of the results for this region, it can be seen that, the Love-wave spectral shapes show higher amplitude values at lower frequencies and lower amplitude values at the higher frequencies than is normally observed in the band (0.02 to 0.05 Hz) of interest. This has caused our automatic spectral fitting procedure to place relatively large focal depths for these earthquakes.

#### G. EARTHQUAKES IN TADZHIK

Five events recorded at NORSAR have been studied for the region in Tadzhik (Table III-9), and the estimated parameters for these events are given in Table III-10. The excitation of the Love-waves are generally lower than those for the Rayleigh waves with the exception of Event 33, which is located to the northeast of the other four events. Generally, the spectral shapes

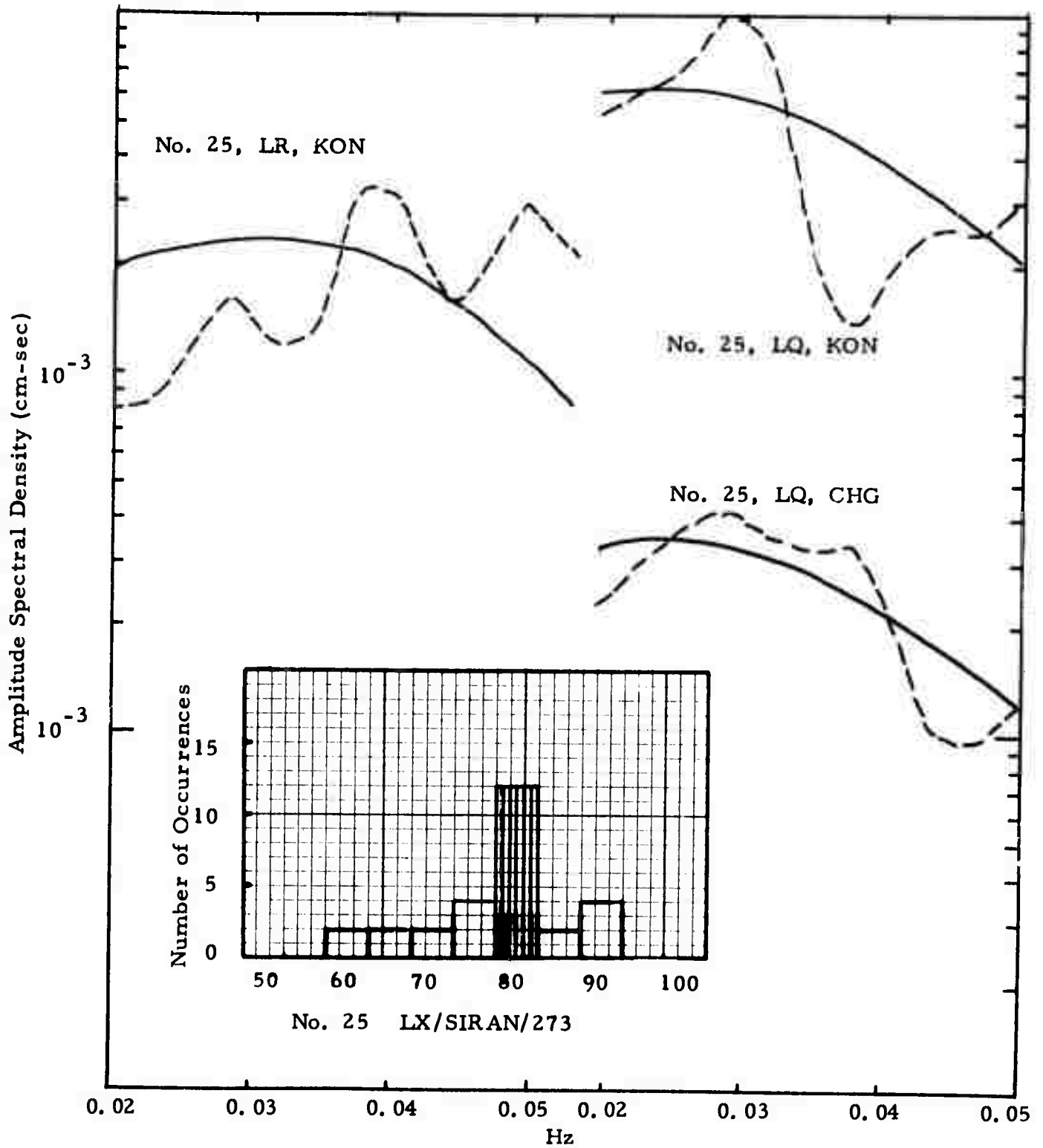


FIGURE III-13

LR AND LQ SPECTRA FOR EVENT 25 (KON; CHG) AND THE  
CORRESPONDING DISTRIBUTION OF ESTIMATED FOCAL DEPTHS

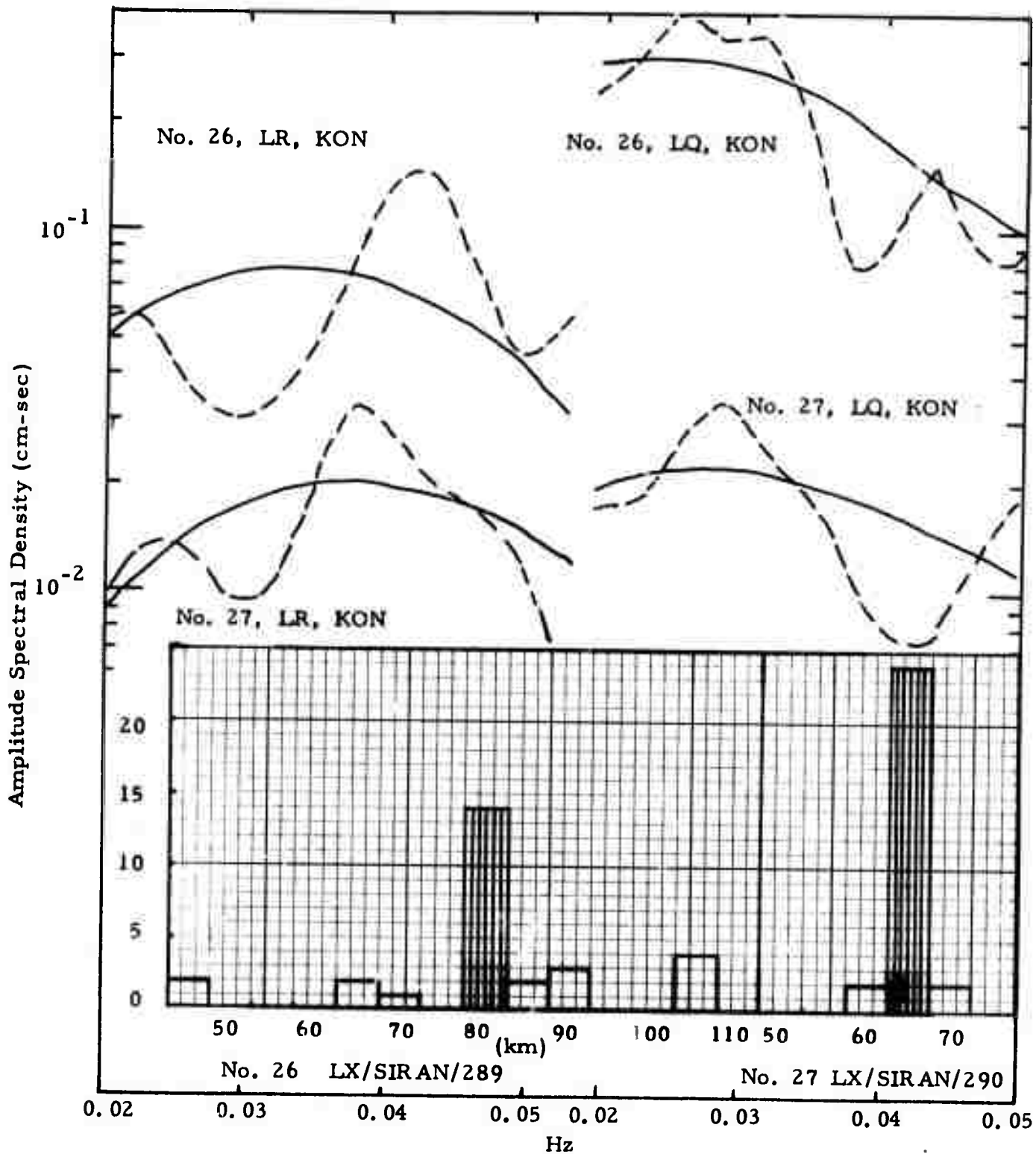
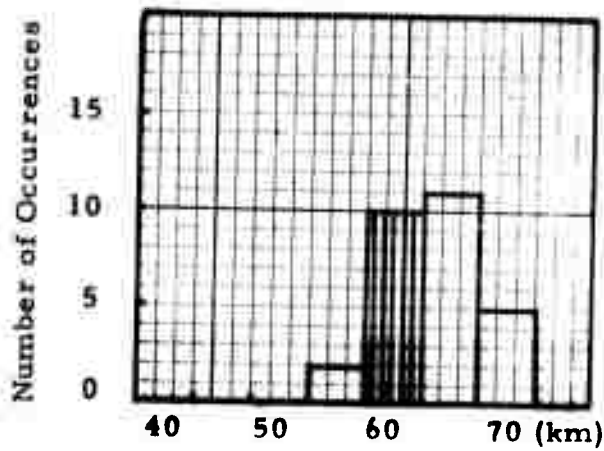
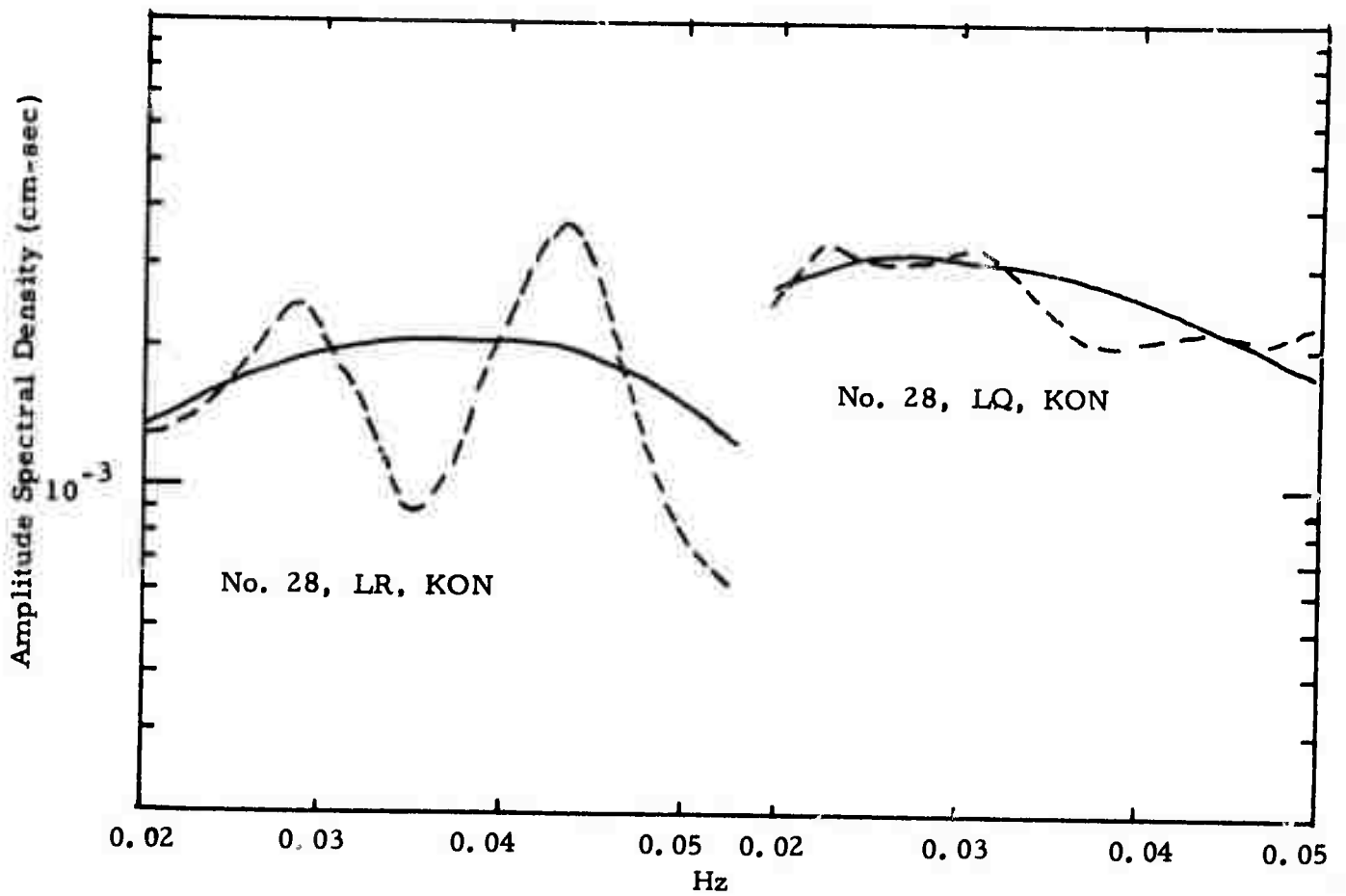


FIGURE III-14

LR AND LQ SPECTRA FOR EVENTS 26 AND 27 (KON) AND THE CORRESPONDING DISTRIBUTION OF ESTIMATED FOCAL DEPTHS



No. 28 LX/SIRAN/276

FIGURE III-15

LR AND LQ SPECTRA FOR EVENT 28 (KON) AND THE CORRESPONDING DISTRIBUTION OF ESTIMATED FOCAL DEPTHS

TABLE III-9  
PDE INFORMATION FOR EVENTS IN TADZHIK

| I. D. No. | Event Name    | Date     | Time     | Location |           | Focal Depth | m <sub>b</sub> | Data Site |
|-----------|---------------|----------|----------|----------|-----------|-------------|----------------|-----------|
|           |               |          |          | Latitude | Longitude |             |                |           |
| 29        | AFG*059*18NL* | 02/28/72 | 18.12.23 | 36.0N    | 68.7E     | N           | 4.4            | NORSAR    |
| 30        | TAD*077*09NL  | 03/17/72 | 09.17.11 | 40.1N    | 69.7E     | 26          | 5.2            | NORSAR    |
| 31        | TDZ/147/00NL  | 05/27/71 | 00.30.28 | 38.3N    | 69.0E     | 36          | 4.8            | NORSAR    |
| 32        | TDZ/274/16NL  | 10/01/71 | 16.27.48 | 38.6N    | 69.8E     | 36          | 4.9            | NORSAR    |
| 33        | KRG/301/13NL  | 10/28/71 | 13.30.57 | 41.9N    | 72.4E     | N           | 5.5            | NORSAR    |

\* = ISB

TABLE III-10  
THEORETICAL SOLUTION OF SOURCE MECHANISM FOR  
EARTHQUAKE-EVENTS IN TADZHIK

| I. D. No. | Event Name   | Strike  | Dip Angle | Slip Angle | Focal Depth (km) | Moment $M(\times 10^{25} \text{ dyne-cm})$ |
|-----------|--------------|---------|-----------|------------|------------------|--|
| 29        | AFG*059*18NL | N 150°E | 60        | 60         | 40               | 0.13x10 <sup>-1</sup>                      |
| 30        | TAD*077*09NL | N 0°E   | 80        | 90         | 20               | 0.68x10 <sup>-1</sup>                      |
| 31        | TDZ/147/00NL | N 80°E  | 70        | -30        | 5                | 0.86x10 <sup>-2</sup>                      |
| 32        | TDZ/274/16NL | N 160°E | 80        | 60         | 5                | 0.20x10 <sup>-1</sup>                      |
| 33        | KRG/301/13NL | N 20°E  | 90        | 60         | 40               | 0.37                                       |

for both the Rayleigh and Love waves are curved up from the lower frequencies to the higher frequencies, and tend to give relatively shallow focal depths.

For Event 29, the residual errors are evenly distributed in the focal depth range of 30 to 50 km, as shown in Figure III-16, and other source parameters suggest an oblique-slip source mechanism. The focal depth for Event 30 is located in the 10 to 30 km range with the greatest possibility at 20 km. The other source parameters of the best-fit solution suggest a dip-slip source mechanism for this earthquake.

Because of the variations of the spectral shapes for Event 31 (Figure III-17), a good estimation of the source parameters is not possible. The residual errors are very close to each other and are scattered in three spots, with the focal depth at 0, 5 or 35 km.

The observed amplitude spectra for Event 32 (Figure III-18) are modulated, with the modulation more severe at the higher frequencies. The profile of residual errors places the focal depth in two ranges, from 5 to 10 km or from 30 to 40 km. The best-fit solution in Table III-10 picks an oblique-slip source mechanism for this event. For Event 33, the focal depth lies in the range of 30 to 45 km with the best-fit dip and slip angles defining an oblique-slip source mechanism. The best-fit theoretical spectra follow quite closely the general shapes of their observed counterparts for Events 32 and 33. Even so, the spectral modulations may still keep the resolution for the best-fit solution relatively low.

#### H. EARTHQUAKES IN SINKIANG, CHINA

Ten events have been studied, using NORSAR data, for the region in Sinkiang, China (Table III-11). The earthquake parameters obtained for these events are shown in Table III-12. In general, the spectral shapes of the Rayleigh waves are characterized by nodes in the 0.025 to 0.035 Hz band. The source

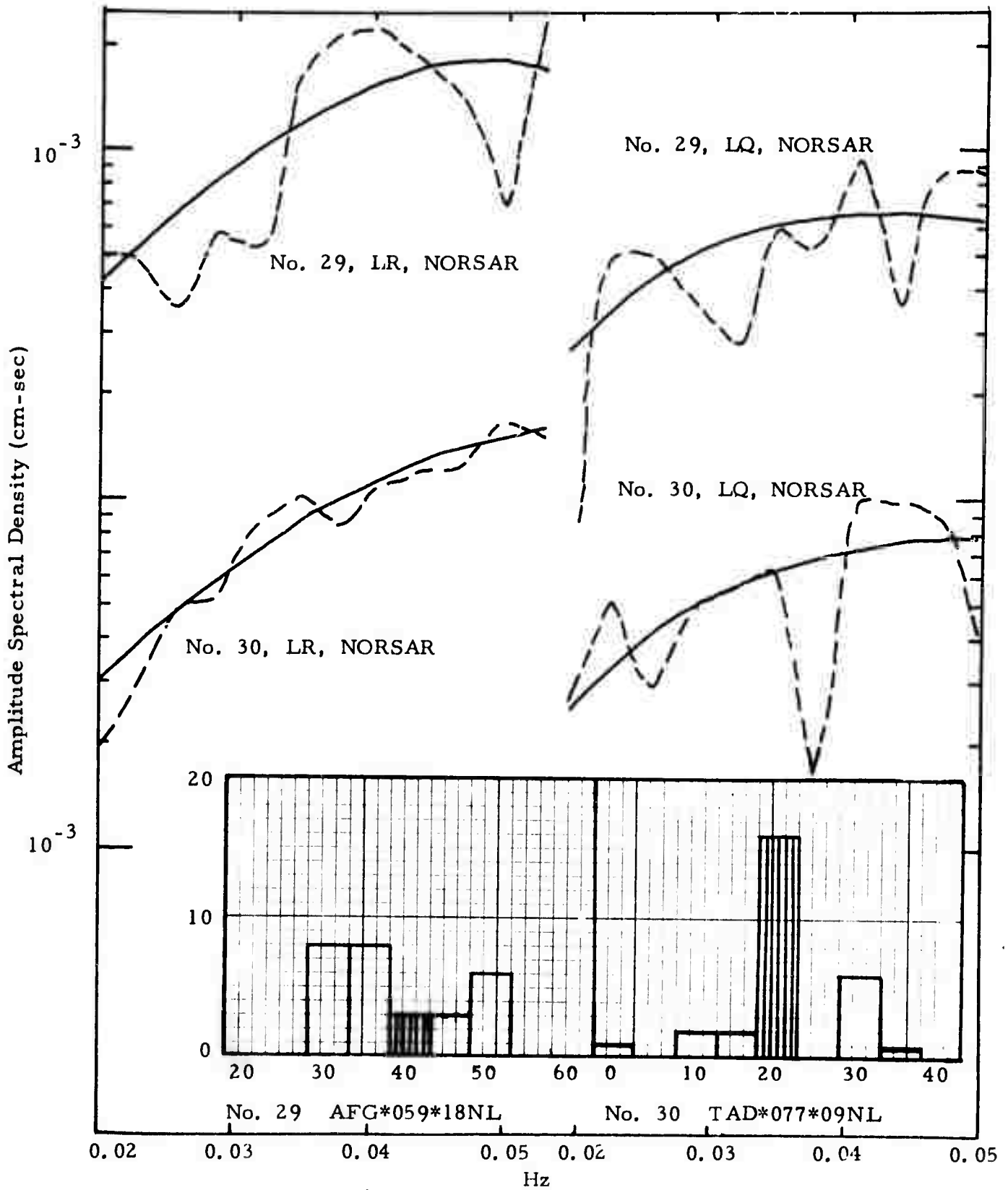
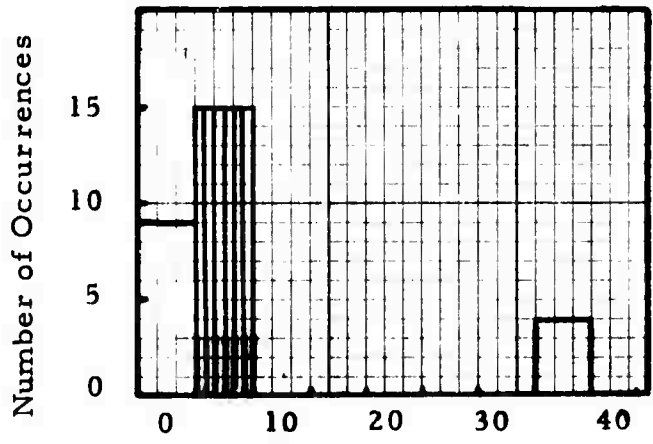
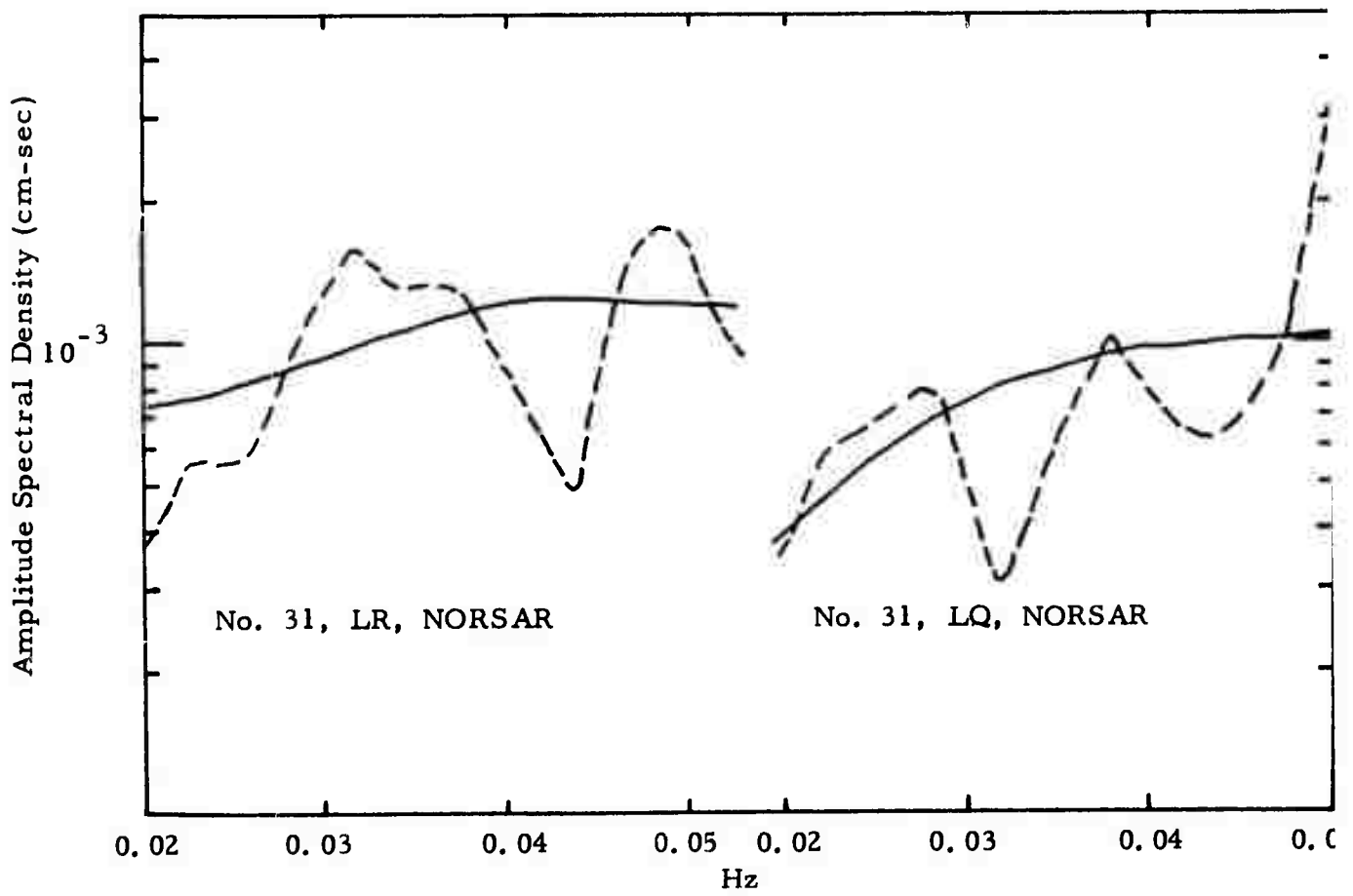


FIGURE III-16

LR AND LQ SPECTRA FOR EVENTS 29 AND 30 (NORSAR) AND THE CORRESPONDING DISTRIBUTION OF ESTIMATED FOCAL DEPTHS



No. 31 TDX/147/00NL

FIGURE III-17

LR AND LQ SPECTRA FOR EVENT 31 (NORSAR) AND THE  
CORRESPONDING DISTRIBUTION OF ESTIMATED FOCAL DEPTHS

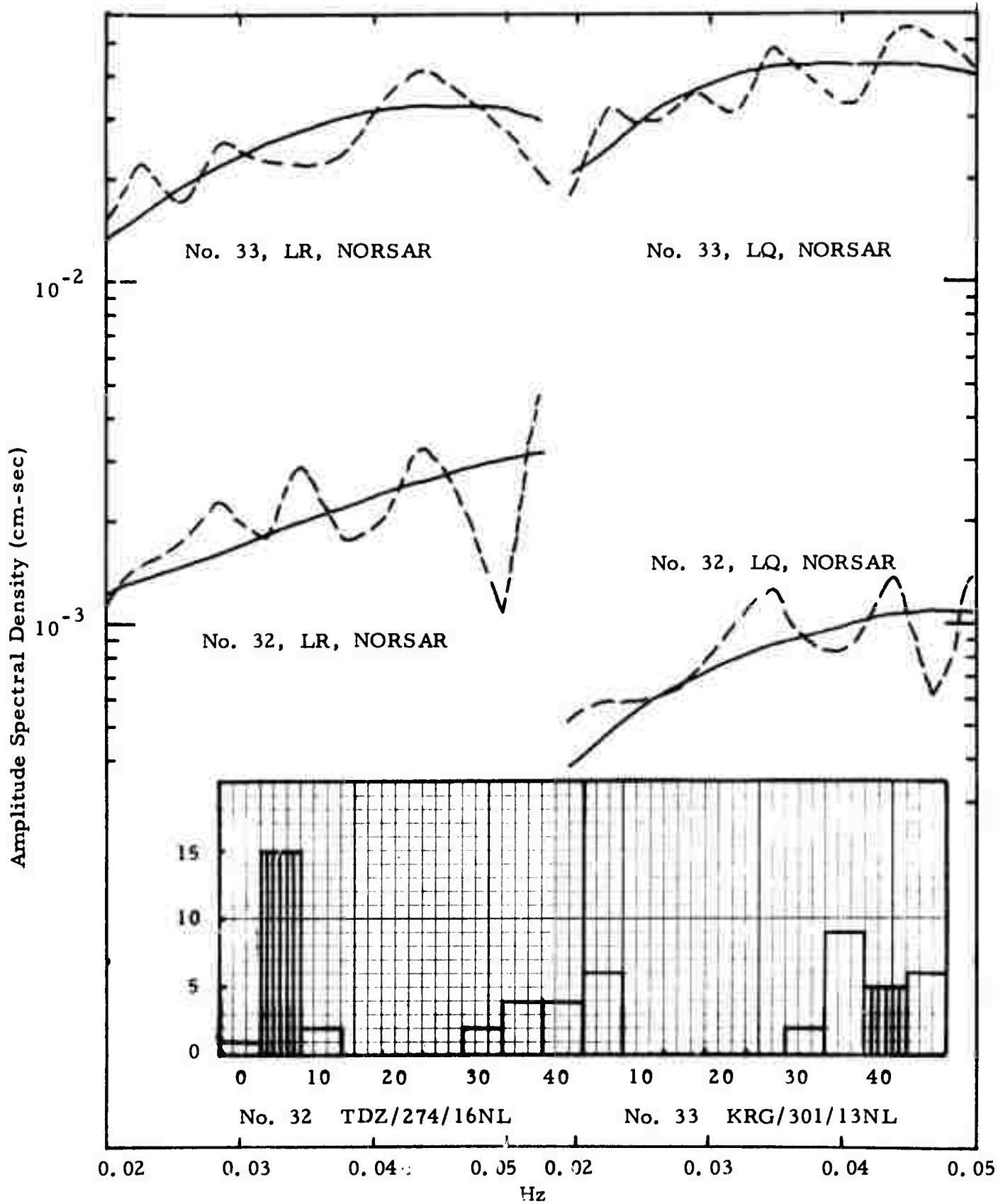


FIGURE III-18

LR AND LQ SPECTRA FOR EVENTS 32 AND 33 (NORSAR) AND THE  
CORRESPONDING DISTRIBUTION OF ESTIMATED FOCAL DEPTHS  
III-35

TABLE III-11

## PDE INFORMATION FOR EARTHQUAKE-EVENTS IN SINKIANG, CHINA

| I. D. No. | Event Name    | Date     | Time     | Location |           | Focal Depth | $m_b$ | Data Site |
|-----------|---------------|----------|----------|----------|-----------|-------------|-------|-----------|
|           |               |          |          | Latitude | Longitude |             |       |           |
| 34        | SIN*075*00NL  | 03/15/72 | 00.21.25 | 38.5N    | 72.3E     | 140         | 3.7   | NORSAR    |
| 35        | SIN/219/15NL  | 08/07/71 | 15.21.53 | 36.1N    | 77.7E     | N           | 4.8   | NORSAR    |
| 36        | SIN*042*05NL  | 02/11/72 | 05.55.46 | 39.9N    | 77.4E     | 23          | 4.9   | NORSAR    |
| 37        | CHI/298/13NL  | 07/27/71 | 12.48.32 | 38.9N    | 78.1E     | N           | 5.3   | NORSAR    |
| 38        | SIN/170/17NL  | 06/19/71 | 17.23.03 | 41.5N    | 79.3E     | N           | 5.2   | NORSAR    |
| 39        | SIN/166/23NL  | 06/15/71 | 23.17.34 | 41.6N    | 79.2E     | N           | 4.9   | NORSAR    |
| 40        | SIN*064*04NL* | 03/04/72 | 04.00.09 | 40.2N    | 79.0E     | N           | 4.5   | NORSAR    |
| 41        | SIN/221/01NL  | 08/09/71 | 01.03.17 | 42.1N    | 83.4E     | N           | 4.2   | NORSAR    |
| 42        | SIN*002*10NA  | 01/02/72 | 10.27.35 | 41.8N    | 84.5E     | N           | 5.2   | NORSAR    |
| 43        | SIN/273/12NL  | 09/30/72 | 12.43.45 | 50.0N    | 88.0E     | N           | 4.5   | NORSAR    |

\* = ISB

TABLE III-12

THEORETICAL SOLUTION OF SOURCE MECHANISM FOR  
EARTHQUAKE-EVENTS IN SINKIANG, CHINA

| L. D. No. | Event Name   | Strike  | Dip Angle | Slip Angle | Focal Depth<br>(km) | Moment<br>$M(x10^{25}$ dyne-cm.) |
|-----------|--------------|---------|-----------|------------|---------------------|----------------------------------|
| 34        | SIN*075*00NL | N 50°E  | 90        | 90         | 45                  | $0.12 \times 10^{-1}$            |
| 35        | SIN/219/15NL | N 160°E | 80        | 0.0        | 65                  | 0.13                             |
| 36        | SIN*042*05NL | N 80°E  | 60        | 60         | 10                  | $0.24 \times 10^{-1}$            |
| 37        | CHI/208/13NL | N 80°E  | 80        | 90         | 5                   | $0.49 \times 10^{-1}$            |
| 38        | SIN/170/17NL | N 70°E  | 70        | -60        | 15                  | 0.17                             |
| 39        | SIN/166/23NL | N 20°E  | 90        | 0          | 5                   | $0.48 \times 10^{-2}$            |
| 40        | SIN*064*04NL | N 0°E   | 70        | 0          | 25                  | $0.20 \times 10^{-1}$            |
| 41        | SIN/221/01NL | N 90°E  | 60        | -60        | 15                  | $0.34 \times 10^{-2}$            |
| 42        | SIN*002*10NA | N 0°E   | 70        | 30         | 25                  | $0.32 \times 10^{-1}$            |
| 43        | SIN/273/12NL | N 90°E  | 70        | -60        | 20                  | $0.76 \times 10^{-2}$            |

parameters suggest a dip angle near  $70^{\circ}$  -  $80^{\circ}$  and the strike direction is approximately  $N90^{\circ}E$  for this region.

For example, Event 34 (Figure III-19) has a node in the Rayleigh-wave spectrum in the 0.025 to 0.035 Hz band. The residual errors yield a focal depth in the range of 30 to 45 km, with the high frequency Love wave energy indicating that a deeper focus is very unlikely. Event 35 (Figure III-19) yielded residual errors indicating a focal depth in the range of 55 to 75 km with a higher possibility in the 60 to 65 km range. The best-fit dip and slip angles define a strike-slip source mechanism. The difference in the Love wave spectral shapes between Events 34 and 35 is remarkable.

The residual errors for Event 36 (Figure III-20) indicate a focal depth in the 5 to 15 km range, with the dip and slip angles consistent with an oblique-slip source mechanism. The spectral shape for Event 37 are similar to those of Event 36. The focal depth is estimated to be in 5 to 15 km range. The best-fit dip and slip angles suggest a dip-slip source mechanism. Both Events 36 and 37 yield a consistent strike direction of  $N80^{\circ}E$ . The difference in the best-fit estimates of dip and slip angles between Events 36 and 37 is questionable.

Events 38 and 39 have nodes at 0.035 Hz in the Rayleigh wave spectra (Figure III-21). The residual errors yield relatively shallow source parameters in Table III-12, Event 38 is an oblique-slip fault whereas Event 39 has a strike-slip source mechanism.

Event 40 has deep nodes in both the Rayleigh and Love wave amplitude spectra (Figure III-22). They are probably due to propagational effects rather than to the source mechanism. Residual errors place the focal depth in the 0-25 km range. For Event 41 (Figure III-22), the focal depth is in the 5 to 30 km range, with the strike direction estimated to be  $N90^{\circ}E$ . According to the best-fit dip and slip angles this event has an oblique-slip source mechanism.

The node on the 'best-fit' theoretical Rayleigh-wave spectra for Event 42 (Figure III-23) seems to be over-characterized. Residual errors

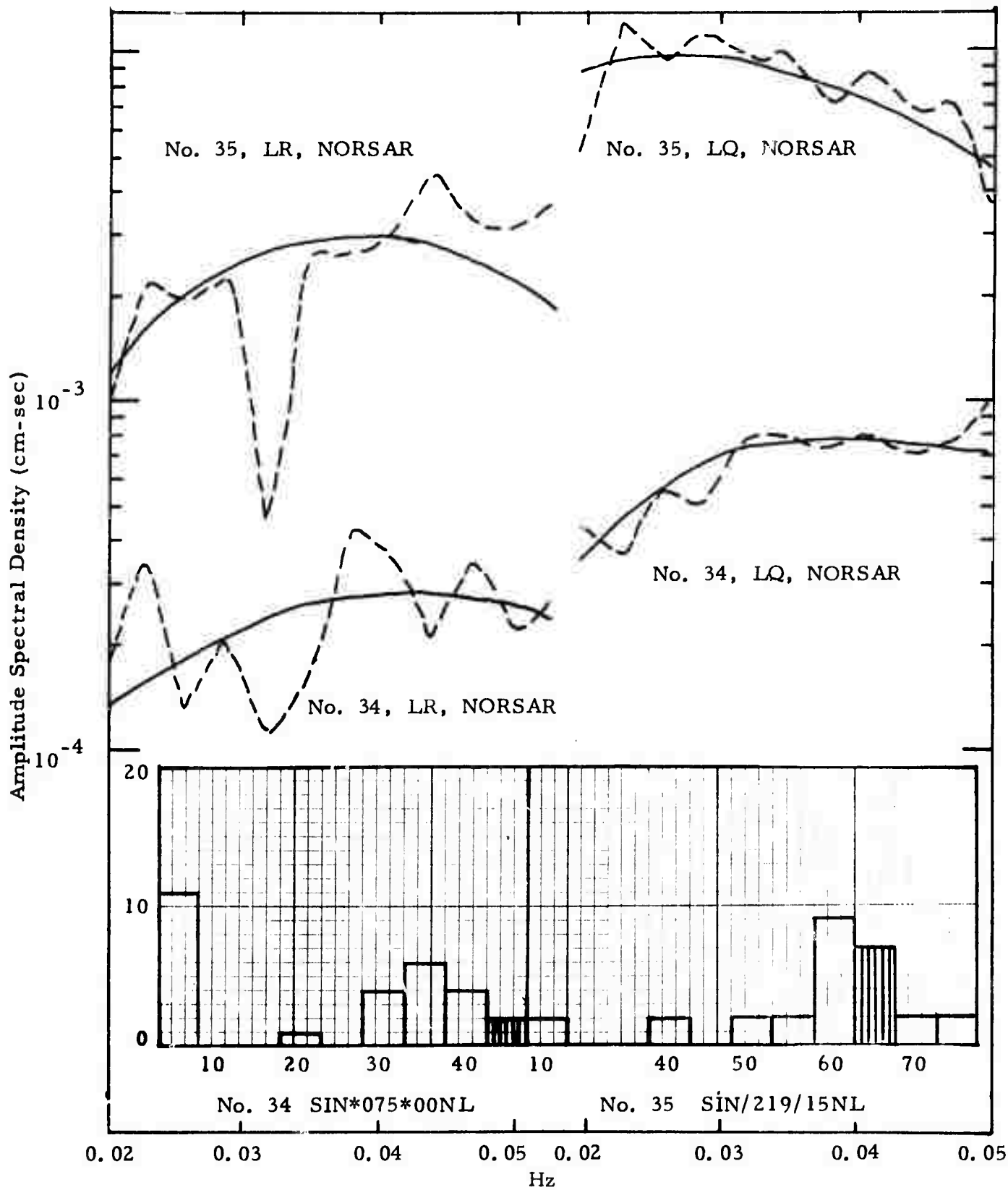


FIGURE III-19

LR AND LQ SPECTRA FOR EVENTS 34 AND 35 (NORSAR) AND THE CORRESPONDING DISTRIBUTION OF ESTIMATED FOCAL DEPTHS

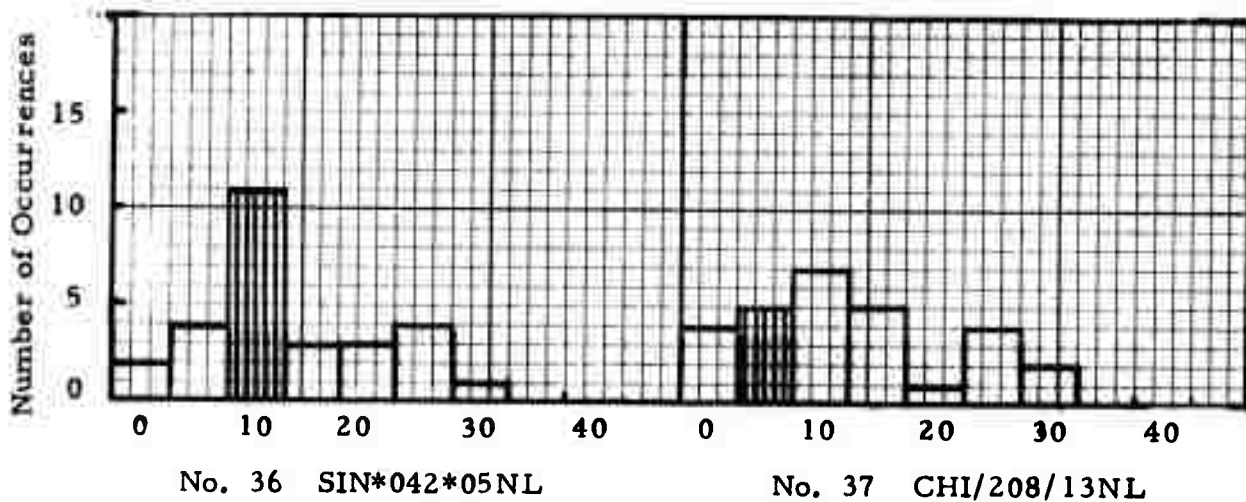
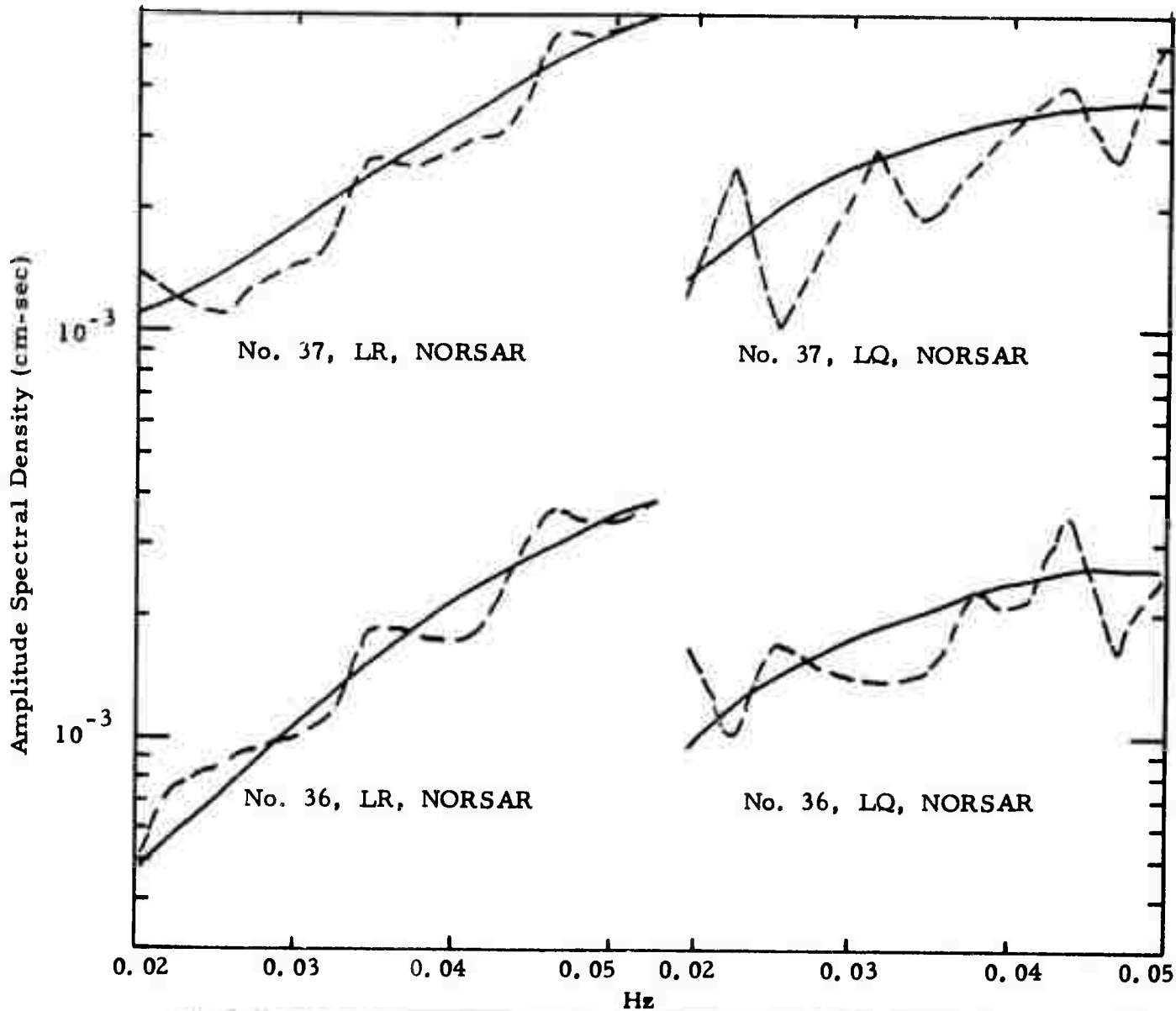


FIGURE III-20

LR AND LQ SPECTRA FOR EVENTS 36 AND 37 (NORSAR) AND THE CORRESPONDING DISTRIBUTION OF ESTIMATED FOCAL DEPTHS

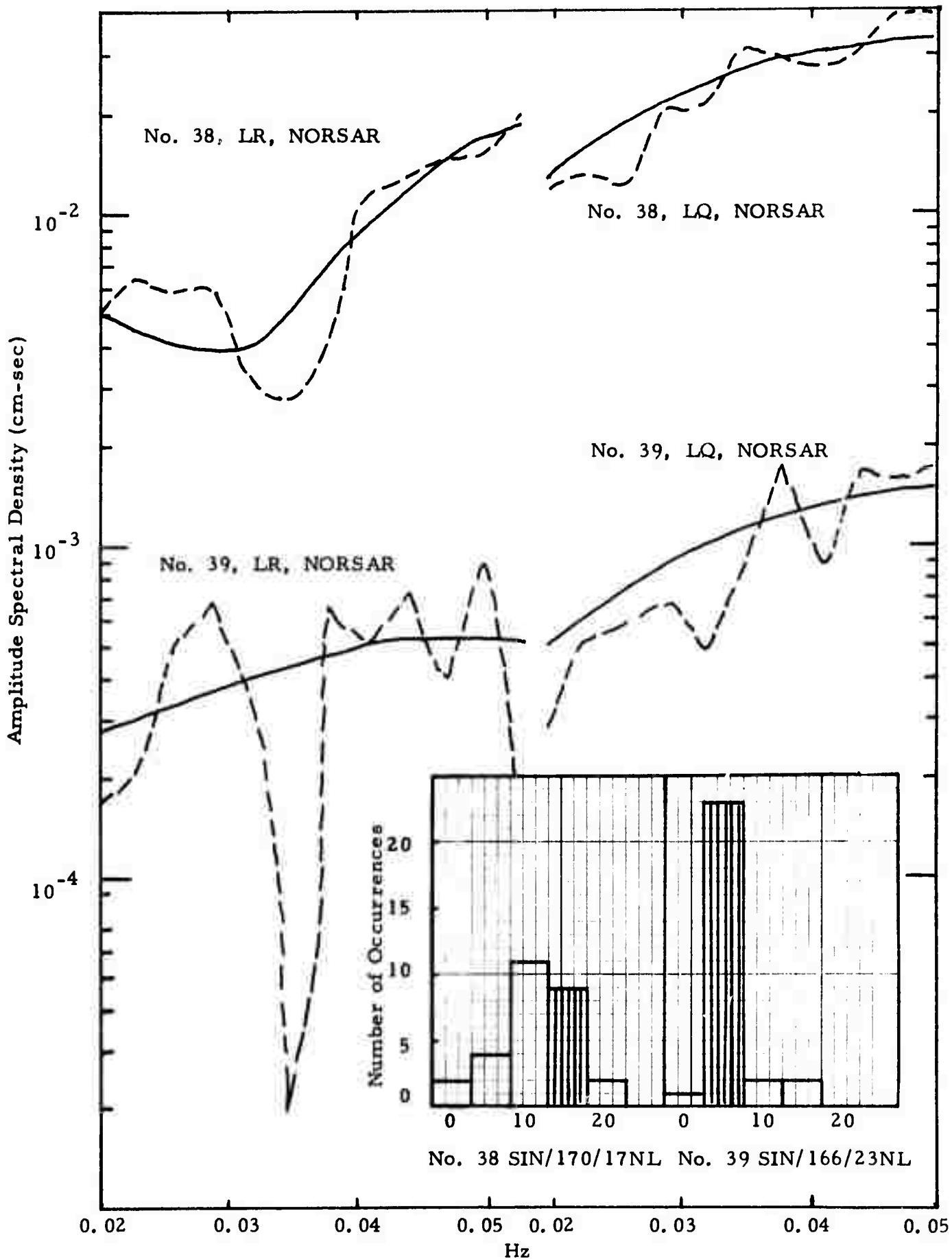


FIGURE III-21

LR AND LQ SPECTRA FOR EVENTS 38 AND 39 (NORSAR) AND THE CORRESPONDING DISTRIBUTION OF ESTIMATED FOCAL DEPTHS

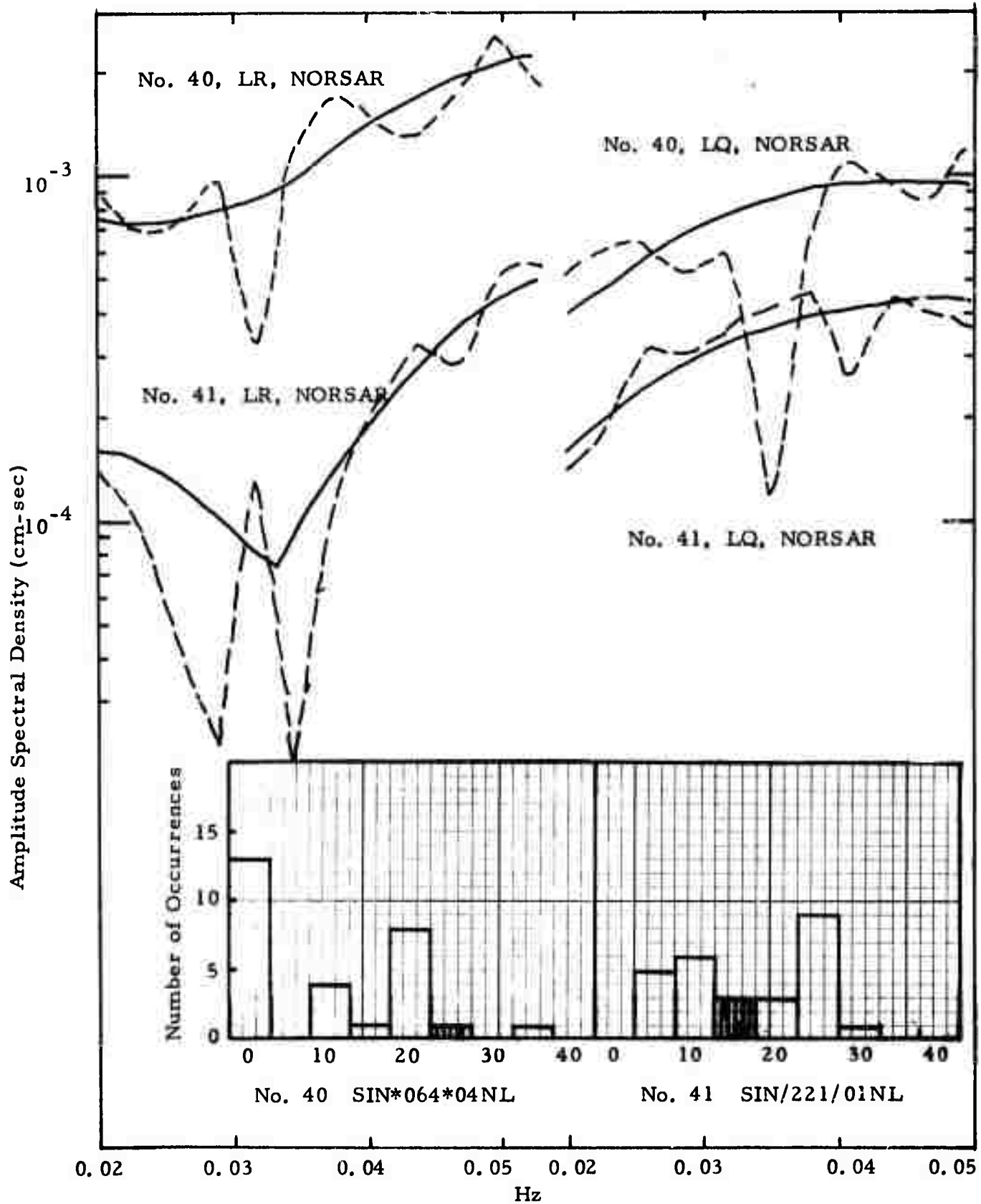


FIGURE III-22

LR AND LQ SPECTRA FOR EVENTS 40 AND 41 (NORSAR) AND THE CORRESPONDING DISTRIBUTION OF ESTIMATED FOCAL DEPTHS

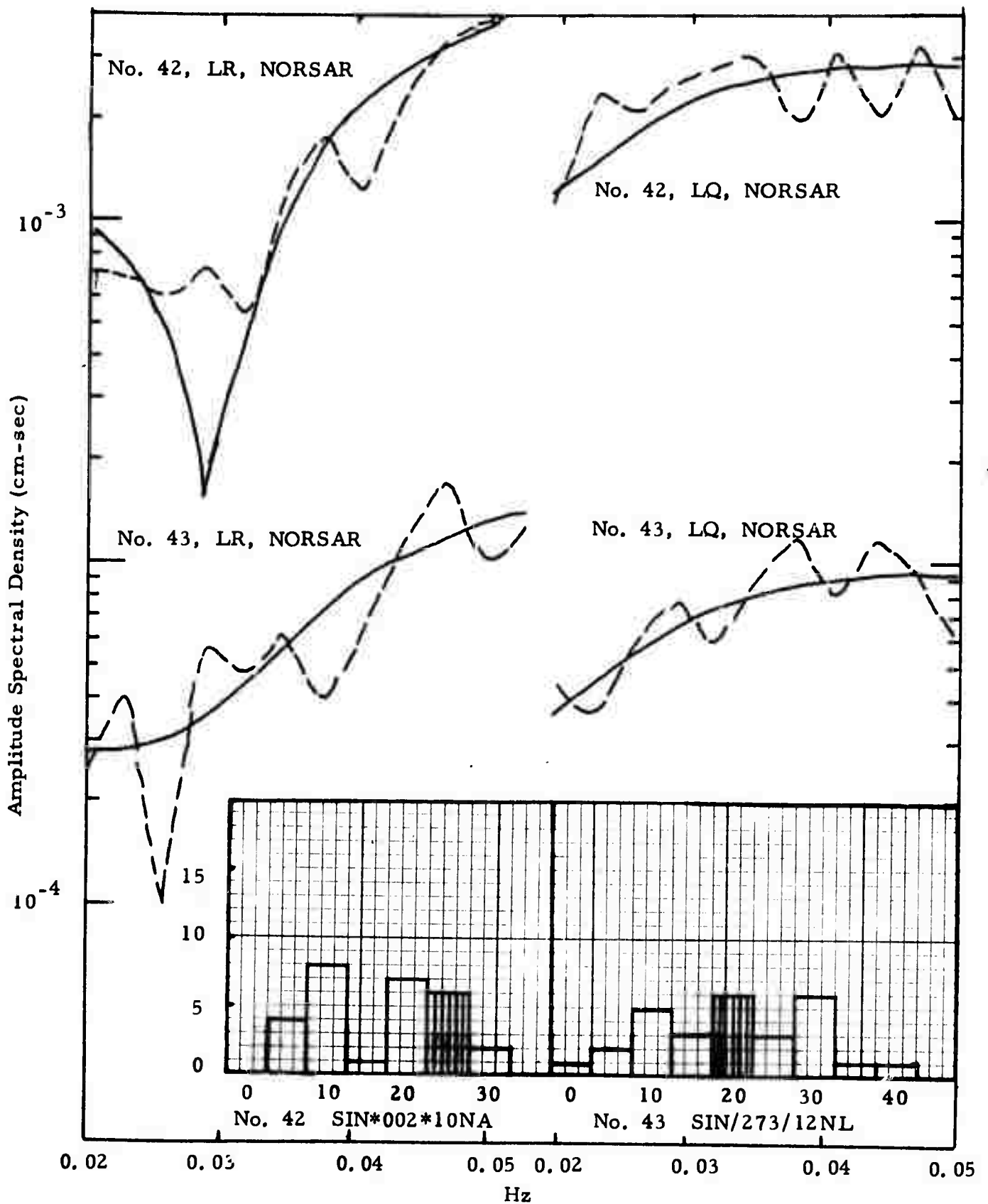


FIGURE III-23

LR AND LQ SPECTRA FOR EVENTS 42 AND 43 (NORSAR) AND THE CORRESPONDING DISTRIBUTION OF ESTIMATED FOCAL DEPTHS

indicate a focal depth of 5 to 30 km with the best estimate at 25 km. The Rayleigh wave spectra for Event 43 also has a deep node, which seems to be due to path effects. Residual errors show the mechanism as an oblique-slip fault with the strike direction,  $N90^{\circ}E$ , consistent with the other events in this region. The distribution of focal depth estimates spreads over a relatively wide range from 0 to 40 km. The best-fit focal depth of 20 km appears to be reasonable because of the relatively good spectral fitting as shown in Figure III-23.

Generally speaking, the LQ spectra are much less variable than the LR spectra observed at NORSAR for the earthquakes in this region. With the exception of Event 35, all of the other nine earthquakes in this region are placed at relatively shallow focal depths in the upper 25 km.

#### I. EARTHQUAKES IN TIBET, CHINA

Five events for the region in Tibet have been studied by using data recorded at NORSAR (Table III-13). The best-fit earthquake parameters are given in Table III-14.

For Event 44, (Figure III-24), the observed Love-wave spectrum is very modulated. The profile of residuals indicate a focal depth of 15 to 35 km, with the estimates of the dip and slip angles suggesting an oblique-slip faulting. The spectral fitting for Event 45 suggests a focal depth in the range of 35 to 45 km and an oblique-slip source mechanism.

The observed Rayleigh-wave spectrum for Event 46 (Figure III-25) is highly modulated and at a lower level than its counterpart for Love waves. All residual errors are close to each other with a maximum to minimum ratio of 1.1. The focal depth may be in the range of 5 to 40 km with the greatest possibility at 30 km, and the dip and slip angles suggest a strike-slip source mechanism. The Rayleigh-wave is very modulated for Event 47 (Figure III-25), with the residual errors confining the focal depth to the vicinity of 45 km. The source mechanism can be described as oblique slip faulting with the strike direction  $N10^{\circ}E$  or its orthogonal solution of  $N100^{\circ}E$ .

TABLE III-13  
PDE INFORMATION FOR EARTHQUAKE-EVENTS IN TIBET, CHINA

| I. D. No. | Event Name   | Date     | Time     | Location |           | Focal Depth | $m_b$ | Data Site |
|-----------|--------------|----------|----------|----------|-----------|-------------|-------|-----------|
|           |              |          |          | Latitude | Longitude |             |       |           |
| 44        | TIB/123/00NL | 05/03/71 | 00.33.23 | 30.8N    | 84.5E     | 16          | 5.4   | NORSAR    |
| 45        | TIB*075*06NL | 03/15/72 | 06.00.32 | 31.0N    | 85.0E     | N           | 5.3   | NORSAR    |
| 46        | TIB/302/17NL | 10/28/71 | 17.16.52 | 34.0N    | 86.0E     | N           | 5.0   | NORSAR    |
| 47        | TIB/155/20NL | 06/04/71 | 20.49.58 | 32.2N    | 92.1E     | N           | 5.0   | NORSAR    |
| 48        | CHI/283/05NL | 10/10/71 | 05.53.57 | 33.9N    | 95.0E     | N           | 4.4   | NORSAR    |

TABLE III-14  
THEORETICAL SOLUTION OF SOURCE MECHANISM FOR  
EARTHQUAKE-EVENTS IN TIBET, CHINA

| I. D. No. | Event Name   | Strike  | Dip Angle | Slip Angle | Focal Depth (km) | Moment $M(x10^{25} \text{ dyne-cm})$ |
|-----------|--------------|---------|-----------|------------|------------------|--------------------------------------|
| 44        | TIB/123/00NL | N 170°E | 60        | 30         | 35               | 0.240                                |
| 45        | TIB*075*06NL | N 70°E  | 60        | -30        | 40               | 0.023                                |
| 46        | TIB/302/17NL | N 160°E | 80        | 0          | 30               | 0.053                                |
| 47        | TIB/155/20NL | N 10°E  | 80        | 30         | 45               | 0.024                                |
| 48        | CHI/283/05NL | N 10°E  | 80        | 0          | 35               | 0.018                                |

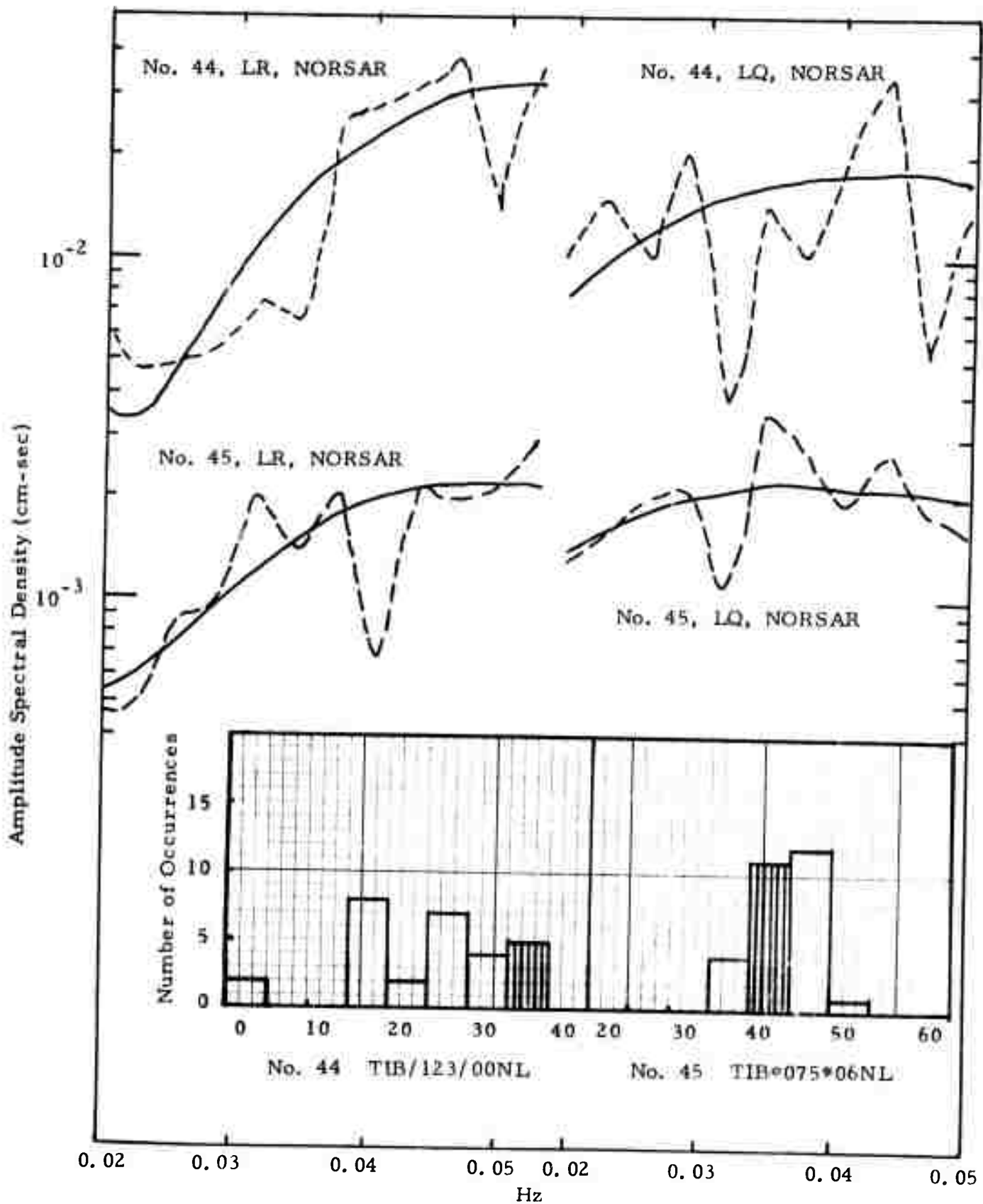


FIGURE III-24

LR AND LQ SPECTRA FOR EVENTS 44 AND 45 (NORSAR) AND THE CORRESPONDING DISTRIBUTION OF ESTIMATED FOCAL DEPTHS

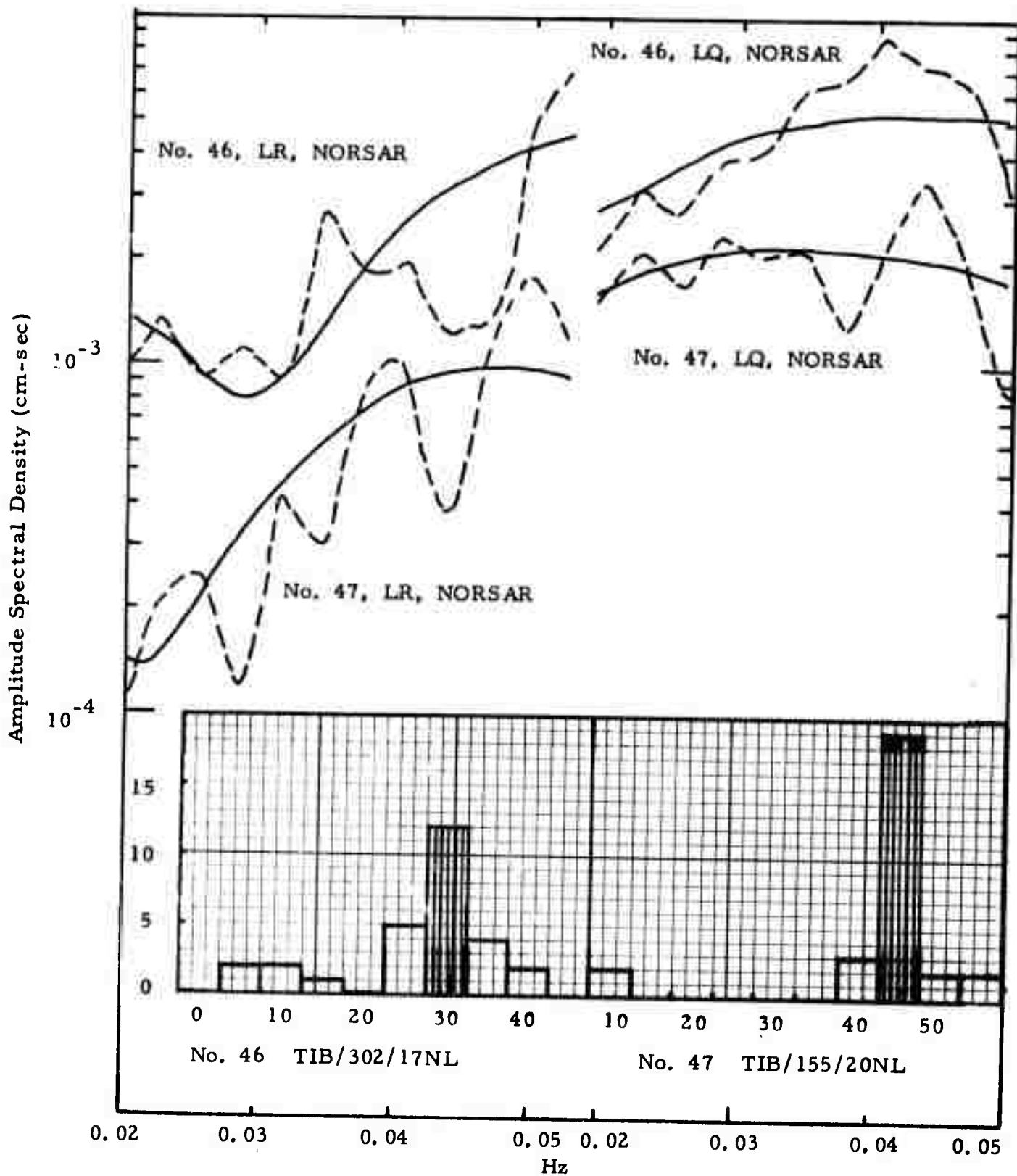


FIGURE III-25

LR AND LQ SPECTRA FOR EVENTS 46 AND 47 (NORSAR) AND THE CORRESPONDING DISTRIBUTION OF ESTIMATED FOCAL DEPTHS

For Event 48, the Rayleigh wave spectrum is also highly modulated (Figure III-26), with the residual error analysis yielding a focal depth of 25 to 40 km.

In general, we see that the Rayleigh wave spectra from events in Tibet are severely modulated, with these modulations probably due to multipath interference.

#### J. EARTHQUAKES IN NORTHEASTERN ASIA

The last three events studied with the data obtained from NOR-SAR are scattered in North Eastern Asia (Table III-15). The source mechanism solutions are given in Table III-16. All the observed spectra are severely modulated, as shown in Figure III-27 for Event 49. There are deep nodes at 0.03 Hz in both the Rayleigh and Love wave spectra, and hence the solutions are not considered reliable.

For Events 50 and 51, the spectra show some characteristics in common even though severely modulated. The focal depths are estimated to lie between 5 and 20 km, as shown in Figure III-28.

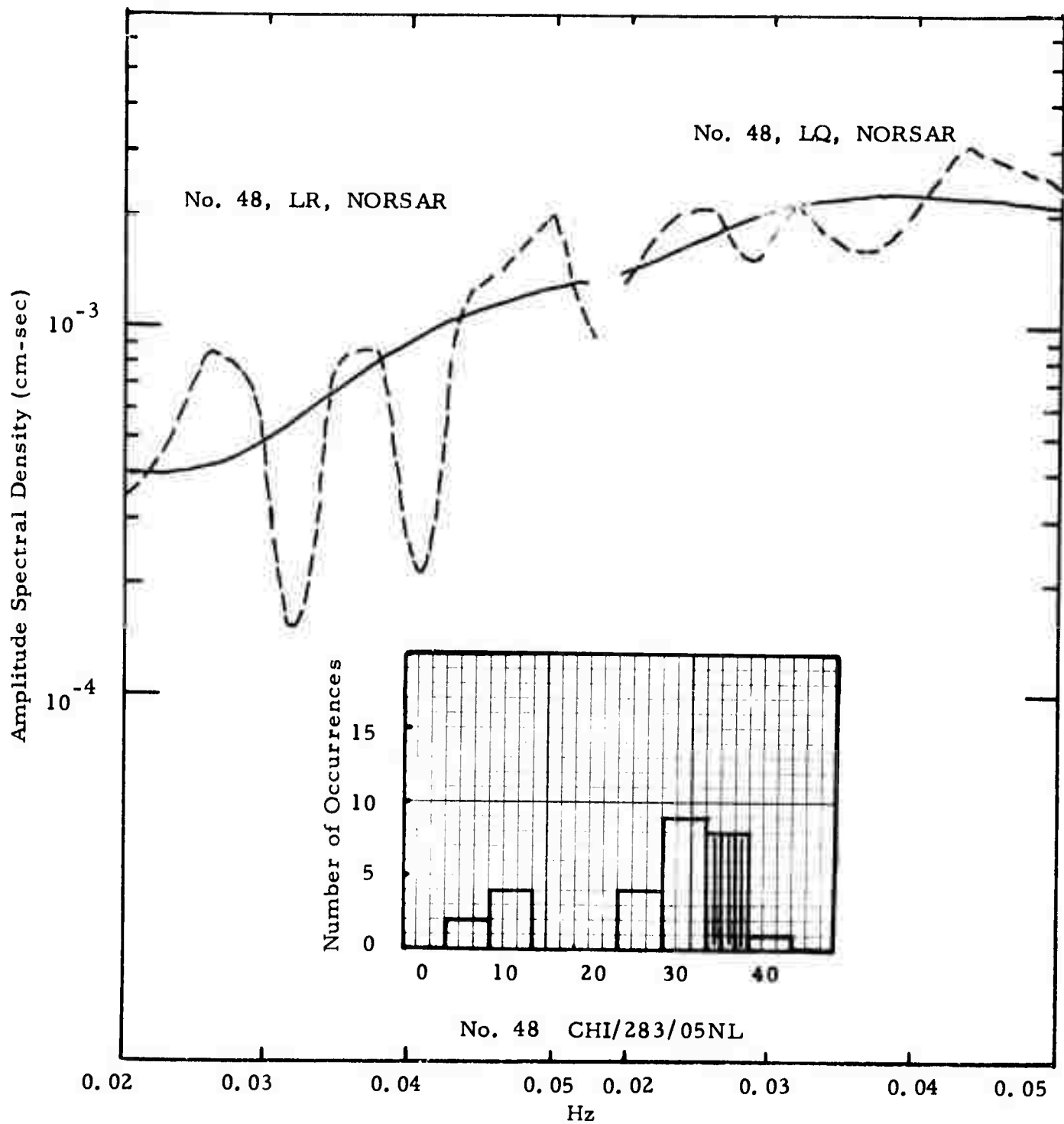


FIGURE III-26

LR AND LQ SPECTRA FOR EVENT 48 (NORSAR) AND THE CORRESPONDING DISTRIBUTION OF ESTIMATED FOCAL DEPTHS

TABLE III-15  
PDE INFORMATION FOR EARTHQUAKE-EVENTS IN NORTHEASTERN ASIA

| I. D. No. | Event Name    | Date     | Time     | Location |           | Focal Depth | $m_b$ | Data Site |
|-----------|---------------|----------|----------|----------|-----------|-------------|-------|-----------|
|           |               |          |          | Latitude | Longitude |             |       |           |
| 49        | BAI*058*22NL* | 02/27/72 | 22.15.01 | 52.0N    | 106.0E    | N           | 4.5   | NORSAR    |
| 50        | CHI/156/10NL  | 06/05/71 | 10.21.28 | 37.3N    | 113.7E    | N           | 4.7   | NORSAR    |
| 51        | ERS/165/13NL  | 06/14/71 | 13.48.56 | 56.2N    | 123.6E    | N           | 5.6   | NORSAR    |

\* = ISB

TABLE III-16  
 THEORETICAL SOLUTION OF SOURCE MECHANISM FOR  
 EARTHQUAKES IN NORTHEASTERN ASIA

| I. D. No. | Event Name   | Strike  | Dip Angle | Slip Angle | Focal Depth (km) | Moment $M(\times 10^{25} \text{ dyne-cm})$ |
|-----------|--------------|---------|-----------|------------|------------------|--|
| 49        | BAI*058*22NL | N 80°E  | 80        | 0          | 40               | 0.0070                                     |
| 50        | CHI/156/10NL | N 150°E | 60        | 30         | 15               | 0.1200                                     |
| 51        | ERS/165/13NL | N 80°E  | 60        | -30        | 15               | 0.7100                                     |

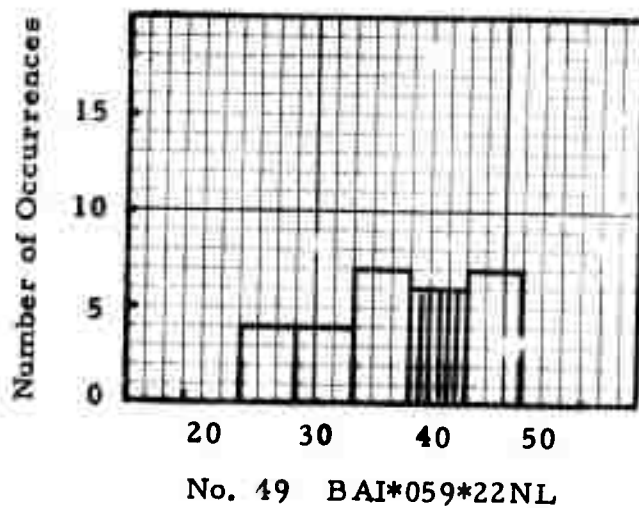
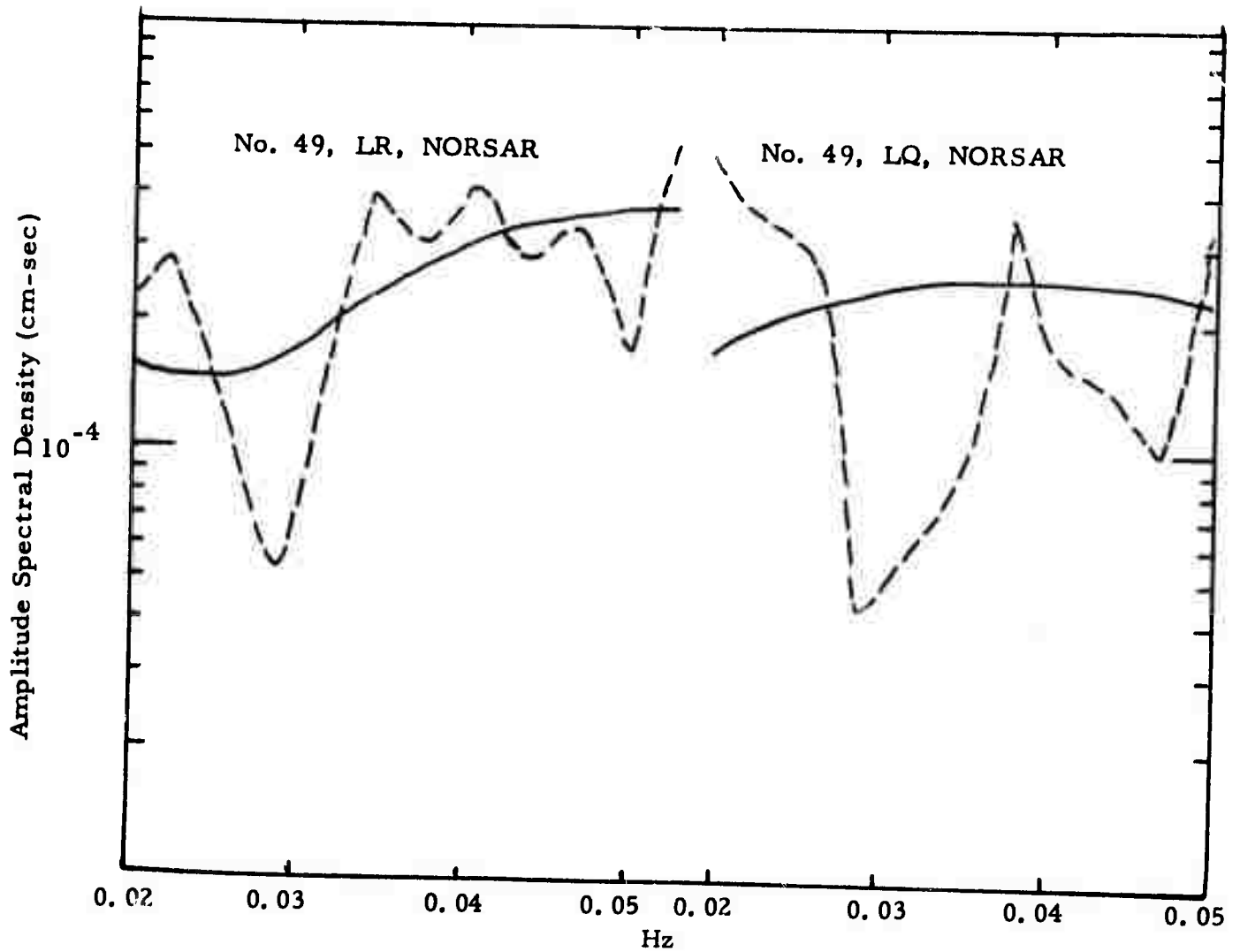


FIGURE III-27

LR AND LQ SPECTRA FOR EVENT 49 (NORSAR) AND THE  
CORRESPONDING DISTRIBUTION OF ESTIMATED FOCAL DEPTHS

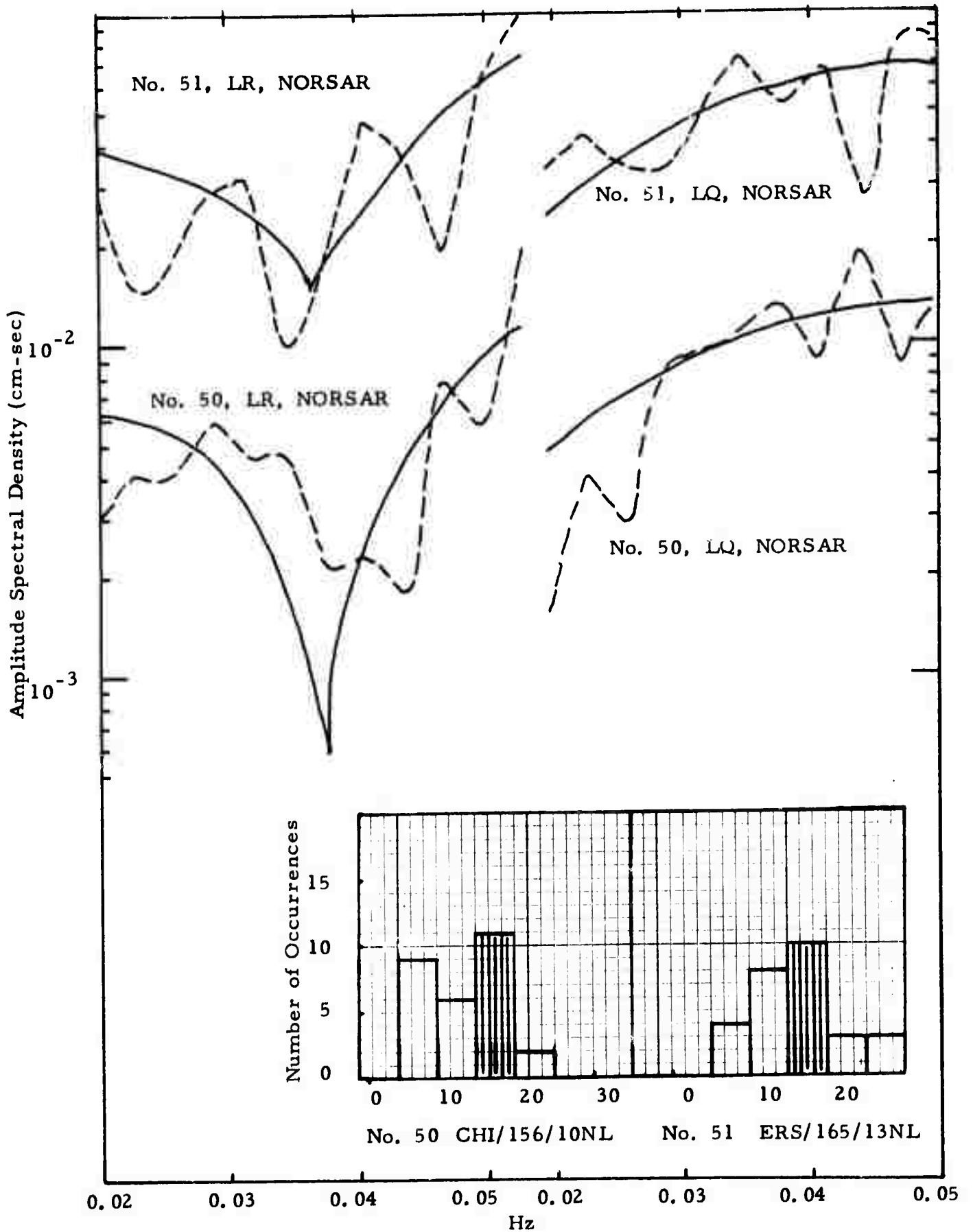


FIGURE III-28

LR AND LQ SPECTRA FOR EVENTS 50 AND 51 (NORSAR) AND THE CORRESPONDING DISTRIBUTION OF ESTIMATED FOCAL DEPTHS

## SECTION IV

### EVALUATION OF THE AUTOMATIC INTERPRETATION PROCEDURE FOR SURFACE WAVE SPECTRA

In the preceding sections we have made a factual presentation of the results obtained from applying an automatic interpretation procedure to surface wave spectra in the frequency band between 0.02 and 0.05 Hz to determine the source parameters, including focal depth, of a sizable suite of fifty-one Eurasian earthquakes. We shall now turn to the important task of making a thorough evaluation on many facets of the procedure which may have varying degrees of influence on the outcomes derived thereby. Among the things to be covered in this section are a preliminary survey of the data availability for the procedure, the effects of attenuation corrections and complex cepstrum technique on the observed spectra, the use of spectral data at multiple sites, and a summary of the estimated values of seismic moment for the fifty-one earthquakes studied. Let us now proceed to discuss these topics in detail.

#### A. DATA AVAILABILITY FOR THE PRESENT PROCEDURE

The automatic interpretation procedure devised in this study is intended for making maximum use of the surface wave data of relatively small earthquakes to extract information useful for seismic discrimination purposes. Basically, the use of this method is limited only by the availability of sufficiently good surface wave data. Thus, some knowledge of the magnitude range of an earthquake for which this method can be used is of particular interest. Table IV-1 gives a summary on the  $m_b$  magnitudes and the epicentral distances at which surface wave data are available for the sixteen earthquakes studied by using the VLPE records. Although the number of earthquakes listed in the table is relatively small, it appears not too unrealistic to expect that for many Eurasian earthquakes having  $m_b$  magnitude above 4.0 a sizable portion of the surface

TABLE IV-1  
 BODY-WAVE MAGNITUDE VS. DISTANCES  
 FROM THE VLPE DATA

| $m_b$ | Number of Station | Delta (degrees)     |
|-------|-------------------|---------------------|
| 4.1   | 1                 | 39.0°               |
| 4.4   | 1                 | 15.3°               |
| 4.4   | 2                 | 25.1°, 26.4°        |
| 4.4   | 3                 | 13.7°, 15.5°, 61.6° |
| 4.5   | 1                 | 27.4°               |
| 4.5   | 1                 | 40.8°, 44.3°        |
| 4.6   | 1                 | 15.3°               |
| 4.6   | 1                 | 24.9°               |
| 4.7   | 1                 | 15.3°               |
| 4.7   | 1                 | 15.7°               |
| 4.8   | 1                 | 15.5°               |
| 4.8   | 1                 | 30.1°               |
| 4.8   | 1                 | 44.9°               |
| 5.1   | 1                 | 45.3°               |
| 5.1   | 3                 | 30.3°, 73.9°, 33.2° |
| 5.6   | 1                 | 44.7°               |

wave data recorded at the VLPE sites within  $\Delta = 40^\circ$  will be usable for analysis by our method. Hence, the amount of suitable surface wave data should increase markedly by the time when the VLPE network is in full operation.

#### B. EFFECTS OF THE COMPLEX CEPSTRUM TECHNIQUE ON THE ESTIMATES OF EARTHQUAKE SOURCE PARAMETERS

When the observed and the best-fit theoretical spectra for both Rayleigh and Love waves for the six earthquakes in the Caucasus area were compared in Section II, we have pointed out that application of the complex cepstrum technique on the VLPE set of data had definitely improved the quality of the observed spectra and in turn resulted in a marked increase in the resolution for picking the correct earthquake source parameters. On the contrary, poorer results were obtained from the NORSAR set of data which were not processed by the complex cepstrum technique. This phenomenon was found to persist throughout the data for the other forty-five earthquakes presented in the preceding section. Table IV-2 compares the ratios of maximum to minimum error counts between ten earthquakes in the VLPE set and ten others in the NORSAR set; all are randomly chosen. It is seen that the ratios of the VLPE group are in general greater than the NORSAR group. Since the solutions for a particular earthquake is a good indicator of the resolution for deciding on the best solution, we can say that the source mechanism solutions for earthquakes from the VLPE data are superior to the NORSAR data. In summary, it is appropriate to emphasize the improvement brought about by the complex cepstrum technique both on the excellence of spectral fitting and on the reliability of source mechanism solution for an earthquake.

#### C. EFFECTS OF ATTENUATION CORRECTIONS

The observed amplitude spectra of surface waves are affected by anelastic attenuation. Corrections for its effects have to be made before the observed spectra can be used for determining the earthquake source parameters.

TABLE IV-2

COMPARISON OF RESOLUTION ERROR BETWEEN THE VLPE  
DATA (CEPSTRUM APPLIED) AND NORSAR DATA  
(NO CEPSTRUM APPLIED)

| VLPE Data (Cepstrum Applied) |                                | NORSAR Data (No Cepstrum Applied) |                                |
|------------------------------|--------------------------------|-----------------------------------|--------------------------------|
| Events                       | Ratio of Residual<br>(max/min) | Events                            | Ratio of Residual<br>(max/min) |
| LX/CAUCA/606                 | 3.28                           | TUR/143/01NL                      | 1.45                           |
| LX/CAUCA/724                 | 2.02                           | TIB /302/17NL                     | 1.12                           |
| LX/CAUCA/688                 | 1.32                           | CAU/283/09NL                      | 1.28                           |
| LX/ITALY/665                 | 1.74                           | KRG/301/13NL                      | 1.53                           |
| LX/SIRAN/290                 | 1.55                           | CAU/288/17NL                      | 1.43                           |
| LX/SIRAN/289                 | 3.94                           | TRS/251/22NL                      | 1.17                           |
| LX/SIRAN/273                 | 2.34                           | TUR/120/04BE                      | 1.16                           |
| LX/SIRAN/276                 | 2.03                           | TUR/221/04NL                      | 1.57                           |
| LX/CITLY/134                 | 2.39                           | IRA*006*09NL                      | 1.70                           |
| LX/ITALY/674                 | 1.66                           | AIG*059*18NL                      | 1.18                           |

Measurement of the attenuation coefficient for both Rayleigh and Love waves in the frequency band between 0.02 and 0.05 Hz have been made by a number of investigators. Unfortunately, these measurements were made either as world-wide averages or for regions outside the area of interest, (i. e., the Eurasian continent) and hence are not readily applicable for the present study. To improve this undesirable condition, we have made an attempt to measure the attenuation coefficient of surface waves. The results are discussed below.

The attenuation coefficient  $\eta(f)$  for a given frequency  $f$  is defined as:

$$A_2(f) = A_1(f) e^{-\eta(f)(r_2 - r_1)} \quad (3)$$

where

$A_1(f)$  and  $A_2(f)$  are the Fourier amplitude of displacement for frequency  $f$  at Sites 1 and 2, respectively;

$r_1$  and  $r_2$  are the epicentral distances to Sites 1 and 2, respectively;

$\eta(f)$  is the attenuation coefficient for frequency  $f$ .

Equation ( 3 ) is valid only if the seismic source and Sites 1 and 2 are aligned on one great-circle path since in this case the effect of source radiation is identical for both recording sites.

Six earthquakes with magnitude  $m_b \geq 5.0$  in the Moluccas-New Guinea region were selected. The pertinent information about these events as given in PDE is listed in Table IV-3. The two VLPE sites CHG (Thailand) and TLO (Spain) happen to be aligned approximately along the same great-circle paths. Hence, the surface wave data recorded at these two sites for the six events are used for this purpose. The Fourier amplitudes at each site are corrected for instrumental response and the geometrical spreading before they are inserted into equation (3) for computing  $\eta(f)$ . Because the data quality of horizontal components for these six particular events is not sufficiently good for

TABLE IV-3  
 EVENTS USED FOR ATTENUATION MEASUREMENT  
 (FROM PDE BULLETIN)

| Event Name   | Date     | Time     | Location |           | Focal Depth | $m_b, M_s$ |
|--------------|----------|----------|----------|-----------|-------------|------------|
|              |          |          | Latitude | Longitude |             |            |
| LX/MOLUC/693 | 01/04/72 | 17.59.54 | 0.2S     | 124.9E    | 69          | 5.3        |
| LX/MOLUC/694 | 01/04/72 | 18.09.46 | 0.0S     | 124.8E    | N           | 5.6        |
| LX/GUINA/695 | 01/07/72 | 06.25.48 | 2.1S     | 139.0E    | N           | 5.9, 5.9   |
| LX/GUINA/699 | 01/19/72 | 03.47.02 | 4.8S     | 145.0E    | N           | 5.1        |
| LX/GUINA/700 | 01/19/72 | 15.00.54 | 4.7S     | 145.0E    | N           | 5.8, 6.4   |
| LX/GUINA/702 | 01/22/72 | 18.41.25 | 4.6S     | 145.0E    | 22          | 5.6        |

the present purpose, we have not been able to measure the attenuation coefficient for Love waves. Only measurements for Rayleigh waves are made and reported here. The attenuation coefficient  $\eta(f)$  of Rayleigh waves is first computed from each of the six events individually. The average of these six values is taken at individual frequencies to result in the dashed curve shown in Figure IV-1. This curve is further smoothed to give the solid curve which has been used to correct all the observed spectra, Rayleigh and Love waves alike, presented in the preceding sections. Our measurements suggest that the attenuation coefficient of Rayleigh waves propagating from CHG to TLO increase steadily with frequency from 0.02 to 0.05 Hz. This behavior is markedly different from the second solid curve shown in Figure IV-1 which was measured by Tryggvasson (1965). Since the attenuation correction is implemented by multiplying the observed spectral value by a factor  $e^{(f)r}$  at any given frequency  $f$ , a frequency dependent attenuation coefficient curve will modify the original spectral shapes. Apparently, the two different attenuation coefficient curves will modify the same original spectral shape in different ways. Our attenuation coefficient curve will result in an increase in the spectral slope from 0.02 to 0.05 Hz whereas Tryggvasson's curve will bring about an opposite effect. Thus, the source parameters estimated from the corrected spectra would differ somewhat for these two different cases. In order to see how much difference there is in the resultant source parameters, we have run six events with three different curves for attenuation coefficient, namely, our present curve, Tryggvasson's curve and a zero attenuation coefficient curve for the whole frequency band. This last curve will not alter the observed spectral shapes. The resultant source parameters for these six earthquakes are listed in Table IV-4. In the table each event is given three different solutions A, B, and C which are obtained according to the three cases of attenuation correction just mentioned above. The results suggest that Solution A which is based on our own attenuation coefficient curve has a tendency to yield a shallower focal depth than Solution B which uses Tryggvasson's

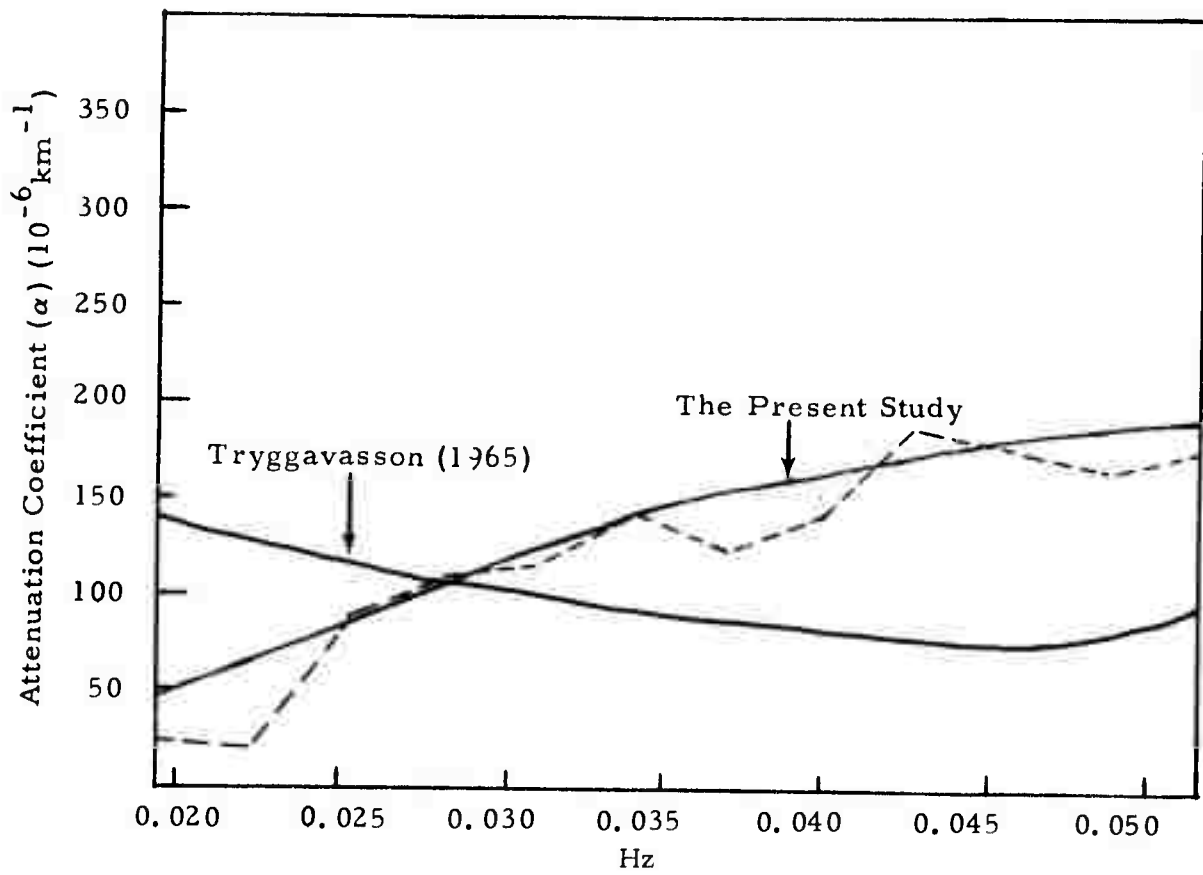


FIGURE IV-1  
 LR ATTENUATION COEFFICIENT CURVES MEASURED BY THE  
 PRESENT STUDY AND BY TRYGGAVASSON (1965)

TABLE IV -4

TEST OF SOLUTIONS FOR SOURCE MECHANISM DUE  
TO VARIOUS ATTENUATION COEFFICIENTS

| Events       | Tests | Strike  | Dip Angle | Slip Angle | Focal Depth (km) | Moment $\times 10^{25}$ dyne-cm |
|--------------|-------|---------|-----------|------------|------------------|---------------------------------|
| LX/CAUCA/668 | A     | N 0°E   | 70        | 30         | 40               | 0.010                           |
|              | B     | N 150°E | 60        | 30         | 45               | 0.0085                          |
|              | C     | N 110°E | 60        | -30        | 40               | 0.0052                          |
| LX/CAUCA/606 | A     | N 100°E | 60        | -30        | 40               | 0.074                           |
|              | B     | N 90°E  | 90        | 0          | 40               | 0.15                            |
|              | C     | N 80°E  | 70        | -30        | 35               | 0.045                           |
| LX/ITALY/667 | A     | N 110°E | 60        | -30        | 35               | 0.0019                          |
|              | B     | N 0°E   | 70        | 0          | 40               | 0.0020                          |
|              | C     | N 0°E   | 70        | -30        | 35               | 0.0016                          |
| LX/ITALY/671 | A     | N 40°E  | 80        | -30        | 45               | 0.0040                          |
|              | B     | N 40°E  | 80        | 0          | 45               | 0.0045                          |
|              | C     | N 40°E  | 80        | 0          | 45               | 0.0038                          |
| LX/TURKY/265 | A     | N 60°E  | 90        | 0          | 50               | 0.040                           |
|              | B     | N 0°E   | 70        | 30         | 65               | 0.030                           |
|              | C     | N 60°E  | 90        | 0          | 55               | 0.032                           |
| LX/CITLY/134 | A     | N 170°E | 90        | ±60        | 30               | 0.0072                          |
|              | B     | N 170°E | 90        | ±60        | 45               | 0.010                           |
|              | C     | N 160°E | 60        | 60         | 45               | 0.0073                          |

curve. Fortunately, the difference stays well within 15 km for most cases. In other words, the present method for determining focal depths is not critically dependent on precise attenuation corrections so long as the attenuation coefficient can be approximated by a smooth curve. In case of an incorrect curve for attenuation coefficient, the resultant estimates of focal depth will be biased all in the same pattern. This will not alter substantially the relative focal depths among a suite of earthquakes which are of particular interest to us. Thus, as far as focal depth is concerned, lack of precise information for making attenuation corrections on the observed spectra is not so serious as one may suspect. It must be cautioned that similar remarks can not be extended to other source parameters such as the strike direction, the dip and slip angles and the seismic moment because substantial differences do take place on the estimates of these parameters from different solutions as can be seen from Table IV-4. For this reason it is strongly hoped that more definite measurements on the attenuation coefficients of both Rayleigh and Love waves can be made on a regional basis for regions of interest in the near future.

#### D. MULTIPLE-SITE SPECTRAL FITTING

The automatic spectral fitting procedure is intended for handling surface wave data at multiple sites. Unfortunately, the applications of this procedure to the earthquakes described in the preceding two sections have been made mostly on single-site data. In order to have some knowledge on the performance of the present procedure for fitting the spectral data at multiple sites, we have made a study of two earthquakes for which data are available at more than one site. The two earthquakes are Event No. 3 (LX/CITLY/134) in Italy and Event No. 21 (LX/CAUCA/724) in Caucasus. The results are presented below.

Figure IV-2 shows the observed spectra in dashed curves for Event LX/CITLY/134. Both LR and LQ spectra are available at KON and OGD



whereas only LQ spectrum is usable at TLO. All these three sites belong to the VLPE Network. The distances from, and the azimuths at the epicenter are  $15.5^{\circ}$  and  $-7.4^{\circ}$  to KON,  $61.6^{\circ}$  and  $-59.0^{\circ}$  to OGD,  $13.7^{\circ}$  and  $-102.8^{\circ}$  to TLO, respectively. The data from OGD clearly suggest that both the LR and LQ spectral shapes deteriorate with increasing epicentral distance. The 'best-fit' theoretical spectra are superimposed on the observed spectra in Figure IV-2 for four different solutions designated as A, B, C, and D, respectively. Solution A is obtained by using the observed spectra at all three sites. The fit between the observed and the theoretical spectra is quite acceptable for all three sites. The corresponding source parameters are given in the second line of Table IV-5. According to Solution A, this earthquake is located at a depth of 30 km and is related to a oblique slip dislocation on a vertical plane. Solution B is obtained by using the observed LR and LQ spectra at KON and OGD. The theoretical spectra of this solution give a reasonable fit with the observed counterparts at OGD but are too low to explain the observed spectra at KON. The corresponding source parameters are given in the third line of Table IV-5. The focal depth is estimated at 25 km in this case. When compared to Solution A, Solution B appears to be less satisfactory in terms of the goodness of spectral fitting. Solutions C and D are obtained by using the single-site spectral data at KON and OGD, respectively. The theoretical spectra for the other site are then 'predicted' according to each single-site solution. For Solution C the predicted spectra for OGD do not agree with their observed counterparts, especially, the LR spectra. Similarly, for Solution D the predicted spectra for KON are much too high to fit both the observed LR and LQ spectra. The corresponding source parameters for these two solutions are given in the last two lines of Table IV-5. The focal depths are given as 45 and 35 km, respectively. In this table we find that the strike direction, the dip and slip angles as well as the focal depth all change from solution to solution with varying degrees. It is difficult to make a definite judgement on whether the multiple-site coverage yields more reliable estimates on the source parameters than the single-site

TABLE IV-5  
COMPARISON OF MULTI-SITES AND SINGLE-SITE SOLUTION FOR EVENT LX/CITLY/134

|   | Tests                               | Strike | Dip Angle | Slip Angle | Focal Depth | Seismic Moment<br>( $\times 10^{25}$ dyne-cm) |
|---|-------------------------------------|--------|-----------|------------|-------------|---|
| A | 3-Sites Solution<br>(KON, OGD, TLO) | N170°E | 90        | +60        | 30          | 0.0072  |
| B | 2-Sites Solution<br>(KON, OGD)      | N 10°E | 80        | +90        | 25          | 0.0089  |
| C | Single-Site Solution<br>(KON)       | N 30°E | 80        | -60        | 45          | 0.011   |
| D | Single-Site Solution<br>(OGD)       | N 0°E  | 60        | 60         | 35          | 0.011   |

coverage using the good quality data at KON alone, because the quality of data are not uniform for the three sites considered in this case. Inclusion of poor quality data will certainly not bring about improvement on the quality of the solution for source parameters. Therefore, data quality at individual sites should not be overlooked in judging the multiple-site solution. This point is brought out clearly by the next example.

Figures IV-3 and IV-4 show the observed spectra for Event LX/CAUCA/724 at the three VLPE sites FBK, KON and OGD. Only the LR spectrum is available at FBK in this instance. The distances from, and the azimuths at the epicenter are  $30.3^\circ$  and  $-39.2^\circ$  to KON,  $73.9^\circ$  and  $3.8^\circ$  to FBK,  $83.2^\circ$  and  $-39.4^\circ$  to OGD. The two sites KON and OGD in this case happen to be located almost on the same great circle path. Therefore, the spectra observed at these two sites should be very similar to each other, if they are not subject to grossly different effects of propagation. A comparison of the observed LR and LQ spectra between KON and OGD clearly reveals that the spectra at OGD markedly differ from their counterparts at KON, especially for the LR waves. This shows that the greater the epicentral distance becomes, the poorer the spectral quality will be. Thus, in this case, addition of the data at OGD to the automatic spectral fitting procedure would actually downgrade the outcomes. Addition of the poor quality data at FBK will have the same effect too. Now let us look at the 'best-fit' theoretical spectra and the related source parameters. Again four solutions are sought and shown as A, B, C, and D in Figures IV-3 and IV-4, respectively. The related source parameters for these solutions are given in Table IV-6. The theoretical spectra corresponding to Solution A which is obtained by using the data at all three sites fail to give a satisfactory fit to their counterparts, especially, for the LQ spectra at both KON and OGD. Solution B which is derived by using data at KON and OGD appears to yield somewhat better results. Still, it fails to produce an acceptable spectral fit for KON. Solution C is obtained by using the data at KON, the spectral fit is excellent at this site. The predicted spectra from this solution again

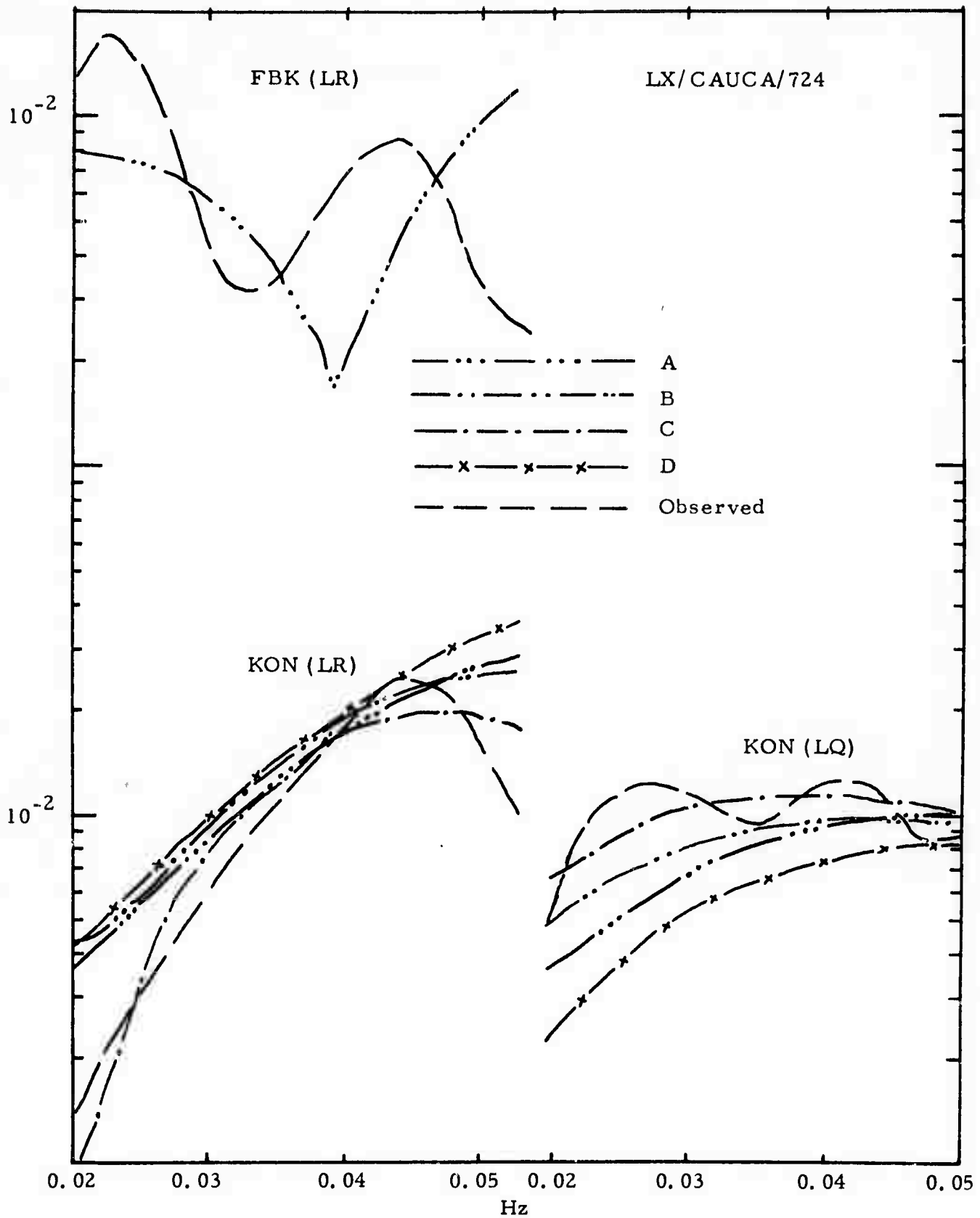


FIGURE IV-3

COMPARISON OF SPECTRAL FITTINGS FOR EVENT 21  
AMONG VARIOUS SITE COMBINATIONS

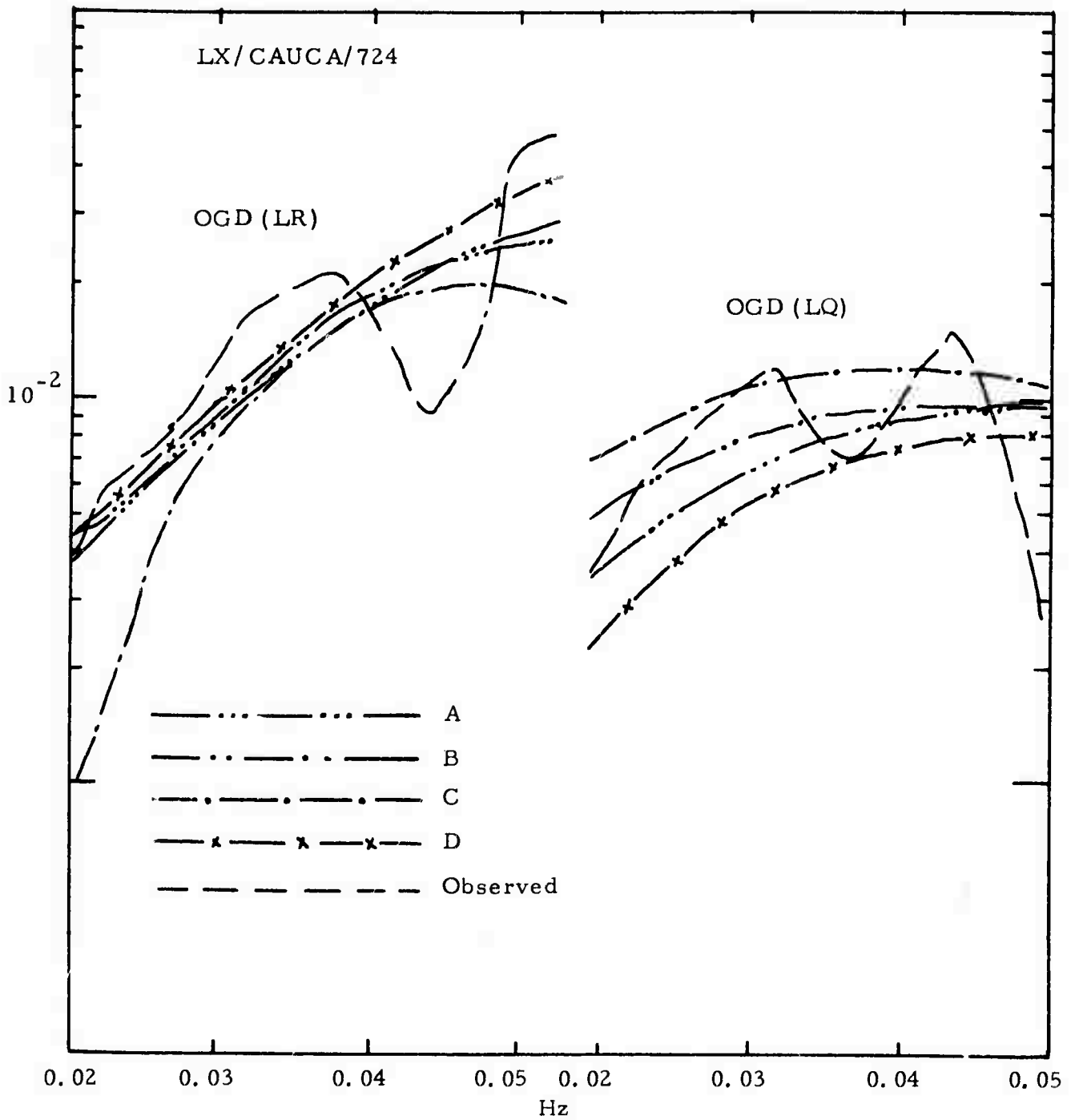


FIGURE IV-4  
 COMPARISON OF SPECTRAL FITTINGS FOR EVENT 21  
 AMONG VARIOUS SITE COMBINATIONS

TABLE IV-6  
 COMPARISON OF MULTI-SITES AND SINGLE-SITE SOLUTION FOR EVENT LX/CAUCA/724

|   | Tests                               | Strike | Dip Angle | Slip Angle | Focal Depth | Seismic Moment<br>( $\times 10^{25}$ dyne-cm) |
|---|-------------------------------------|--------|-----------|------------|-------------|---|
| A | 3-Sites Solution<br>(KON, OGD, FBK) | N 20°E | 60        | -60        | 10          | 0.21 $\times 10^{-1}$                         |
| B | 2-Sites Solution<br>(KON, OGD)      | N120°E | 60        | -60        | 30          | 0.13 $\times 10^{-1}$                         |
| C | Single-Site Solution<br>(KON)       | N160°E | 60        | 30         | 45          | 0.28 $\times 10^{-1}$                         |
| D | Single-Site Solution<br>(OGD)       | N 0°E  | 90        | +90        | 5           | 0.30 $\times 10^{-1}$                         |

fall short of giving a satisfactory spectral fit at OGD. As for Solution D, the outcome is even less desirable because it fails to reproduce large enough LQ spectra at both KON and OGD. The focal depth estimates in this case are highly variable among the four solutions. In summary, the addition of more data with poor quality in our automatic spectral fitting procedure definitely would have negative effects on the solution for source parameters. Thus, one should be careful during the selection of spectral data to be used for this purpose. Conversely, we can expect that addition of more data with good quality would improve the outcomes of the present procedure. The extent of this improvement still remains to be evaluated when such data become available.

#### E. ESTIMATION OF SEISMIC MOMENT

As pointed out earlier in Section II, the seismic moment is used as a parameter for minimizing the error in our spectral fitting procedure. Thus, the seismic moment is determined along with other source parameters in the process. Figure IV-5 shows the seismic moment corresponding to the "best-fit" theoretical spectra that is plotted against the PDE  $m_b$  magnitude for each of the fifty-one earthquakes processed by the present method. The solid line in the figure represents the theoretical curve based on the revised  $2$ -model for earthquake source spectra previously proposed in our second semi-annual technical report (Tsai, 1972b). The curve was calibrated then with observations for earthquakes in the magnitude range higher than most of the earthquakes shown in the present figure. It is remarkable that the theoretical curve agrees so closely with the data obtained in the present study. If we convert  $m_b$  to  $M_s$  magnitude, this implies that the seismic moment is directly proportional to the  $M_s$  magnitude for  $M_s$  smaller than 5.0.

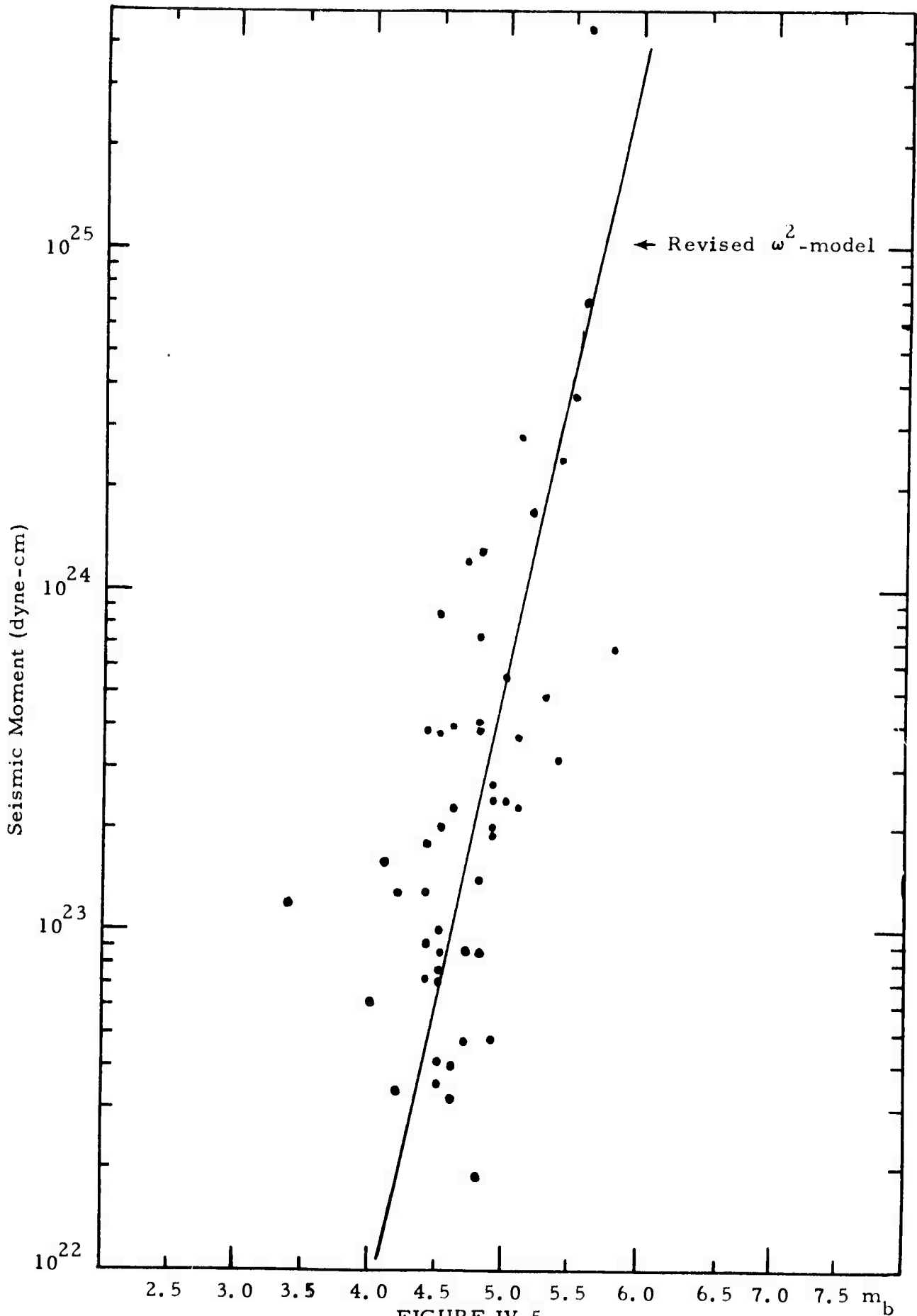


FIGURE IV-5

THE OBSERVED AND THEORETICAL RELATIONSHIPS OF SEISMIC  
MOMENT VERSUS THE  $m_b$  MAGNITUDE

## SECTION V

### CONCLUSIONS AND DISCUSSIONS

To summarize the results obtained from application of the automatic spectral-fitting procedure to the data presented in the preceding sections the following remarks are in order:

- The use of a relatively large number of unmodified spectral data in this study has been intended for the purpose of gaining first-hand knowledge on the spectral behavior of surface waves carried by the original recordings for earthquakes in regions of interest. It is found that a sizeable proportion of the unmodified spectral data are severely contaminated by modulations related to multipath interference. In the meantime, the occurrence of this phenomenon is found to be highly erratic. In some cases the spectral modulations take place on both Rayleigh and Love waves, whereas in other cases, they are present on only one of these two types of surface waves. There is indication that the spectral modulations become more serious with increasing epicentral distance. This last phenomenon is not surprising because the longer the propagation path becomes, the more lateral heterogeneities the surface wave will encounter. This, in turn, will result in more severe spectral modulations. For our purpose the presence of such undesirable spectral modulations will degrade the outcomes from applications of the present procedure to the data. Fortunately, such spectral modulations can be removed by using the complex cepstrum technique. This improvement brought about by the technique is clearly demonstrated in the sixteen earthquakes for which the VLPE data

are processed with the complex cepstrum technique. Thus, a combination of this technique with the automatic spectral fitting procedure will make it possible for us to use the surface wave data for estimating an earthquake's source parameters which may not be available otherwise.

- Our primary objective has been centered on developing a practical procedure for exploiting the long-period surface wave data to provide us useful information for seismic discrimination purposes in terms of not only the  $M_s$  magnitude but also some other source parameters. In presenting the results of this study we have singled out one such parameter, the focal depth, for special emphasis. The rationale behind this approach is the following: For a given set of surface wave data if we can estimate the focal depth within a relatively narrow range, then we shall be able to make a judgement on whether the seismic event is natural or man-made based on its location in depth. Unfortunately, based on the present data it is not yet possible to make a definite estimate of the depth range attainable by the present procedure. It should be emphasized once again that the automatic spectral fitting procedure is basically limited only by the availability of sufficiently good data. There is reason to expect that when proper multiple-site data are available, the focal depth of an earthquake can be estimated within a range of twenty kilometers. Further investigations on this aspect are needed.
- Since our present procedure depends on the theoretical surface wave spectra computed for a layered, nondissipating earth model, detailed knowledge on the elastic and anelastic properties of the crust and the upper mantle in the regions of interest will improve the performance of the automatic spectral fitting procedure.

Preliminary measurements on the attenuation coefficient of Rayleigh waves have been made for the path between CHG and TLO. Data for the central part of the Eurasian continent remains to be desired.

SECTION VI  
REFERENCES

- Ben-Menahem, A., and D. G. Harkrider, 1964, Radiation Patterns of Seismic Surface Waves from Buried Dipolar Point Sources in a Flat Stratified Earth, *J. Geophys. Res.*, 69, 2605-2620.
- Canitez, N., and M. N. Toksoz, 1972, Static and Dynamic Study of Earthquake Source Mechanism, *J. Geophys. Res.*, 77, 2583-2594.
- Harkrider, D. G., 1964, Surface Waves in Multilayered Elastic Media, 1, Rayleigh and Love Waves from Buried Sources in a Multilayered Elastic Halfspace, *Bull. Seismol. Soc. America*, 54, 627-679.
- Haskell, N. A., 1964, Radiation Pattern of Surface Waves from Point Sources in a Multilayered Medium, *Bull. Seismol. Soc. America*, 54, 377-393.
- McGarr, A., 1972, Comments on some Papers Concerning Amplitudes, Seismic Surface Waves, *J. Geophys. Res.*, 77, 3823-3826.
- Mendiguren, J., 1971, Focal Mechanism of a Shock in the Middle of the Nazca Plate, *J. Geophys. Res.*, 76, 3861-3879.
- Saito, M., 1967, Excitation of Free Oscillations and Surface Waves by a Point Source in a Vertically Heterogeneous Earth, *J. Geophys. Res.*, 72, 3689-3699.
- Texas Instruments Incorporated, 1970a, Long-Period Experiment Software Package, Services Group, Dallas, Texas.
- Texas Instruments Incorporated, 1970b, Array Evaluation Software Package, Services Group, Dallas, Texas.

- Tryggvasson, E. , 1965, Dissipation of Rayleigh Wave Energy, J. Geophys. Res. , 70, 1449-1455.
- Tsai, Y. B. , and K. Aki, 1970a, Source Mechanism of the Truckee, California Earthquake of September 12, 1966, Bull. Seismol. Soc. America, 60, 1199-1208.
- Tsai, Y. B. , and K. Aki, 1970b, Precise Focal Depth Determination From Amplitude Spectra of Surface Waves, J. Geophys. Res. , 75, 5729-5743.
- Tsai, Y. B. , 1972a, Utility of Tsai's Method for Seismic Discrimination; Semiannual Technical Report No. 1, Texas Instruments Incorporated, Dallas, Texas.
- Tsai, Y. B. , 1972b, Utility of Tsai's Method for Seismic Discrimination; Semiannual Technical Report No. 2, Texas Instruments Incorporated, Dallas, Texas.